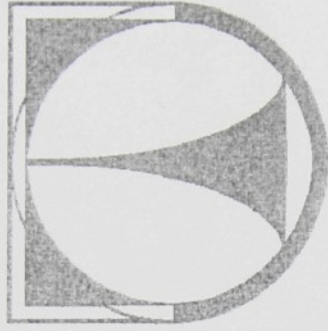


TECHNICKÁ UNIVERZITA V LIBERCI

FAKULTA TEXTILNÍ



**Pevnost příze jako stochastický proces
(Yarn Strength as a Stochastic Process)**

Dipayan Das

TEZE DISERTAČNÍ PRÁCE

Název disertační práce: **Pevnost příze jako stochastický proces**
(*Yarn Strength as a Stochastic Process*)

Autor: **Dipayan Das**

Obor doktorského studia: textilní technika

Forma studia: prezenční

Školící pracoviště: Katedra textilních technologií

Školitel: Prof. Ing. Bohuslav Neckář, Dr.Sc.

Školitel specialista: -

Liberec 2005

1 Předmět a cíl práce (Subject and Aim of Work)

1.1 Prediction of Yarn Strength Behavior at Different Gauge Lengths

Usually, yarn strength measurement is performed at 500 mm gauge length. However, in practice, yarns are stressed at different lengths. Therefore, yarn strength measurements carried out only at 500 mm gauge length is not sufficient. It is necessary to know yarn strength behavior at different gauge lengths. However, it is not at all a realistic idea to carry out strength measurements using a tensile tester at different gauge lengths. Therefore, a new scientific way should be developed for predicting yarn strength behavior at different gauge lengths. In order to have sufficient information on this behavior, it is necessary to know not only the basic statistical parameters of yarn strength, say the mean value and the coefficient of variation, but also the frequency distribution of yarn strength.

1.2 Understanding Yarn Strength Variability

It is well known that yarn strength variability is one of those very critical factors that determine the performances of the subsequent technological processes as well as of the textile products during their various end-uses. Many attempts were made in the past to investigate the causes of yarn strength variability, but most of them were confined to establish only empirical equations relating yarn strength variability to yarn mass irregularity and to the variations in fiber properties. Nevertheless, no attempt has been made till date to investigate the nature of yarn strength variability. Moreover, the physical bases of yarn strength variability are still not enough clear. It is therefore of extreme importance to gain new knowledge leading to improved understanding of yarn strength variability.

2 Přehled současného stavu problematiky (Summary of State-of-the-Art of the Problem)

Yarn strength versus gauge length behavior was probably first theoretically modeled by Peirce [1]. He considered a long length of yarn equally divided into several short sections and imagined that 1) strength of the long section is equal to that of the weakest short section (weakest-link principle), 2) the breakage of any short section does not influence the breakage of other short sections (concept of strength independency), and 3) strength of the short sections follow Gaussian (normal) distribution. Under these assumptions, he theoretically derived the following relations

$$\bar{S}^* = \bar{S} + 4.2\sigma_s \left[(l/l_0)^{-1/5} - 1 \right], \quad (1)$$

$$\sigma_{S'} = \sigma_S (l/l_0)^{-1/8}; \quad (2)$$

where \bar{S}' and \bar{S} are the mean strength of yarn specimens with lengths l and l_0 , respectively; $\sigma_{S'}$ and σ_S are the standard deviations of strength corresponding to lengths l and l_0 , respectively. Here, $l > l_0$. Later on, Morton & Hearle [2] and Meredith [3] observed that these relations did not correspond well to the reality. As a reason for this discrepancy, Spencer-Smith [4] imagined that strength of successive fracture zones along a yarn is dependent. (Fracture zone is that small region where actual breaking takes place while strength testing of a long length of yarn [5].) The imagination of strength dependency and the consequent theoretical model of Spencer-Smith have not verified with the actual results till date due to the fact that the fracture zone is very ill defined [2]. Later on, performing statistical tests on the actual strength data, Knox & Whiwell [6] and Realfe *et al.* [7] concluded that Peirce's assumption of the independent weakest-link is not appropriate. The assumption of Gaussian distribution of yarn strength was also questionable, as reported by Realfe *et al.* [7] and Kapadia [8], however, on the contrary, this assumption was reasonable, as concluded by Truevstev *et al.* [9], Pozdniakov *et al.* [10], Perepelkin [11]. According to Zurek [12], the yarn breakages occur at different gauge lengths depending on yarn twist and this consideration was neglected in Peirce's theory. Also, the types of yarn breakages are different at different gauge lengths, as observed by Radhakrishnaiah & Huang [13]. Additionally, the physical mechanism of yarn breakages are different at different gauge lengths depending on yarn structure [7] and fiber properties [14]. These facts were not accounted by Peirce's model. After Peirce, several attempts were made to study the behavior of yarn strength at different gauge lengths; however, those were empirical only [15-19].

3 Použití metody (Used methods)

3.1 Materials

In this research work, 100% cotton carded and combed yarns with different fineness and twist characteristics produced by ring, rotor, compact, and new¹ spinning technologies were used.

¹ The Cotton Research Institute (VUB) of Czech Republic has invented a new spinning technology, which is not yet commercialized, and no specific name is given to that technology. Throughout this report, that technology is called "New Spinning Technology" and the yarns made from that technology are called "New Yarns."

3.2 Methods of Measurements

Different standard and nonstandard methods were applied in this research work to measure yarn strength, yarn mass, and yarn twist.

3.2.1 Yarn Strength at Different Gauge Lengths

In this research work, yarn strength measurements at short gauge length, which is longer than the longest fiber in the yarn, were performed using a special methodology (Figure 1). Let us imagine a long yarn section divided into sixty successive short sections of equal length ($l_0 = 50$ mm), as marked by the serial numbers 1, 2, 3, 4, ..., 59, 60 in Figure 1. Then the strength of the sections marked by the numbers 1, 3, ..., 59 was measured one after another; the remaining sections (shown by the symbol \times) were used for clamping. Thus, the strengths S_1, S_3, \dots, S_{59} of 30 alternate sections were measured. This procedure was repeated 30 times at different places of the same yarn randomly chosen from many bobbins. As a result, 900 strength values were obtained on each yarn. This methodology was applied on all yarns. The strength datasets were used to calculate the statistical parameters (mean value, standard deviation, and coefficient of variation, and autocorrelation characteristics) as well as the frequency distribution.

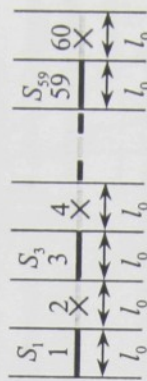


Figure 1 Yarn strength measurements procedure at short gauge length

Yarn strength was also measured conventionally with some yarns at other gauge lengths: 100 mm, 200 mm, 350 mm, 500 mm (ČSN 80 0700), and 700 mm, and then the basic statistical parameters (mean value, standard deviation, and coefficient of variation) as well as the frequency distribution were calculated.

3.2.2 Yarn Mass by Capacitive Method

All yarns were tested using the USTER TESTER 4 instrument following the Czech Standard (ČSN 80 0706), and different mass characteristics (U%, CV%, imperfection counts, mass diagram, mass spectrogram, mass variance-length curve, and mass correlogram) were estimated.

3.2.3 Yarn Mass by Gravimetric Method

In order to obtain the descriptive statistical characteristics of yarn count, each yarn was also tested gravimetrically following the Czech Standard (ČSN 80 0702).

In addition, 900 gravimetric mass measurements were carried out manually each with 20 tex and 35.5 tex carded rotor yarns. The method of measurements was almost similar to that of the strength measurements at short gauge length (Figure 1), except the fact that in case of the former, mass of every successive section (each of 50 mm length) was measured; whereas, in case of the latter, strength of every alternate section (each of 50 mm length) was measured. The mass datasets were used to estimate the mass correlograms.

3.2.4 Measurements of Yarn Twist with Yarn Specimens of Different Lengths

With each yarn, 50 twist measurements were performed each at 250 mm length manually following the Czech Standard (ČSN 80 0701), and then the common descriptive statistical parameters (mean value, standard deviation, and coefficient of variation) were estimated.

In order to estimate yarn twist correlogram, 900 twist measurements were carried out on 35.5 tex cotton carded rotor yarn. The method of measurements was analogous to that of yarn strength measurements at short gage length (Figure 1).

3.3 Method of Computer Simulations

Using the autocorrelation characteristics estimated from the actual strength data corresponding to 50 mm gauge length and assuming that the strength data follows Gaussian distribution, numerical simulations were performed on computer with 30000 yarn sections each of 5000 mm length; thus, 3×10^6 strength values each corresponding to 50 mm length were generated. Then, applying the weakest-link principle [1] on them, strength of yarn specimens with different length (a whole number multiple of 50 mm) was obtained. Thereby, basic statistical parameters as well as frequency distribution of simulated strength of yarn specimens with different length (50 mm – 5000 mm) were estimated.

4 Přehled dosažených výsledků (Summary of achieved results)

4.1 Basic Statistical Parameters of Actual Yarn Strength

Table 1 shows the basic statistical parameters of yarn strength measured at different gauge lengths with 7.4 tex cotton combed ring yarn. These results with other yarns are in [22].

Table 1 – Basic statistical parameters of actual strength of 7.4 tex combed ring yarn

Gauge length [mm]	50	100	200	350	500	700
Mean value [cN/tex]	21.81	20.22	20.44	19.61	18.74	17.18
Coefficient of variation [%]	12.25	11.76	10.90	11.96	9.91	9.56

4.2 Frequency Distribution of Actual Yarn Strength

The strengths S_l corresponding to 50 mm gauge length were standardized according to the expression $U_l = (S_l - \bar{S})/\sigma_s$, and the strengths S_l^* corresponding to the other gauge

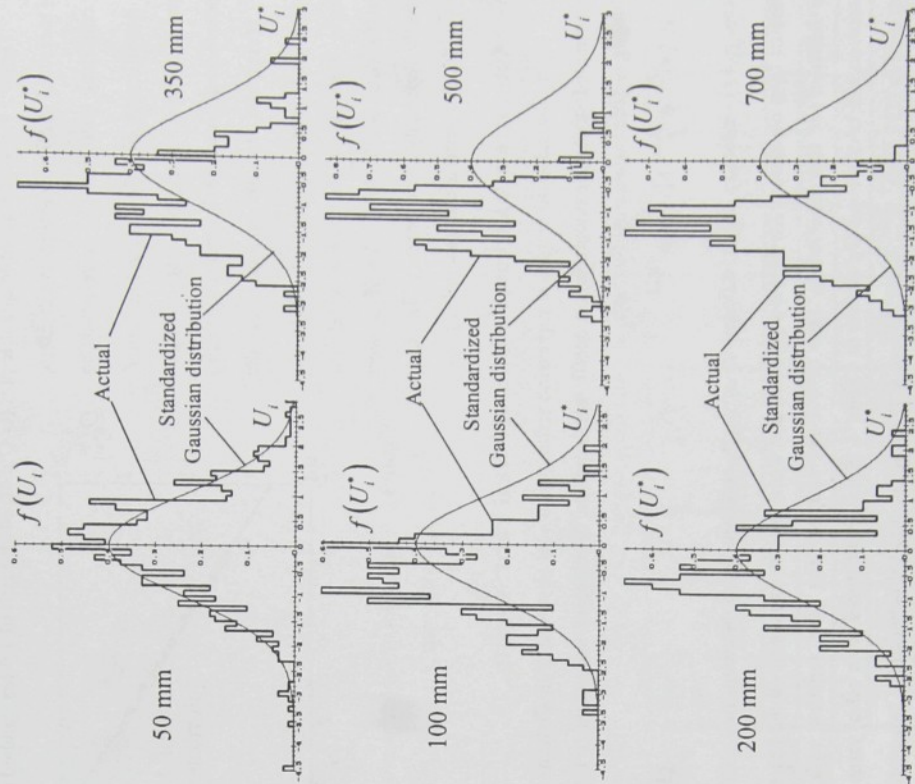


Figure 2 Strength histograms in case of 7.4 tex combed ring yarn
lengths were transformed according to $U_l^* = (S_l^* - \bar{S})/\sigma_s$. Here, \bar{S} and σ_s are the mean value and standard deviation of yarn strength related to the gauge length $l_0 = 50$ mm, but S_l^* are related to the gauge length l , $l > l_0$. Then, their frequencies $f(U_l)$ and $f(U_l^*)$ were

calculated. The frequency distribution of the strengths of 7.4 tex combed ring yarn measured at different gauge lengths is shown by the histograms in Figure 2 together with the probability density function of the standardized Gaussian distribution. These results with other yarns are presented in [22].

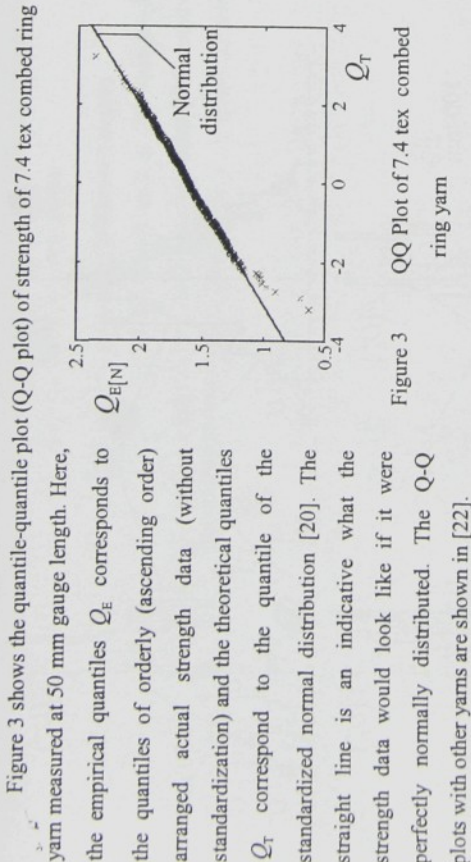


Figure 3 QQ Plot of 7.4 tex combed ring yarn

Using the standard statistical regression technique, it was observed with all yarns that the estimated strength autocorrelation coefficients could be represented satisfactorily by the following double exponential function

$$\rho_s(x) = ae^{-bx_{[mm]}} + (1-a)e^{-cx_{[mm]}} \tag{3}$$

where $\rho_s(x)$ indicates the coefficient of strength autocorrelation between two sections separated by a distance x , a is the coefficient and b , c are the exponents of the function. The behavior of this function in case of 7.4 tex combed ring yarn together with the autocorrelation coefficients are shown in Figure 4. Similar behaviors with other yarns are illustrated in [22]. Here, $x_{[mm]} = 50k$, where k is the lag or interval between the two sections.

Then, Equation (3) can be expressed in another form

$$\rho_s(k) = ae^{-bk} + (1-a)e^{-ck} \tag{4}$$

This expression is comparable to the following theoretical strength autocorrelation function obtained under the assumption that yarn strength is a summation of two independent SEMG – stationary, ergodic, Markovian, and Gaussian – stochastic processes [21]

$$\rho_s(k) = \frac{^{(1)}\sigma_s^{(1)}r^k + ^{(2)}\sigma_s^{(2)}r^k}{\sigma_s^2} \tag{5}$$

where $^{(1)}\sigma_s$, $^{(1)}r^k$ represents the standard deviation and autocorrelation coefficient, respectively, corresponding to the first SEMG-stochastic process and $^{(2)}\sigma_s$, $^{(2)}r^k$ denotes the same for the second SEMG-stochastic process. The value of these characteristics can be easily obtained by comparing Equations (5) and (3). These, for different yarns, are shown in Table 2 together with the corresponding values of the coefficient and exponents of the double exponential function expressed by Equation (4).

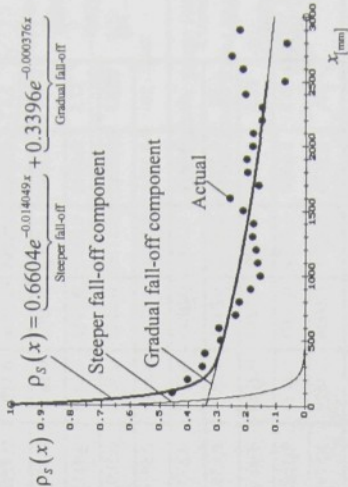


Figure 4 Strength correlogram and autocorrelation function in case of 7.4 tex combed ring yarn

Table 2 Strength autocorrelation characteristics and parameters of different yarns

Yarn	Count [tex]	a	b	c	⁽¹⁾ σ _s [N]	⁽¹⁾ r ^k [-]	⁽²⁾ σ _s [N]	⁽²⁾ r ^k [-]	A	B
Combed Ring	7.4	0.6604	0.7025	0.0188	0.1607	0.4953	0.1153	0.9814	5.33	1/8.66
	10	0.6214	1.1042	0.0411	0.1698	0.3314	0.1325	0.9597	5.08	1/8.16
	14.5	0.6601	0.4378	0.0031	0.1735	0.6455	0.1245	0.9695	5.53	1/9.78
	16.5	0.6129	0.3484	0.0106	0.1945	0.7058	0.1546	0.9895	6.08	1/12.19
	20	0.7032	0.1934	0.0168	0.2311	0.8242	0.1502	0.9834	5.83	1/11.75
Carded Ring	20	0.6659	0.4532	0.0164	0.2363	0.6356	0.1674	0.9837	5.69	1/10.38
	25	0.7048	0.2796	0.0182	0.2792	0.7561	0.1807	0.9820	5.45	1/10.55
	29.5	0.7450	0.8122	0.0122	0.3956	0.4439	0.2314	0.9879	5.22	1/8.49
Carded Rotor	20	0.7830	1.0057	0.0003	0.1947	0.1025	0.3658	0.9966	4.69	1/7.29
	35.5	0.5968	1.2042	0.0409	0.3754	0.3000	0.3086	0.9599	5.28	1/8.66
	42	0.5507	0.6360	0.0002	0.3148	0.5294	0.2843	0.9978	6.17	1/12.97

Using the standard statistical regression technique, it was observed that the above results were approximated well by the following type of expression

$$\bar{S}^* = \bar{S} + A \sigma_s \left[\left(l/l_0 \right)^{-B} - 1 \right], \quad (6)$$

$$\sigma_s^* = \sigma_s \left(l/l_0 \right)^{-B}; \quad (7)$$

where A and B are the coefficient and the exponent, respectively. The other symbols are already defined in Equations (1) and (2). The values of A and B for different yarns are presented in Table 2.

Figure 5 illustrates the simulation results (Table 3), the actual results (Table 1), and the results obtained from Equations (1) and (2) in case of 7.4 tex combed ring yarn. These results with other yarns are shown in [22].

Note: In some yarns, the actual strength at longer gauge length was found nearly the same or a little higher than the actual strength at short gauge length (50 mm). Imaginatively, this might happen because the "micro-slippage" of fibers and/or fiber segments was not fully realized in a region near to the jaw gripping line. Evidently, this was relatively more prominent during tensile testing at short gauge length (50 mm).

4.5 Frequency Distribution of Simulated Yarn Strength

The histograms of the simulated strengths corresponding to three selected specimen lengths in case of 7.4 tex cotton

Yarn	Count [tex]	a [-]	b [-]	c [-]	$^{(1)}\sigma_s$ [N]	$^{(1)}r^k$ [-]	$^{(2)}\sigma_s$ [N]	$^{(2)}r^k$ [-]	A [-]	B [-]
Combed Compact	7.4	0.7624	1.2309	0.0186	0.1632	0.2920	0.0911	0.9816	4.80	1/7.44
	10	0.3858	0.5061	0.0007	0.1740	0.6029	0.2196	0.9930	7.60	1/19.19
	11.8	0.6719	0.8629	0.0179	0.2236	0.4219	0.1562	0.9823	5.29	1/8.89
Carded Compact	20	0.7162	1.2012	0.0353	0.2937	0.3009	0.1849	0.9653	4.87	1/7.40
	29.5	0.5336	0.8508	0.0004	0.3780	0.9184	0.3535	0.9961	7.69	1/23.92
Combed New (TM ² - 38)	7.4	0.6160	0.3258	0.0106	0.1596	0.7220	0.1260	0.9895	5.94	1/12.21
	10	0.5160	0.5569	0.0201	0.1810	0.5730	0.1753	0.9801	6.04	1/11.91
	12.5	0.6140	0.8397	0.0113	0.2568	0.4318	0.2036	0.9888	5.72	1/10.46
	16.5	0.6363	0.2116	0.0143	0.3674	0.8093	0.2778	0.9859	6.06	1/12.77
	20	0.5394	0.5421	0.0290	0.3387	0.5816	0.3130	0.9714	5.77	1/10.82
Combed New (TM - 56)	7.4	0.5907	1.2129	0.0173	0.2207	0.2973	0.1837	0.9829	5.60	1/9.89
	10	0.7584	0.7905	0.0181	0.2317	0.4536	0.1308	0.9821	5.01	1/7.91
	12.5	0.6774	0.8499	0.0365	0.2728	0.4275	0.1883	0.9642	5.12	1/8.19
	16.5	0.6038	1.0126	0.0209	0.2773	0.3633	0.2246	0.9793	5.49	1/9.67
	20	0.5178	0.5277	0.0004	0.3629	0.5900	0.3502	0.9957	6.86	1/15.08
Combed New (TM - 81)	7.4	0.8529	11.71	0.0427	0.2269	8×10^{-6}	0.0942	0.9957	3.74	1/4.85
	10	0.7925	11.24	0.1163	0.3031	1×10^{-5}	0.1551	0.8902	4.27	1/5.55
	12.5	0.5802	11.38	0.0005	0.4051	1×10^{-5}	0.3446	0.9954	3.61	1/5.90
	16.5	0.7134	11.53	0.0307	0.4102	1×10^{-5}	0.2600	0.9698	4.86	1/7.19
	20	0.6574	1.0964	0.0002	0.5012	0.3341	0.3619	0.9998	3.87	1/6.35

Note: The nature of the strength autocorrelation function, when the strength data contained periodicity, is shown in [22]. Studying this was, however, beyond the scope of this work.

4.4 Basic Statistical Parameters of Simulated Yarn Strength

The basic statistical parameters calculated from the simulated strength values corresponding to the lengths ranging from 50 mm to 5000 mm in case of 7.4 tex combed ring yarn are shown in Table 3.

Table 3 – Basic statistical parameters of simulated strength of 7.4 tex combed ring yarn

Gauge length [mm]	50	...	500	...	1000	...	5000
Mean value [cN/tex]	21.81	...	18.79	...	17.94	...	16.06
Coefficient of variation [%]	12.25	...	11.23	...	10.90	...	9.98

² TM stands for twist multiplier (Phrix type), expressed in $\text{tex}^{2/3} \text{cm}^{-1}$.

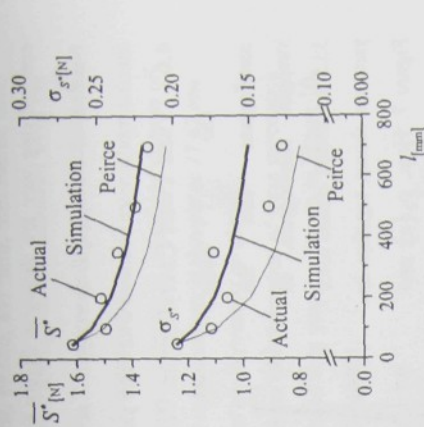


Figure 5 Strength vs. gauge length relation in 7.4 tex combed ring yarn

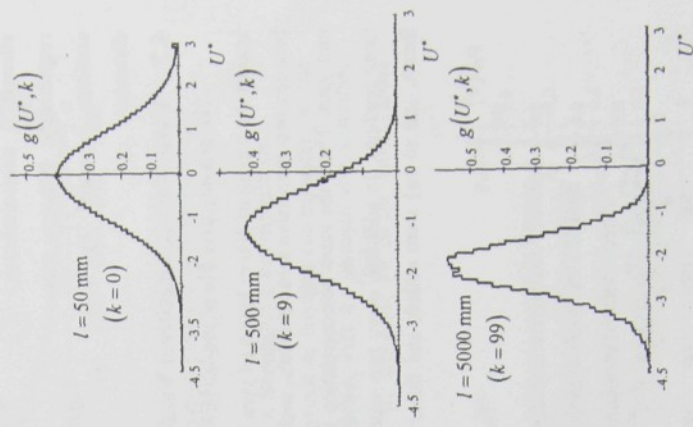


Figure 6 Simulated strength histograms

combed ring yarn are shown in Figure 6. Here, $g(U^*, k)$ indicates the probability density function of the strength quantity U^* at a gauge length parameter k , where $k = l/l_0 - 1$. Similar results were obtained with other yarns.

4.6 Yarn Twist Correlation Versus Yarn Strength Correlation

The twist correlation and the strength correlation of 35.5 tex cotton carded rotor yarn are shown together in Figure 7. Here, $\rho_s(x)$ and $\rho_t(x)$ indicates the coefficients of twist and strength autocorrelation, respectively, between two sections separated by a distance x

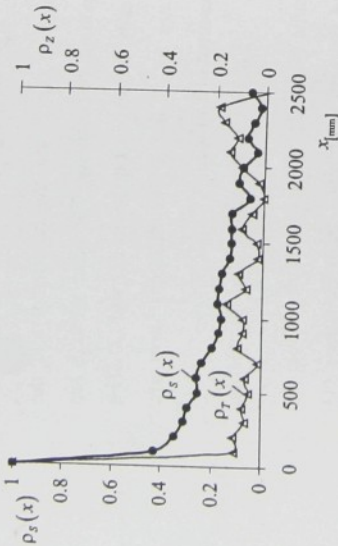


Figure 7 Strength and twist correlations of 35.5 tex cotton carded rotor yarn

4.7 Yarn Mass (Capacitive) Versus Yarn Strength Correlations

The primary data file of the USTER TESTER 4 always showed 18458 mass readings against the testing of 400 m length of yarn. Under the hypothesis that no yarn was wasted in between two successive measurements, each reading corresponded to the mass of about 21.67 mm yarn. Then, the mass autocorrelation coefficients $\rho_m(x)$ were estimated directly from those readings. In addition, every two successive readings (first and second, then third and fourth, and so on) were added; and then, the mass correlation was estimated from those

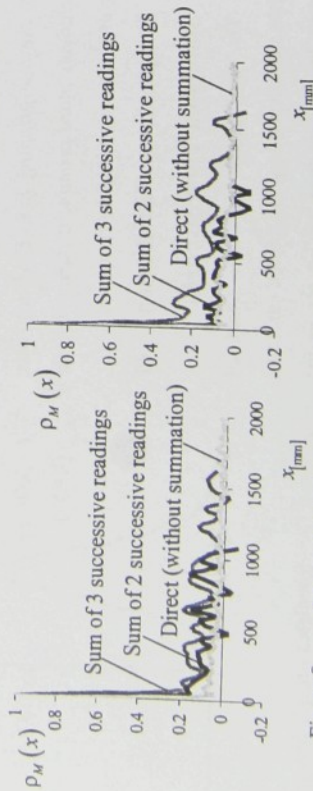


Figure 8 Mass correlations (capacitive) of 7.4 tex combed ring yarn

Figure 9 Mass correlations

resulting readings. Also, three successive readings (first, second, and third, then fourth, fifth, and sixth, and so on) were added; and then, the mass correlation was estimated from the resulting readings. The estimated mass correlations for 7.4 tex combed ring yarn and 20 tex carded compact yarn are shown in Figure 8 and Figure 9, respectively.

Note: Sometimes, each reading, as appeared in the primary data file, is considered as mass of 10 mm yarn, and the distance between two successive measurements is thought as 11.67 mm. Based on this, the estimated mass correlations showed similar results as above.

The mass autocorrelation function, estimated from the summation of three successive readings, and the strength correlation of 7.4 tex combed ring yarn are shown in Figure 10. The same for 20 tex carded compact yarn is shown in Figure 11.

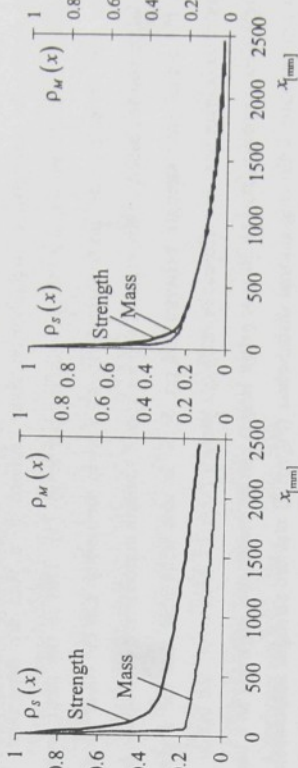


Figure 10 Mass (capacitive) and strength autocorrelation functions in case of 7.4 tex combed ring yarn

Figure 11 Mass (capacitive) and

strength autocorrelation functions in case of 20 tex carded compact yarn

4.8 Yarn Mass (Gravimetric) Versus Yarn Strength Correlations

The mass correlation and the mass autocorrelation function corresponding to the mass data of 35.5 tex cotton carded rotor yarn together with the strength autocorrelation function of the same yarn are represented in Figure 12. The same for 20 tex cotton carded rotor yarn is shown in Figure 13.

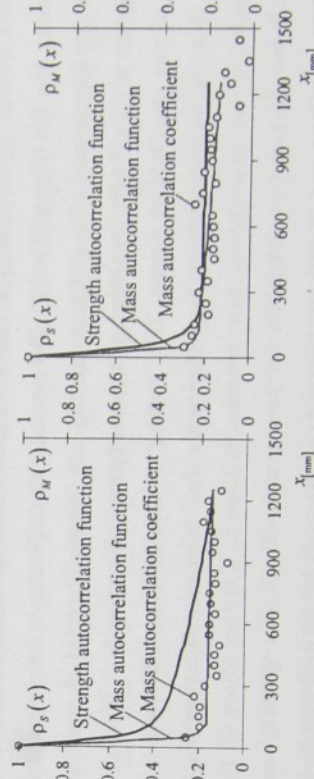


Figure 12 Strength and mass (gravimetric) autocorrelations in 35.5 tex carded rotor yarn

Figure 13 Strength and mass (gravimetric)

autocorrelations in 20 tex carded rotor yarn

5 Zhodnocení výsledků a nových poznatků (Estimation of Results and New Knowledge)

The mean value and the standard deviation of actual yarn strength are decreasing with the increase in gauge length (Table 1). This is also evident from the relative shifting of the actual strength histogram towards the left-hand side and the change in shape of the histogram – it becomes higher and narrower – with the increase in gauge length (Figure 2). Similar trends were obtained with the simulated strength as well (Table 3 and Figure 6). Therefore, it can be said that the weakest-link principle is evident in yarns. Figure 4 reveals the existence of strength autocorrelation among the neighboring short sections (50 mm) along a yarn. In other words, the strengths of neighboring short sections in a yarn are dependent. This contradicts Peirce's assumption of strength independency [1]. This is the most probable reason why Peirce's model does not correspond well to the reality. On the other hand, the simulation results, based on the verified assumption of strength dependency, correspond better with the actual yarn strength behavior (Figure 5). It is also noticeable that the degree of strength autocorrelation is different in different yarns (Table 2). Moreover, the actual yarn strength data corresponding to 50 mm gauge length can be reasonably regarded as a sample from a population following normal distribution (Figure 3) and the strength autocorrelation can be satisfactorily characterized by a summation of two exponential functions, where each function possesses very different nature than the other. This autocorrelation function is in agreement with that obtained theoretically under the assumption of yarn strength as a summation of two independent SEMG stochastic processes [21]. It therefore issues the probable existence of two highly different and mutually independent phenomena that are acting together on the yarn so as to impart variability to yarn strength.

It is evident that the capacitive mass correlogram, based on the summation of three successive readings, shows significantly higher correlation than that estimated directly from the primary data file (Figures 8 and 9). The reason for this difference is not yet precisely known. At this moment, this difference can be very roughly imagined as a natural consequence of fiber distribution along a yarn caused by the drafting operations at different stages of yarn manufacturing process. This "working" hypothesis needs to be verified in future. However, the results obtained from the capacitive mass measurements are comparable to those found from the gravimetric mass measurements (Figures 10, 12 and Figure 11, 13). The influence of yarn mass irregularity on yarn strength variability is generally very significant. Sometimes yarn strength variability is found due solely to yarn mass irregularity

and sometimes, besides the mass irregularity, influence of another variability on yarn strength variability is evident. Certainly, this is not related to yarn twist (Figure 7). The physical basis of that variability is still unknown. At this present moment, it is an open question. Very roughly speaking, it may be a structural irregularity, say the packing density variation along the yarns; however, future research works need to be conducted to scientifically answer this question.

6 Práce autora se vztahem ke studované problematice (Authors Work in Relation to the Studied Problems)

- "Yarn Strength as a Stochastic Process," Neckář, B., and Das, D., *Textile Research Journal* (Accepted for Publication)
- "Yarn Strength Behavior at Different Gauge Lengths," Das, D., and Neckář, B., *Indian Journal of Fiber and Textile Research* (Accepted for Publication)
- "Yarn Strength as a Function of Gauge Length – A Critical Review," Das, D., *Vlákna a Textil* (Communicated for Publication)
- "Mathematical Modeling and Experimental Investigation of Yarn Strength as a Stochastic Process," Das, D., *The Fiber Society 2004 Annual Meeting and Technical Conference* (Oral), Ithaca (USA), 2004
- "A Stochastic Approach to Yarn Strength," Das, D., and Neckář, B., *7th Asian Textile Conference* (Oral), New Delhi (India), 2003

7 Literatura (Literature)

- [1] Peirce, F. T., *Journal of Textile Institute* **17**, pp. T 355-T368, 1926.
- [2] Morton, W. E. & Hearle, J. W. S., "Physical Properties of Textile Fibers," Butterworths & Co. (Publishers) Ltd., The Textile Institute, Manchester, 1992.
- [3] Meredith, R., *Journal of Textile Institute* **37**, p. T205, 1946.
- [4] Spencer-Smith, J. L., *Journal of Textile Institute* **38**, pp. P257-P271, 1947.
- [5] Turner, A. J., *Journal of Textile Institute* **19**, pp. T280-T314, 1928.
- [6] Knox, L. J., Jr. & Whitwell, J. C., *Textile Research Journal* **41**, pp. 510-517, 1971.
- [7] Realfe, M. L., Seo, M., Boyce, M. C., Schwartz, P. & Backer, S., *Textile Research Journal* **61**, pp. 517-530, 1991.
- [8] Kapadia, D. F., *Journal of Textile Institute* **25**, pp. T355-T370, 1934.
- [9] Truetsev, N. N. et al., *Journal of Textile Institute* **88**, pp. 400-414, 1971.
- [10] Pozdniakov, B. P., "Methods of Statistical Control and Investigation of Textile Material," Light Industry, Moscow, 1978.

- [11] Perepelkin, K. E., *Fibre Chem.* **23**, pp. 115-133, 1991.
- [12] Zurek, W., "The Structure of Yarn," The National Center for Scientific, Technical, and Economic Information, Warsaw, 1975.
- [13] Radhakrishnaiah, P. & Huang, G., *Papers of the 10th EFS[®] System Research Forum*, North Carolina, 1997
- [14] Perepelkin, K. E. et al., *Khim. Volok.* **29**, pp. 47-48, 1987.
- [15] Zurek, W. et al., *Papers of The Technical University of Lodz.* **33**, pp. 62-73, 1976.
- [16] Hussain, G. F. S. et al., *Textile Research Journal* **60**, pp. 69-77, 1990.
- [17] Kapadia, D. F., *Journal of Textile Institute* **26**, pp. T242-T260, 1935.
- [18] Mark, H., "The Physics and Chemistry of the Cellulose," J. Springer, Berlin, 1932.
- [19] Sippel, A., *Faserforschung und Textiltechnik* **9**, p. 163, 1958.
- [20] Meloun, M. et al., "Chemometrics for Analytical Chemistry, Volume 1: PC-Aided Statistical Data Analysis," Ellis Horwood, New York, 1992.
- [21] Neckář, B., "Morphology and Structural Mechanics of General Fibrous Assemblies", Technical University of Liberec, Liberec, 1998.
- [22] Das, D., "Yarn Strength as a Stochastic Process," Ph.D. Thesis, Technical University of Liberec, Liberec, 2005.

8 Summary

In this research work, strength of thirty-one cotton yarns with different fineness and twist characteristics produced by four different spinning technologies was studied under the model of yarn strength as a summation of two independent stationary, ergodic, Markovian, and Gaussian (SEMG) stochastic processes. A special methodology was applied to measure the strength of every alternate short section – each of 50 mm length – along a yarn and the strength autocorrelation characteristics were determined. Those characteristics were found different in different yarns. Using those characteristics, computer simulations were performed to obtain the frequency distribution as well as basic statistical parameters (mean value and standard deviation) of strength of yarn specimens with different lengths (50 mm – 5000 mm). It was found that depending on the degree of strength autocorrelation, the empirical strength versus gauge length relations were different in different yarns and those relations were in a better correspondence with the actual ones as compared to those derived traditionally on the basis of strength independency. It was revealed that probably two highly different and mutually independent phenomena are acting together so as to cause yarn strength variability and those phenomena are partially related to yarn mass irregularity.



DOCTORAL THESIS



Computer Simulation of Wetting and Wicking Phenomena

Věra Soukupová

A thesis submitted in partial fulfilment of the
requirements of Technical University of Liberec
for the degree of Doctor of Philosophy

October 2004

UNIVERZITNÍ KNIHOVNA
TECHNICKÉ UNIVERZITY V LIBERCI



3146115310

KNT

TECHNICKÁ UNIVERZITA V LIBERCI
Univerzitní knihovna
Moravčická 1203, Liberec
PSČ 461 02

1597 T

1022, 515. pro
ob, Liberec.

Acknowledgments

First and foremost, I would like to express my sincere gratitude to my family, especially my parents, for their unwavering support, love, and guidance throughout my life. Their sacrifices and sacrifices have been the foundation of my success. I would also like to express my thanks to my friends and colleagues for their encouragement and assistance during my journey. Finally, I would like to thank the Department of Education for providing me with the opportunity to pursue my education and the staff and faculty of the institution.

I also want to thank Dr. Rajesh Arora for his support during the last year of my study. His guidance and advice were invaluable. I also want to thank my friends and colleagues for their support and encouragement.

Dedicated to my dearest parents

Acknowledgements

First and foremost, I would like to express sincere thanks to Prof. RNDr. David Lukas, CSc. for his valuable supervision, interest and guidance through out the research period. I would also like to express my thanks to academic staff, technicians and students of the Department of Nonwovens for providing their support in all areas related to successful completing of the thesis.

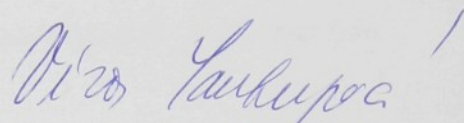
Thanks to Dr. Rajesh Anadjiwala for his support during the last period of the thesis completion at CSIR M&MTek Port Elizabeth.

I would also like to thank my friend Marlon Chetty for supporting me morally during my stay in Port Elizabeth and his help with the final formation of the thesis and language corrections.

Declaration of word of honour

I Věra Soukupová declare that this thesis has been elaborated independently with the support of mentioned literary sources.

In Port Elizabeth 23th October 2004


Věra Soukupová

Annotation

The transport and absorption of liquids play significant role in textile processes such as, dying, finishing, coating and hot-melt bonding. The structural parameters, such as, fibre fineness, fibre composition, fibre orientation, etc., influence the desired properties of the final products. The analytical description of liquid sorption and transport is very difficult due to complex shapes of pore in textile materials and complicated surface phenomena based on physical and chemical properties of polymer surfaces.

The computer technique helped the rapid development of analytical calculations, however, its main contribution was in the field of computer simulation of real phenomena by developing models of real systems and employing different statistical methods. The advantage of computer simulation is its possibility to develop an accurate model approximation of a real system and the arbitrary selection of inter-atomic and inter-molecular interactions. The model configuration and properties are easy to modify even with high variability. The computer simulation allows to examine the inside structure of the system and to evaluate the results in selected step of the simulation process.

This thesis concerns with the results of computer simulation of wetting and wicking phenomena into fibrous structures. The three dimensional lattice model and the Monte Carlo simulation methods are used for computer simulation. The several model configurations are investigated, from simple model of a liquid drop placed on horizontal surfaces to liquid penetration into complex fibrous structure. The computer simulation and experimental results are compared. The computer simulation brings interesting view about the liquid behaviour inside textile structures made of different fibre arrangement.

Anmerkung

Der Transport und die Absorption von Flüssigkeiten spielen eine bedeutende Rolle in Textilprozessen wie Färben, Veredeln, Umhüllen und „hot-melt“-Bindung. Die strukturellen Parameter wie Faserfeinheit, Faserzusammensetzung, Faserorientierung etc. beeinflussen die gewünschten Eigenschaften der Endprodukte. Die analytische Beschreibung von Flüssigkeitsabsorption und -transport ist aufgrund der komplexen Formen von Poren in Textilmaterialien und des komplizierten Oberflächenphänomens, das auf physikalischen und chemischen Eigenschaften von Polymeroberflächen beruht, sehr schwierig.

Die Computertechnik unterstützte die schnelle Entwicklung von analytischen Berechnungen, jedoch lag ihr Hauptbeitrag im Bereich der Computersimulation von Realphänomenen durch die Entwicklung von Modellen von Realsystemen und durch die Benutzung verschiedener statistischer Methoden. Der Vorteil der Computersimulation liegt in ihrer Möglichkeit eine genaue Modellannäherung an ein Realsystem und die willkürliche Auswahl von inter-atomaren and inter-molekularen Wechselwirkungen zu entwickeln. Die Modellanordnung und -eigenschaften sind einfach zu verändern, sogar mit großer Variabilität. Die Computersimulation erlaubt es, die innere Struktur des Systems zu untersuchen und die Ergebnisse in ausgewählten Schritten des Simulationsprozesses zu bewerten.

Diese Arbeit befaßt sich mit den Ergebnissen von Computersimulationen von Benetzungs- und Transport- und Absorption-Phänomen in Faserstrukturen. Das dreidimensionale Gittermodell und die Monte Carlo Simulation werden zur Computersimulation benutzt. Die verschiedenen Modellanordnungen werden untersucht, vom einfachen Modell eines flüssigen Tropfens, der auf horizontale Oberflächen gesetzt wird, bis zur Flüssigkeitseindringung in komplexe Faserstrukturen. Die Computersimulation und experimentelle Ergebnisse werden verglichen. Die Computersimulation verschafft einen interessanten Überblick über das Verhalten von Flüssigkeiten innerhalb von textilen Strukturen, die aus verschiedenen Faseranordnungen gemacht sind.

Publications

- [1] Soukupova, V.: The Complete Wetting of Fibre Truss, Textile Science, Liberec 1998.
- [2] Soukupova, V.: Absorbency Measuring on Tenziometr KRÜSS K12, Strutex, Liberec 1998.
- [3] Lukas, D., Soukupova, V.: Recent Studies of Fibrous Materials Wetting Dynamics, INDEX 99 Congress, Geneva 1999.
- [4] Soukupova, V.: Computer Simulation of Droplet Motion on Heterogenous Substrate, Textile Science For XXI. Century, Guimaraes 1999.
- [5] Soukupova, V.: Study of Sorption of Highloft Textile Fabrics, Strutex, Liberec 1999.
- [6] Adams, N., Soukupová, V.: Tendencies in Thin Fibre Bond Wetting, Strutex, Liberec 1999.
- [7] Soukupova, V., Lukas, D., Jirsak, O., Parikh, D.V.: Sorption Kinetics and Capacity of Highloft Cotton Fabrics, Beltwide Cotton Conferences, San Antonio 2000.
- [8] Lafova, Z., Soukupova, V.: Tendencies in wetting fibre bonds, Strutex, Liberec 2000.
- [9] Soukupova, V. – Sedlacek, R. – Ptacek, P.: Liquid speed measured by wetting fibre bonds, Strutex, Liberec 2001.
- [10] Saunders, T.- Mackova, I.- Soukupova, V.: Industrial Struto Applications, Beltwide Cotton Conferences, Atlanta 2002.
- [11] Soukupova, V.- Gregr, J.- Semanova, G.: Contact Angle Measurement and Surface Energy Determination, Strutex, Liberec 2002.
- [12] Soukupova, V. – Gregr, J.: Solid Surface Energy Investigation, Autex, Gdansk 2003.
- [13] Grégr, J., Soukupová, V.: Surface Energy Determination of Composites and Reinforcing Fibers, Czech-Polish workshop Testing of Composite Materials, 2003, IRSM ASCR, Praha.
- [14] Soukupova, V. – Kotasova, P.: The Simulation of Liquid Penetration into Textile Materials, Strutex, Liberec 2003.
- [15] Lukas, D., Soukupova, V., Landeryou, M.: Three-dimensional monte carlo simulation of droplet motion on heterogenous surface, In.: Wissenschaftliche abhandulgen, IX, pp. 193-196, 2003.
- [16] Soukupova, V.- Lukas, D., Roubinkova, L.: Computer Simulation of Liquid Sorption into Textile Structures, XXI Textile Technician Congress, Natal Rio Grande do Norte 2004.

CONTENTS

NOTATIONS.....	3
1. INTRODUCTION.....	6
1.1 HISTORY OF WETTING AND WICKING PHENOMENA.....	7
2. OBJECTIVES OF THE THESIS	10
3. THEORETICAL BACKGROUND.....	11
1.2 SURFACE FREE ENERGY AND SURFACE TENSION	11
3.1 WORK OF COHESION AND ADHESION	14
3.2 WETTING AND WICKING	15
3.3.1 Wetting of Solid Flat Surface.....	17
3.3.2 Wetting of Single Fibre.....	18
3.3.3 Wetting of Fibrous Assembly.....	20
3.3.4 Wicking into Single Capillary.....	21
3.3.5 Wicking into Fibrous Structure	23
3.4 LIQUID TRANSPORT THROUGH EQUIVALENT PORE RADIUS	26
4. SIMULATION MODELS AND COMPUTER SIMULATION TECHNIQUE.....	28
4.1 THE ISING MODEL AND ITS MODIFICATIONS.....	30
4.2 MODELS FOR WETTING AND WICKIN PHENOMENA SIMULATION	31
4.3 MONTE CARLO METHOD	36
4.3.1 History of Monte Carlo Method	36
4.3.2 Monte Carlo Method and Statistical Mechanics	37
5. EXPERIMENTAL WORK AND COMPUTER SIMULATION PROCESS	40
5.1 EXPERIMENTAL TECHNIQUES.....	41
5.2 THREE DIMENSIONAL LATTICE MODEL AND SIMULATION PROCESS	43
5.2.1 Three Dimensional Lattice Model.....	43
5.2.2 Computer Simulation Process	47
5.3 COMPUTER SIMULATION OF TWO PHASE SYSTEM	48
5.3.1 Thermodynamic Relations in the Sphere of Phase Interface	48
5.3.2 Two Phase System in Three Dimensional Lattice Model.....	51
5.4 WETTING OF HOMOGENEOUS SURFACE.....	54
5.4.1 Experimental Results of Contact Angle Measurement.....	55
5.4.2 Computer Simulation of Wetting Process on Homogeneous Surface	56
5.4.3 Influence of Interface Energy on Wetting of Homogeneous Surface	60
5.5 COMPUTER SIMULATION OF DROPLET MOTION ON A HETEROGENEOUS SUBSTRATE	64
5.6 COMPUTER SIMULATION OF WETTING OF SINGLE FIBRE.....	67
5.7 WETTING OF FIBROUS ASSEMBLES.....	70
5.7.1 Wetting of Assemblies from Parallel Filaments.....	70
5.7.2 Computer Simulation of Wetting of Fibrous Assemblies	74
5.8 LIQUID PENETRATION INTO FIBROUS STRUCTURES OF DIFFERENT FIBROUS ORIENTATION.....	79
5.8.1 Liquid acquisition and Liquid Distribution	79
5.8.2 Computer Simulation of Liquid Penetratin Process	82
6. DISCUSSION.....	92
7. CONCLUSION.....	96
8. REFERENCES	97
APPENDIX 1	103
APPENDIX 2	105
APPENDIX 3	110
APPENDIX 4	116

APPENDIX 5 120

APPENDIX 6 127

APPENDIX 7 136

APPENDIX 8 145

Notations

A, A_p, A_A	area, area of pore
b	fibre radius
b_c	constant
B_O	exchange energy
c	concentration
\bar{c}	mean speed of particles
C_{a0}, C_{a1}, C_{a2}	adhesion energy
C_{c1}, C_{c2}, C_{c3}	cohesion energy
C_{ij}	exchange energy
C_{aa}	exchange energy between two air cells
C_{al}	exchange energy between air cell and liquid cell
C_{as}	exchange energy between air cell and solid cell
C_g	gravitational constant
C_{ll}	exchange energy between two liquid cells
C_{ls}	exchange energy between liquid cell and solid cell
C_{ss}	exchange energy between two solid cells
d_e	effective radius of fibre
da	change of distance
$dA, \partial A$	change of area
$dF, \partial F$	change of total free energy
dF_l	change of free energy of liquid phase
dF_s	change of free energy of surface phase
dF_v	change of free energy of vapour phase
dh	change of high of liquid column
dh_v	change of distance of liquid front motion
$dn_{l1,2,\dots}$	change of number of moles of component 1,2,...in liquid phase
$dn_{s1,2,\dots}$	change of number of moles of component 1,2,...in surface phase
$dn_{v1,2,\dots}$	change of number of moles of component 1,2,...in vapour phase
dp, dP	change of pressure, pressure drop
dP_l	change of pressure in liquid phase
dP_v	change of pressure in vapour phase
dr	change of radius of liquid drop
dt	change of time
$dT, \partial T$	change of temperature
dV	change of volume
dV_d	change of drop volume
dW_A	change of surface free energy
dz	difference of
D	diffusion coefficient
e	thickness of liquid film
E	radius of liquid body
E_n	energy of system
E_i, E_1, E_2	energy of cell/cells
f	density of Helmholtz energy
$f_{1,2,3}$	constants
F	Ising variable
F_S, F_l, F_v	Helmholtz energy
F_t	total free energy
F_A	force
F_l	free energy of liquid phase
F_s	free energy of surface phase
F_v	free energy of vapour phase
g	acceleration of gravitational field
G	Gibbs energy
h, h_d	length of liquid column, high of liquid drop
$H, H(xi), H(xi+1)$	Hamiltonian, Hamiltonian of system in configuration xi, xi+1 respectively
H_a, H_c, H_g	adhesion energy, cohesion energy, gravitational energy
J	velocity

k, l	coefficient
k_B	Boltzman constant
K	permeability
K_c	coefficient
l, L	length
m	number of configurations
M	intensity of magnetic field
m_b	body mass
MC	Monte Carlo
M_w	molar weight
n, n_m	number of fibres, number of moles
n_f	number of fibres in assemble
n_l, n_v	number of moles in liquid phase, air phase
N, n	number of cells in system
N_{ac}	number of adsorption sites occupied
N_{av}	number of adsorption sites available
N_m	number of magnetic moments
p, p_1, p_2	pressure
P_l	pressure of liquid phase
P_{TR}	probability of transition
P_v	pressure of vapour phase
$P_{(xi)}, P_{(xi+1)}$	probability of system in configuration $xi, xi+1$
PET	polyethylene terephthlate
PP	polypropylene
Q	liquid flow
r	radius of liquid drop
r_c	radius of capillary
r_e	equivalent pore radius
$r_{1,2}$	radii of curvature
R	gas constant
s	area
S	Ising variable
S_e	total entropy
S_c	Harkinson spreading coefficient
S_l	entropy of liquid phase
S_s	entropy of surface phase
S_v	entropy of vapour phase
ST	simulation time
t	finesses of fibre
T	temperature
T_l	thickness
U_{ij}	exchange energy
V	volume
V_d	volume of liquid drop
V_l	volume of liquid phase
V_v	volume of vapour phase
W_A	surface free energy
W_a	work of adhesion
W_c	work of cohesion
W_l	energy of liquid surface
W_s	energy of solid surface
W_{sl}	energy of solid – liquid interface
$W(xi \rightarrow xi+1)$	transition probability
$W(xi+1 \rightarrow xi)$	transition probability
$xi, xi+1$	configurations of system
y_i	vertical co-ordinate in two dimensional lattice
z_i	vertical co-ordinate in three dimensional lattice
Z	particular function
α	orientation of magnetic moment in magnetic field
β	angle of capillary incline

δ_i	Dirac function
ΔE	difference of energy
ΔH	difference of energy
$\Delta p, \Delta P$	pressure drop
ΔP_v	vapor pressure drop
γ	surface tension
γ_l	liquid surface tension
γ_s	solid surface tension
γ_{sl}	solid – liquid interface tension
γ_0	liquid surface tension for 0°C
γ_1	surface tension of liquid 1
γ_2	surface tension of liquid 2
$\gamma_{1,2}$	interface tension of liquid 1 and liquid 2 interface
η	viscosity of liquid
λ	distance
μ	elementary magnetic charge
μ_p	chemical potential
$\mu_{l,1,2,\dots}$	chemical potential of component 1,2,... in liquid phase
$\mu_{s,1,2,\dots}$	chemical potential of component 1,2,... in surface phase
$\mu_{v,1,2,\dots}$	chemical potential of component 1,2,... in vapour phase
π	Ludolfovo cislo
$\theta, \theta_1, \theta_2$	contact angle
ρ	density of liquid
σ, σ_{ij}	Ising variable
Θ	surface coverage
$d\mu_{l,1,2,\dots}$	change of chemical potential of component 1,2,... in liquid phase
$d\mu_{s,1,2,\dots}$	change of chemical potential of component 1,2,... in surface phase
$d\mu_{v,1,2,\dots}$	change of chemical potential of component 1,2,... in vapour phase
$d\Theta$	change of surface coverage
∂G	difference of Gibbs energy
∂N	difference of number of mols
∂V	difference of volume
2D	two-dimensional
3D	three-dimensional

1. INTRODUCTION

Textile materials are important part of human live from ancient times. They are used as technical textiles in industrial applications, as household textiles to improve comfort of living environment, and cloth to guarantee the comfort of human body in environmental conditions.

The important applications for using textiles fabrics are absorption materials, cleaning textiles, filters, materials used for liquid transport, etc. The demands depend upon quality characteristics, like absorption, wetting, liquid transport properties, etc. These mentioned qualities are important in some technical processes, like printing, coating, chemical finishing, production of composite materials, preparation of hair and cosmetics products, etc.

Frequently used nonwoven products are mainly disposable or short term used products. The evolution for designing of these products using nonwoven technologies started from sixties of the 20th century, and the main reason was their lower production costs in comparison with traditional textile processes, like weaving and knitting. The result is the wide range of nonwoven structures used today in medical and hygiene textiles, cleaning textiles, drainage materials, insulation materials and barrier layers, filters, etc. The highest increase of nonwoven production in 1994-1998 was recorded in the sector of disposable cleaning textiles 28% (swabs, rubbers, wipes, towels) and disposable hygiene products 15% (baby diapers, feminine hygiene products, diapers for persons with incontinence defect) [1]. The nonwovens used in hygiene products achieved the highest range of 34.7 % from total nonwoven production in the end of 20th century. Hand in hand with increasing demands of customers it is necessary to design new and more comfortable products of very high quality. With this evolution, development of technologies in the nonwoven production and development of new produced materials is required.

The mutual behaviour of liquids and fibre structures is often used in praxis, but still not a lot is dedicated today. Several testing methods exists to describe absorption and transport properties of textiles [2, 3], some measuring equipment exists [4, 5, 6] to evaluate behaviour of different materials and structures, but none of these techniques gives any evidence of fundamental knowledge about the phenomena present in the processes.

1.1 History of Wetting and Wicking Phenomena

It is necessary to delve more into history to find works dealing with the theoretical description of the phenomena when a liquid is in contact with a single fibre, a fibre bundle or a fibre layer.

Goren described in 1963 [7] the break-up of liquid cylindrical body around a cylindrical wire into identical liquid drops periodically distributed on the wire. He derived the theory for liquid drop shape expression using the dependency of liquid shape regular amplitudes on the constant distance between drops.

Roe [8] presented more detail work about the liquid film instability on a wire. He solved the hydrodynamic equations to obtain the rate of growth of the film disturbance and the wavelength of the most rapidly growing disturbance. The influence of liquid viscosity was also studied, the thickness of the film and the influence of wire radius on the film disturbance were studied.

Brochard [9] studied the spreading of a liquid on a thin solid cylinder caused by the effect of attractive Van der Waals forces and Laplace pressure. The critical spreading coefficient is calculated from the energy balance of the liquid – solid system.

Mc Hale [10] considered the theoretical profile of a barrel droplet approximately spherical in its cross section on a high - energy cylindrical solid surface. It was calculated that the level to which the decreasing of the fibre radius changes the surface energy as well as the maximum slope of the drop profile.

It is very difficult to measure the contact angle on system drop – fibre. Song [11] developed the drop length – height method for the determination of a contact angle in the drop-on-fibre system to describe the quality of wetting.

Recently, some experimental works dealing with measuring of quality of the wetting of fibres were achieved. Barsberg [12] examined useful information on plant fibre surfaces from wetting experiments such a dynamic contact angle measurement by the Wilhelmy Technique and the Lifshitz – Van der Waals acid- base theory for theoretical data processing.

Wei [13] used modern technique for direct contact angle measurement of a barrel liquid drop shape on cylindrical fibres.

So far, there is only one theoretical work that describes the spreading condition for bundle of fibres. The theoretical background is adapted from [9]. Lukas [14] expressed the critical spreading coefficient for a liquid volume placed on a fibre bundle.

Several authors dealt in detail with the principles related to mutual behaviour between liquids and complex fibre structures.

Barci and Brochard – Wyart studied liquid droplet penetration into a porous media [15]. They observed two different regimes of small spherical liquid droplets penetration into porous structure, a locked regime and unlocked regime. As well as three regimes of liquid flat puddles penetration into porous structure – gravitational locked, gravitational unlocked regimes and unlocked regime. All the results are interpreted assuming a quasi-equilibrium shape for drops and Darcy Law for suction.

Starov presented in the contribution [16] an attempt to use Brinkman's equation for investigation of the spreading of liquid drops over thin porous substrates filled with the same liquid.

The phenomena of liquid drop is spread over a dry porous layer is presented in the Starov's next paper [17]. The problem is treated under the lubrication theory approximation and in the case of complete wetting.

Holman and col. observed simultaneous spreading and infiltration process of inject – printed droplets into high green density porous ceramic beds [18]. They use the dependency of the droplet radius on time through the process for spreading kinetics description, and Washburn equation to determine the differential liquid volume drawn into material.

Martic characterised a porous media by dynamic contact angle and this solution was used in the modification of Lucas – Washburn equation [19].

The rapid progress of computer technology brought new approaches into all aspects of science – the complicated numerical solution of problems or computer simulation of arbitrary phenomena. Different numerical and computer modelling are used for liquid – solid systems behaviour simulation.

Marmur [20] investigated an oscillatory dependence of the highest and lowest possible contact angles on the simple two - dimensional model of a cylindrical drop placed on periodically heterogeneous smooth solid surface. By the simple model emerged successful experimental results about the fundamental knowledge, that the drop volume influences the contact angle hysteresis.

Brandon and Marmur presented in the paper [21] the same model for investigation of changes in free energy, discontinuous changes of contact angle, etc. The simulated contact

angle hysteresis, including discontinuous changes in the contact angle, and the drop size of the drop base are very similar to experimental observation. The dependence of advancing and receding contact angles on the energy available for overcoming energy barriers was illustrated.

The next paper of these authors [22] brought three – dimensional liquid drop model on the heterogeneous solid surface. The drop shape changes are influenced by incremental changes in volume.

Lukas and Pan [14] studied the spreading of non-volatile liquid drop on a homogeneous solid substrate of a fibre shape using three – dimensional Ising model. This simulation process demonstrated the droplet spreading along a fibre and the model critical wetting condition was discovered.

Schwartz [23] introduced a method for calculation of simulated time – dependent three – dimensional motion of liquid droplets on solid surface. The evaluation of the equation is presented using lubrication approximation including viscose, capillary, disjoining and gravitational forces. The results of simulation correspond to experimental behaviour of real systems.

Zhong [24] used the variant of two-dimensional modification of Ising model, for simulating liquid wicking into fibre material.

Valery Roy and col. [25] presented the lubrication model of dynamics for coating film over a curved substrate. The model includes the effects of curvature and gravity. The numerical simulation exhibits some features like dynamics of thin liquid films on substrate with complex curvature.

In the next paper, Schwartz [26] worked with the same mathematical model [23], and used its modification in simulation of Non - Newtonian Shear – thinning liquid coating on a planar substrate. The simulation results are compared with experimental observation of the drainage flow out in a vertical substrate.

Flow of a liquid droplet over a flat plane and a spherical pellet was studied by Gunjal and col [27]. Drop spreading and recoiling velocities were reconstructed from the experimental data. A computational fluid dynamic model based on the volume of fluid method was used to simulate drop dynamics on the surfaces. Surface tension and wall adhesion are included in the model.

Samsonov and group [28] simulated simple and polymer nanosize droplet spreading over heterogeneous solid substrates on the basis of isothermal molecular dynamics.

2. OBJECTIVES OF THE THESIS

The dissertation thesis is concerned with the problematic of wetting and wicking phenomena present in situations when liquid and fibre structure come into a contact. The objective of the thesis is to establish computer simulation as a tool of investigation for the mentioned phenomena. There are two aspects for the computer simulation process. Firstly, it is composition of a model for a system of three components – solid, liquid and air, which is similar to a real system (a liquid drop on a heterogeneous solid flat surface, a liquid in contact with a textile fibre, a liquid in contact with a textile structure, etc.). Secondly, it is the setting of simulation process variables consistent with wetting and wicking phenomena in real systems known from experimental measurement.

Chapter 3 describes theoretical background of the thesis and contains analytical descriptions of phenomena influencing wetting and wicking processes.

Chapter 4 is dedicated to tools used for computer simulating, like Ising model, Monte Carlo kinetics and statistical thermodynamics.

Chapter 5 presents the three dimensional lattice model used for computer simulations in the thesis, reviewed results of experimental work as mutual behaviour of liquids in contact with diverse fibre structures, on evaluation of their wetting characteristics using presented theoretical principles. The ability the model to be used for simulation of wetting processes and absorption phenomena in fibre systems and nonwoven structures is shown.

Chapter 6 discusses the results and advantages of computer simulation approach. The computer simulation makes possible to evaluate the processes in arbitrary simulation step and allows find out characteristics, which are not available using recent measuring technique on real systems. The benefit of the model is easy change of any parameter. The simulation allows observe the influence of this change on the system behaviour. These attributes lead to prediction of the real system behaviour after concrete parameter changes or environmental factor changes.

3. THEORETICAL BACKGROUND

The wetting and absorption phenomena mainly depend on properties of solids and liquids. The type of material, size and geometry of surface and surface energy are considered for solids. The main quantities of liquids causing the phenomena are surface tension, density and viscosity.

1.2 Surface Free Energy and Surface Tension

Any system, containing two phases, an interfacial region exists. The thickness of the interfacial region is not exactly determined but includes those parts of the system that are influenced by surface forces. The two phase system consists of two bulk phases (liquid and vapour) which are separated by a surface phase. Although the surface phase is not the true phase in physical sense, the physical description is used for the expression of the total free energy of the system [29]

$$F_t = F_l + F_v + F_s, \quad (3.1.1)$$

where subscript l refers to liquid bulk phase, subscript v to vapour bulk phase and s to the surface phase. The calculation of bulk phases free energies follow the assumption that they both remain homogeneous right up to a hypothetical geometric surface. In the case of small, reversible change occurs in the system, the free energy change is expressed

$$dF_t = dF_l + dF_v + dF_s. \quad (3.1.2)$$

For bulk phases the free energy changes are expressed by

$$dF_l = -S_l \cdot dT + V_l \cdot dP_l + \mu_{l1} \cdot dn_{l1} + \mu_{l2} \cdot dn_{l2} + \dots \quad (3.1.3a)$$

$$dF_v = -S_v \cdot dT + V_v \cdot dP_v + \mu_{v1} \cdot dn_{v1} + \mu_{v2} \cdot dn_{v2} + \dots \quad (3.1.3b)$$

where $S_{l,v}$ is entropy, T is temperature, $V_{l,v}$ is volume and $P_{l,v}$ is pressure. The notation n_i refers to the number of moles relevant to component 1, 2, ... with chemical potentials μ_1, μ_2, \dots

The term of work used to increase surface area of an infinitesimal amount dA is included into change of surface free energy dW_A . The work of surface expansion is done against surface tension γ .

In the case of liquid surface tension γ is defined as a force F_A acting perpendicular to the length of surface L . The vector of the force lies in a tangent plane to the surface in the

point of the cross section. Maxwell [30] described the liquid surface tension acting on the soap film stretched over frame with one movable arm, as shown in Figure 3.1.1. The surface tension γ is acting on the two surfaces along the arm of length L against the force F_A .

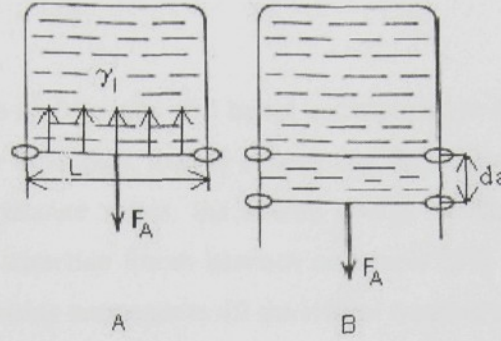


Figure 3.1.1: Maxwell approach to define liquid surface tension γ .

$$\gamma_l = \frac{F_A}{2 \cdot L}. \quad (3.1.4)$$

The surface tension γ can be defined too as a work dW_A necessary to move the frame arm L about the infinitesimal distance da

$$\gamma_l = \frac{dW_A}{dA}, \quad (3.1.5)$$

where $dA = 2L \cdot da$ is the surface area addition.

Since the surface contribution to the whole volume is negligible, the quantity of $V \cdot dP$ can be omitted. For arbitrary surface with surface tension γ , for surface free energy change applies [29]

$$dF_s = -S_s \cdot dT + \gamma \cdot dA + \mu_{s1} \cdot dn_{s1} + \mu_{s2} \cdot dn_{s2} + \dots \quad (3.1.6)$$

where μ_{s1} , μ_{s2} , ... are chemical potentials of the various components of the system. The total free energy change is the sum of 3.1.3a, 3.1.3b and 3.1.6

$$dF = -S_e \cdot dT + V_l \cdot dP_l + V_v \cdot dP_v + \gamma \cdot dA + \sum \mu_{li} \cdot dn_{li} + \sum \mu_{vi} \cdot dn_{vi} + \sum \mu_s \cdot dn_{si},$$

(3.1.7)

where $S_e = S_l + S_v + S_s$ is the total entropy of system. In the special case at constant temperature, pressure and composition from (3.1.7) is transformed to

$$dF = \gamma \cdot dA \quad \text{or} \quad \gamma = \left(\frac{\partial F}{\partial A} \right)_{T, P, n_m} = F_s. \quad (3.1.8)$$

The Equations 3.1.8 express fundamental relation of surface chemistry [29].

The entropy S_e of any system at constant pressure, surface area and composition is

$$-S_e = \left(\frac{\partial F}{\partial T} \right)_{P, A, n_m}. \quad (3.1.9)$$

The work to increase the surface area of a liquid is consumed to bring additional molecules from the interior volume to surface, then to overcoming the attraction forces of surrounding molecules. As the temperature raises, the kinetic energy of the molecule increases and partially overcomes the attraction forces between molecules [29]. Consequently the surface tension decreases with raising temperature till the critical temperature of the liquid is reached and the surface tension diminishes and finally disappears. There are numbers of equations relating the liquid surface tension γ_l to temperature T , Ramsay and Shield equation [31], McLeod's experimental equation [32], etc. One of simplest equations is

$$\gamma_l = \gamma_0 \cdot (1 - b_c \cdot T), \quad (3.1.10)$$

where γ_0 is surface tension for $T=0^\circ\text{C}$ and b_c is a constant [29].

An increase in the pressure of vapour over a liquid surface has an effect to bring more vapour molecules into contact with liquid surface and cause higher pressure onto the liquid surface. The attraction of these molecules neutralized some extent of internal molecules attraction. Consequently, the surface tension decreases with increasing pressure [29].

The influence of surface curvature is shown on a liquid drop. In the absence of external fields influence, a liquid drop is spherical. The surface free energy is $4\pi r^2 \gamma_l$, where r is the drop radius. If the radius increases by dr , the free energy change increases by $8\pi r \gamma_l \cdot dr$. The lower radius, the lower the surface free energy of the drop is. The natural tendency of the drop is to shrink and decrease its energy. The balance state of the drop is caused by a pressure difference ΔP across the drop surface. The decrease in surface free energy is in balance with the work against the pressure difference

$$\Delta P 4\pi r^2 \cdot dr = 8\pi r \gamma_l \cdot dr \quad \text{or} \quad \Delta P = 2 \frac{\gamma_l}{r}. \quad (3.1.11)$$

The smaller the drop is, the higher pressure is inside, compared to outside. The Equation (3.1.11) describes spherical drop. In the case of curved, the surface is characterized by two radii of curvature r_1 and r_2 , the pressure difference across the surface is given by Young and Laplace equation

$$\Delta P = \gamma_l \left(\frac{1}{r_1} + \frac{1}{r_2} \right). \quad (3.1.12)$$

There is no pressure difference across the flat surface, due to ΔP equal to 0.

The increase of vapour pressure ΔP_v over spherical liquid drop of radius r in comparison with the vapour pressure P_v over flat liquid surface is

$$RT \cdot \ln \left(1 + \frac{\Delta P_v}{P_v} \right) = 2\gamma_l \frac{M_w}{r\rho}, \quad (3.1.13)$$

where M_w is the molecular weight, ρ is the liquid density, γ_l is the liquid surface tension.

3.1 Work of Cohesion and Adhesion

The work of cohesion was defined by Harkins [33]. The situation, when two equal liquid volumes exist separately is shown in Figure 3.2.1A. After they come into a contact, the two liquid surfaces disappear, as shown Figure 3.2.1B. The total free energy of system (3.1.7) is cut by the two surface free energies $2\gamma_l$ and it is called work of cohesion W_c

$$W_c = 2 \cdot \gamma_l. \quad (3.2.1)$$

It also can be defined as a work necessary to exert two liquid surfaces from homogeneous phase.

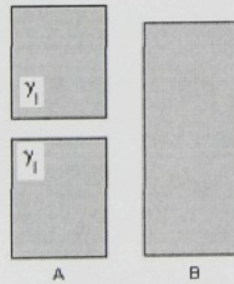


Figure 3.2.1: A - two separated liquid volumes, B - after contact, the free surfaces disappeared.

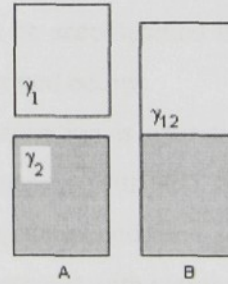


Figure 3.2.2: A - two separated volumes of two liquids, B - after contact a liquid interface arised.

In the case when surface of different liquid 1 and 2 come into a contact, the two individual surfaces disappear and the interface of to liquids is arises, as shown in Figure 3.2.2.

The work of adhesion is equal to the change in surface free energy of separate liquid surfaces γ_1 and γ_2 , and liquid interface γ_{12}

$$W_a = \gamma_1 + \gamma_2 - \gamma_{12}. \quad (3.2.2)$$

The comparison between work of cohesion and work of adhesion gives an indication of the relative attraction between molecules of one liquid 1, and between molecules of the liquid 1 and liquid 2.

3.2 Wetting and Wicking

The interaction of liquids with textile materials may involve several fundamental physical phenomena: wetting of fibre surface, transport of the liquid into assembly of fibres, adsorption on the fibre surface or diffusion of the liquid into the interior of the fibres [34]. Wetting and wicking are not different processes. Wetting is a prerequisite for wicking. A liquid that does not wet fibres can not wick into a fabric. If the fibres in assemble with capillary spaces between fibres are wetted by a liquid, the resulting capillary forces drive the liquid into the capillary spaces in wicking process.

Harnet and Metha distinguished wettability and wickability [35]. The wettability was defined as behaviour between liquid and solid surface and describes the interaction between liquid and substrate prior to wicking taking place. The wickability was defined as an ability to sustain a capillary flow.

In real textile processing, the wicking process can be accompanied by other physical phenomena which is divided into four categories [34] described below:

- I. Wicking of a liquid – only capillary penetration is operating, no diffusion into fibre surface, e.g. hydrocarbon oil in contact with PET fabric.
- II. Wicking accompanied by diffusion – capillary penetration and diffusion into fibres surface are operating, e.g. water in contact with cotton fabric.
- III. Wicking accompanied by adsorption on fibres – capillary penetration and adsorption on fibres are operating, e.g. aqueous surfactant solution in contact with PET fabric.
- IV. Wicking involving adsorption and diffusion into fibres - capillary penetration and diffusion into fibres surface and adsorption on fibres are operating, e.g. an aqueous surfactant solution in contact with cotton fabric.

Diffusion

Diffusion is a transport of particles caused by different concentration of particles in two phases in a contact. The particles (in gases or liquids or solids) diffuse down a concentration gradient until the composition is uniform [36]. The diffusion is characterised by diffusion coefficient D

$$D = \frac{1}{3} \cdot \lambda \cdot \bar{c}, \quad (3.3.1)$$

where λ is distance of transport and \bar{c} is a mean speed of particles.

Adsorption at surfaces

The accumulation of particles at a surface is called adsorption [36]. The substance that adsorbs is called adsorbate; the underlying material is called adsorbent or substrate. The adsorption is characterised by adsorption rate defined as the rate of change of surface coverage $d\Theta$ in time dt .

$$\text{The rate of adsorption} = \frac{d\Theta}{dt},$$

where surface (fractional) coverage is defined

$$\Theta = \frac{N_{ac}}{N_{av}}, \quad (3.3.2)$$

where N_{ac} is the number of adsorption sites occupied and N_{av} is number of adsorption sites available.

Molecules or atoms can stick to surface in two ways. In physisorption, Van der Waals interactions (dispersion or polar interaction) act between adsorbate and substrate. These are a long range but weak interactions and the energy released when the particle is physisorbed. This energy can be absorbed as vibrations of the surface lattice or dissipated as heat, and a particle bouncing across the surface will gradually lose its energy and finally stick to it [36].

In chemisorption, the particles stick to the surface by forming chemical (covalent) bonds, and tend to find sites that maximize their coordination number with the substrate [36]. A chemisorbed molecule can be torn apart at the demand of the unsatisfied valences of the surface atoms. Chemisorption is exothermic process.

3.3.1 Wetting of Solid Flat Surface

Wetting is the displacement of solid – air interface with a solid – liquid interface. Spontaneous wetting is the migration of a liquid over a solid surface toward thermodynamic equilibrium. Forced wetting, involves external hydrodynamics or mechanical forces to increase the solid – liquid interface beyond static equilibrium [34].

The surface energy of solid depends on a character of the solids [37]. The kind of interactions plays important role (covalent or ion or metal interactions), or molecular crystals bonded by Van der Waals forces or by hydrogen bonds. Two kinds of surfaces are distinguished, these are low and high energy surfaces.

The surface energy of both solid and surface energy of liquid, influence the quality of wetting of solid surface by liquid. Three regimes are possible when a finite liquid volume is placed on a flat solid surface, shown in Figure 3.3.1. Indicator of the wetting quality is contact angle θ measured when the solid – liquid – air system is in a stable stay. The contact angle is the angle between the tangent to liquid – air interface and liquid - solid interface [34]. It is formed at the contact line, which is the region where three interfaces (solid – air, solid – liquid and liquid - air) intersect.

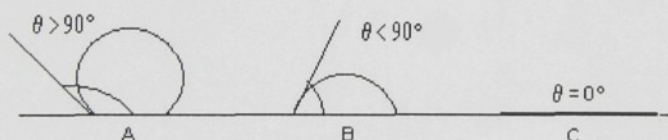


Figure 3.3.1: A - the liquid does not wet solid surface; B - the liquid does wet solid surface; C - the liquid film is spread over solid surface in the case of complete wetting.

When the contact angle θ is higher than 90° , the liquid does not wet the solid flat surface, as shown in Figure 3.3.1A. When contact angle θ is lower than 90° , the liquid wets the solid flat surface, shown in Figure 3.3.1B. The case when liquid drop is spread into a liquid film over a solid flat surface is called complete wetting and contact angle θ is equal to 0, as shown in Figure 3.3.1C.

The basic description of flat homogeneous solid surface wetting by liquid was brought independently by Young and Dupre [38]. The stable stay of solid – liquid – air system, as shown in Figure 3.3.2, is qualified by equilibrium of interface energies of these three phases Young equation

$$\gamma_s - \gamma_{sl} - \gamma_l \cdot \cos \theta = 0, \quad (3.3.3)$$

where γ_s is solid surface energy, γ_{sl} is solid-liquid interface energy, γ_l is liquid surface tension and θ is contact angle between solid –liquid interface and the tangent to liquid surface at the contact lih. The term $\gamma_l \cos \theta$ has been called “adhesion tension” or “specific wettability” [39,40,41].

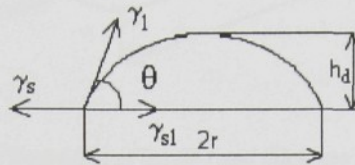


Figure 3.3.2: A liquid drop in the stable stay on a homogeneous solid flat surface in incomplete wetting regime. .

The condition of complete wetting expressed by Harkinson spreading coefficient S_c means [42], that the complete wetting applies when the solid surface energy is equal or higher than the sum of interface tension γ_{sl} and liquid tension factor $\gamma_l \cos \theta$, when $\cos \theta = 1$.

$$S_c = \gamma_s - \gamma_{sl} - \gamma_l \geq 0. \quad (3.3.4)$$

3.3.2 Wetting of Single Fibre

Wetting of fibre is a displacement of fibre – air interface with fibre – liquid interface [43,44].

The different surface shape of a single fibre from a flat surface causes that the wetting of single fibre is controlled by different rules than wetting of flat solid surfaces. Brochard [45] derived the critical spreading coefficient S_c for fibre complete wetting transition. The complete wetting of a single fibre is achieved when the equilibrium of surface energies is realized on the system, when a cylindrical fibre is covered by a thin cylindrical liquid film, as shown in Figure 3.3.3. The fibre has radius b , the liquid film has the thickness e and length l .

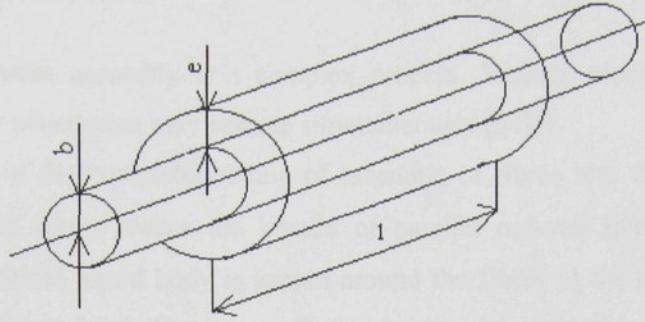


Figure 3.3.3: The scheme of liquid film of length l and thickness e covering a single fibre of the radius b .

According to surface tension definition (3.1.5) Brochard [45] expressed the solid surface energy W_s , solid – liquid interface energy W_{sl} and the liquid surface energy W_l . The system is in stable stay if condition for complete wetting is valid

$$W_s - W_{sl} - W_l \geq 0. \quad (3.3.5)$$

The surface is circular, than the length of acting surface tension is expressed as fibre cross section circumference or liquid cylindrical body cross section circumference

$$2\pi \cdot b \cdot l \cdot \gamma_s - 2\pi \cdot b \cdot l \cdot \gamma_{sl} - 2\pi \cdot (b + e) \cdot l \cdot \gamma_l \geq 0. \quad (3.3.6)$$

After rearrangement of (3.3.4) into (3.3.6) is possible to express the complete wetting condition using the Harkinson spreading coefficient

$$S_c \geq \frac{e}{b} \cdot \gamma_l. \quad (3.3.7)$$

The condition of complete wetting depends only on the geometrical parameters of fibre and liquid body, and on the liquid surface tension. The values of all quantities in (3.3.7) are higher than zero that means that it will always exists a number on the right side of the equation (3.3.7) higher than zero. The conclusion arises from comparison of (3.3.4) and (3.3.7). If the flat surface is wetted by concrete liquid, the single fibre could not discharge condition of complete wetting [45].

The condition (3.3.7) is valid only for liquid films of very low thickness [45]. The liquid films of macroscopic thickness were studied by Rayleigh [46] and Quéré [47]. Both discovered some dependencies in the instability of the thick liquid films over the cylindrical bodies.

3.3.3 Wetting of Fibrous Assembly

Wetting of fibrous assembly is a complex process. Various mechanisms such as immersion or capillary penetration may operate simultaneously [34].

The condition of the complete wetting of assembly of fibres was derived by Lukas [48]. The assembly of fibres means the bundle of parallel ordered fibres in horizontal orientation. The cylindrical liquid body is spread around the fibres in the case of complete wetting, as shown in Figure 3.3.4. There are n fibres of radius b in assembly. The liquid body has radius E and length l .

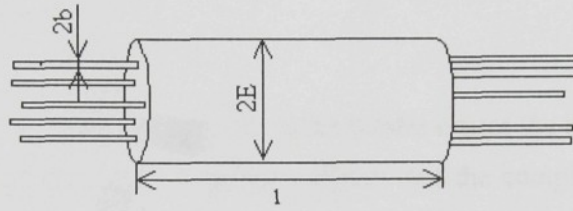


Figure 3.3.4: The fibrous assembly with $n=5$ fibres of radius b . The liquid body has radius E and length l .

The equilibrium (3.3.5) is valid for complete wetting of fibrous assembly. The surface energies have different expression. The solid surface energy W_s is a sum of surface energies of n single fibres in the assembly. The same holds for the solid-liquid interface energy W_{sl} . If the energies are included into (3.3.5), the condition for complete wetting of fibre bundle is expressed

$$n \cdot 2\pi \cdot b \cdot l \cdot \gamma_s - n \cdot 2\pi \cdot b \cdot l \cdot \gamma_{sl} - 2\pi \cdot E \cdot l \cdot \gamma_l \geq 0. \quad (3.3.8)$$

After rearrangement of (3.3.4) into (3.3.8), it is possible to use Harkinson spreading coefficient for complete wetting condition

$$S_c \geq \frac{E - n \cdot b}{n \cdot b} \gamma_l. \quad (3.3.9)$$

As in the case of single fibre complete wetting, the condition (3.3.9) depends on geometrical parameters of fibres and liquid body, the number of fibres, and the liquid surface tension.

From a special ideal case of fibre arrangement ensues a principle conclusion. There are seven fibres of radius b as close as possible arranged in the bundle in the Figure 3.3.5. The cylindrical liquid body surrounds the bundle and the radius of the bundle is $E = 3b$.

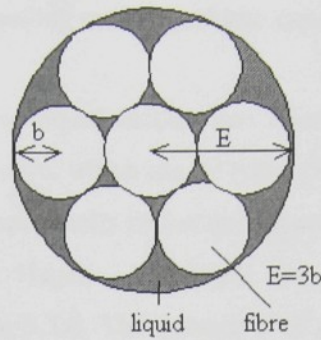


Figure 3.3.5: Seven fibres of radius b in the bundle. The liquid body has the radius E .

This is instituted into (3.3.9) and then

$$S_c \geq -\frac{4}{7} \cdot \gamma_l. \quad (3.3.10)$$

This very simplified case of fibres arrangement in the bundle causes the negative value of the Harkinson spreading coefficient. It is possible to expect that the complete wetting of fibre assemble occurs, although the complete wetting condition was not reached for flat surface from the equal material and for equal liquid. This conclusion predicts the better wetting properties of fibre structures than solid materials.

The more detail work dealing with liquid body shapes on fibre assemblies were done by Princen [49,50].

3.3.4 Wicking into Single Capillary

Transport of liquid into a fibrous assembly, or into textile fabric, can be caused by external forces or by capillary forces only [34]. A spontaneous transport of liquid driven into porous system by capillary forces is termed as wicking. Due to capillary forces are caused by wetting, wicking is a result of spontaneous wetting in a capillary system. For theoretical description of capillary flow into a fibrous assembly is usually considered to consist of a number of parallel capillaries [51]. The advancement of liquid front into the capillaries is occurred in small jumps. The ability of liquid to wet the capillary wall (represented by liquid surface tension), and the circular cross section of capillary, causes reformation of liquid surface into the meniscus. The advancing wetting line in a single capillary stretches the meniscus of the liquid surface until the elasticity of meniscus and the inertia of flow are

exceeded. The meniscus contracts pulling more liquid into capillary to restore the equilibrium state of meniscus.

The theoretical description of liquid suction into fibre material was reduced on the wicking of a liquid into linear tube pore, which can be represented by a capillary. The theory of liquid motion was developed independently by Lucas [52] and Washburn [53].

The theory comes out the Hagen – Poiseuille law [54] of liquid flow through cylindrical tube, as shown in Figure 3.3.6. The volume V of a viscose Newtonian liquid of viscosity η passes the length h in the tube of the radius r_c during the time t . The pressure difference on the ends of length h is $(p_1 - p_2)$.

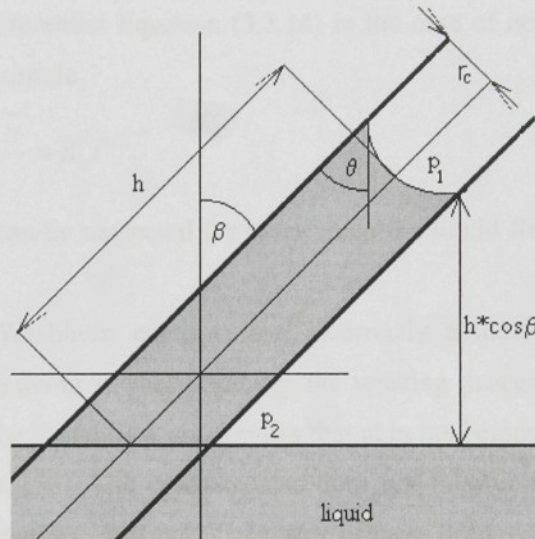


Figure 3.3.6: The liquid flow in a capillary. The pressure p_1 is under the curved liquid surface and pressure p_2 is on the liquid level.

It is possible to express the liquid flow dV/dt through the tube

$$\frac{dV}{dt} = \frac{\pi(p_1 - p_2)r_c^4}{8h\eta}. \quad (3.3.11)$$

The curved liquid surface causes the pressure p_1 . The tangent line of the liquid meniscus in the capillary contains with the capillary wall angle θ measured at the point of three-phase line, as shown in Figure 3.3.6. The p_1 is so called Laplace pressure (described in Chapter 3.1)

$$p_1 = \frac{2\gamma_l \cos \theta}{r_c}. \quad (3.3.12)$$

The pressure p_2 corresponds with the hydrostatic pressure on the liquid level in the vicinity of capillary, as shown in Figure 3.3.6,

$$p_2 = \rho g h \cos \beta, \quad (3.3.13)$$

where ρ is liquid density, g is acceleration of gravitational field and h is the length of liquid body inside the capillary. The angle β is the angle between the normal line to liquid level and capillary axis.

The speed of liquid suction into the capillary was derived and is expressed as a change of liquid column high in capillary dh in time interval dt .

$$\frac{dh}{dt} = \frac{r_c \gamma_l \cos \theta}{4\eta h} - \frac{r_c^2 \rho g \cos \beta}{8\eta}. \quad (3.3.14)$$

The solution of the Differential Equation (3.3.14) in the case of neglecting the gravitational field influence is quite simple

$$h = \sqrt{\frac{r_c \gamma_l \cos \theta \cdot t}{2\eta}} \equiv K_c t^{1/2}. \quad (3.3.15)$$

The gravity influence can be neglected for cases when the liquid flow in horizontal capillary or tube is investigated.

The Lucas – Washburn equation has incorrectly assume the constant advancing contact angle of the moving meniscus during the wicking process [55], does not take in account the inertia of the liquid flow and implies that at in the beginning of wicking process is the liquid flow infinite [56]. The equation also does not involve swelling of fibres, which influence reducing of capillary spaces [57]. In spite of these limitations, the Lucas - Washburn Equation (3.3.15) has been successfully used for description of wicking of a variety of liquid kinetics [58, 59, 60, 61].

3.3.5 Wicking into Fibrous Structure

The theoretical description of fluid transport through porous media gives Darcy's law [62]. The fluid flow Q passes through a porous structure of area A and thickness T_l . The viscosity of fluid is η . The pressure difference which the porous layer causes in fluid flow is characterised by pressure drop Δp , as shown in Figure 3.3.7.

$$Q = \frac{K}{\eta} A \frac{\Delta p}{T_l}. \quad (3.3.16)$$

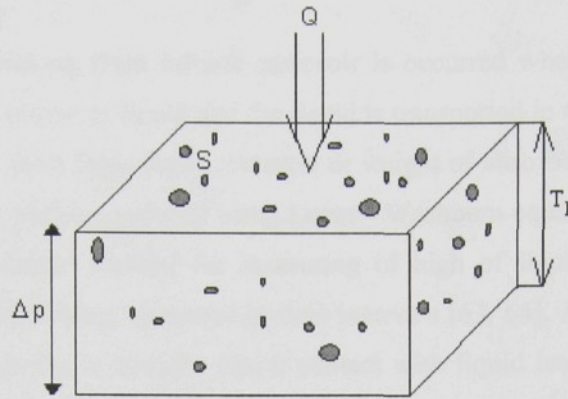


Figure 3.3.7: The liquid flow Q through porous structure driven by Darcy's law.

The permeability K in Darcy's law (3.3.16) is the characteristic parameter of porous structures in contact with fluid flow. Permeability is important parameter for structures used in air and liquid filtration area and as breathable materials. The different textile production processes include different ways of wicking.

Immersion into Infinite Reservoir

Textile treatments like sizing, dyeing, dispersion or other finishing agents treating applications, processed on foulard are based on complete immersion of a fabric into a liquid phase. The liquid enters the fabric from all directions [63]. The speed of suction and amount of sucked liquid are important parameters. A fabric specimen sinking time into a liquid can be measured evaluated as absorption time using several standard methods [64, 65, 66]. The sinking time is related to advancing contact angle or the dynamic surface tension of the wetting front measured, which can be measured using Draves test [67].

Transplanar Wicking

The sorption of water into wipes, towels, baby diapers are examples of liquid sorption in direction perpendicular to fabric flat, so called transplanar wicking from infinite reservoir [34]. A wetting test was developed to measure the volume of absorbed liquid into textile structure [68]. Lucas Washburn equation (3.3.15), or Darcy's law (3.3.16) can be used for theoretical description of this process.

Longitudinal Wicking

Logitudinal wicking from infinite reservoir is occurred when the fabric is partially immersed into large volume of liquid and the liquid is transported in the fabric plane. Usually the distance of liquid front from liquid reservoir or weight of absorbed liquid are recorded in time to determine the wicking velocity using Lucas - Washburn equation (3.3.14). The liquid wicking rate is a standard method for measuring of high of liquid front rising up from reservoir into the vertical hang specimen in time intervals [63, 64]. Also the plate method is used, where the fabric flat is brought into a contact with liquid level and transport rate of liquid into the fabric is measured [69,70,71].

Wicking from finite reservoir

Textile processes like spraying, printing, disperse bonding bring small drops of dyes, disperse binders, print inks into contact with fabrics. The sorption of stains or rain drops attack fabrics through practical using. The suction of a liquid drop into fibre structure is called wicking from finite reservoir [34]. It is more complicated process than wicking from finite reservoir. It can be divided in two phases of different kinetics [72, 73]. At first, the drop spreads and penetrates the porous substrate underneath. In this phase the capillary penetration is kinetically similar to the one from an infinite reservoir [73]. After the whole drop volume is contained within the substrate, it is spread in radial direction under the influence of capillary forces. The method for measuring the radius of spot on very thin fabric or paper was developed [72]. Also the Darcy's law (3.3.16) is used for description of liquid drop penetration into a porous material [74]. The liquid flow Q (3.3.16) was calculated from the decrease of liquid drop volume on the porous membrane surface A_A (penetrating drop was scanned from top and side). The velocity J was plotted against a quotient containing pressure drop Δp , liquid viscosity η and porous membrane thickness T_l

$$J = \frac{Q}{A_A}. \quad (3.3.17)$$

Kissa [75,76] measured the area covered of spreading liquid A during time t and the spreading is driven by equation

$$A = K_e \left(\frac{\gamma_l}{\eta} \right)^{f_1} \cdot V_d^{f_2} \cdot t^{f_3}, \quad (3.3.18)$$

where V_d is the initial drop volume, γ_l is liquid surface tension, η is liquid viscosity, f_1, f_2, f_3 are constants and K_e is coefficient [75,76,77]. Kissa measured the area of n-alkane spreading

on polyester fabrics and found the values of exponents $f_1 = 0.3$, $f_2 = 0.7$ and $f_3 = 0.3$. The exponents are valid only for fibres impermeable to liquids [78].

3.4 Liquid Transport through Equivalent Pore Radius

The equivalent pore diameter d_e is derived from fibre diameter definition [79] in [80] as the diameter of a circle cross section of pore of the same area A like the area of non circular cross section of a fibre

$$d_e = \sqrt{\frac{4A}{\pi}} = \sqrt{\frac{4t}{\pi\rho}}. \quad (3.4.1)$$

The area A can be calculated from pore cross-section area using image analyzer.

This definition was inspiration for the equivalent radius determination in the thesis. The equivalent pore radius is derived for more exact description of liquid transport through the fibrous assemble. The horizontally oriented fibrous assemble contains seven fibres of radius b as close as possible arranged in the bundle. The cross section is in the Figure 3.4.1. The liquid body, of radius E , surrounds the bundle and the liquid fills in the pores between fibres.

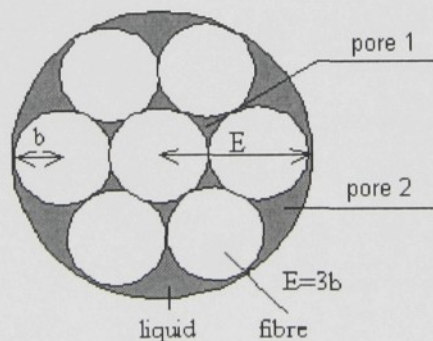


Figure 3.4.1: The size of pore 1 and the size of pore 2 in fibrous assemble.

It is possible to investigate the total pore area, but it is very complicated. The easier solution is to determine an equivalent pore area.

A pore of arbitrary shape of cross section can be considered. In this case, there are 12 pores in Figure 3.4.1 of two different sizes. Equivalent pores to pore 1 have different size from

equivalent pores to pore 2. The total pore area in cross section is A_p . It is calculated as a difference between total area of circle with radius E and sum of fibre cross-section areas.

$$A_p = \pi \cdot E^2 - 7 \cdot \pi \cdot b^2. \quad (3.4.2)$$

When the expression $E=3b$, in Figure 3.4.1, is instituted, than the pore cross section area is

$$A_p = 2 \cdot \pi \cdot b^2.$$

The equivalent pore is the pore of circular cross section with the equal area of cross section as A_p . Then the equivalent pore radius r_e is derived as

$$2 \cdot \pi \cdot b^2 \approx \pi \cdot r_e^2, \text{ then } \sqrt{2} \cdot b \approx r_e. \quad (3.4.3)$$

This is the relationship between the fibre radius b and the radius of equivalent pore r_e . It is possible to institute into solution of Lucas – Washburn equation (3.3.15) the equivalent pore radius r_e or the fibre radius b , and to reach the equation of liquid transition through the fibrous assemble from seven parallel fibres in horizontal orientation

$$h = \sqrt{\frac{r_e \gamma_l \cos \theta}{2\eta}} \cdot t^{1/2} \text{ or } h = \sqrt{\frac{\sqrt{2} \cdot b \cdot \gamma_l \cos \theta}{2\eta}} \cdot t^{1/2}. \quad (3.4.4)$$

For more complicated fibrous assemble structures, does not exit any easy relationship between liquid body radius E and fibre radius b like the one derived in Figure 3.4.1. In this case is possible only to determine the equivalent pore area from real cross section of fibre bundles or from theoretical models.

4. SIMULATION MODELS AND COMPUTER SIMULATION TECHNIQUE

The next method for theoretical description of phenomena in real systems is statistical mechanics. The statistical mechanics works with models of real systems composed from a final number of elementary units with defined degrees of freedom. In a basic model, the units are randomly ordered into different configurations and each configuration occurs with an equal probability. The energy of the model in each specific configuration is calculated as Hamiltonian. When the basic model is placed into an external field or it comes into a contact with another system, the probability of occurrence of particular configurations is different, and it is possible that not all configurations are allowed for the case of more complicated situations. The statistical mechanics deals with models with continuous degrees of freedom as Heisenberg model, XY magnets, Φ^4 model, etc., or with discrete degrees of freedom as Ising model, Potts model, etc [81].

The applications of the Ising model and its description follows in Chapter 4.1 and 4.1.1, respectively. The motivation of using of Ising model for computer simulation of wetting processes and its particular modifications are expressed in Chapter 4.2.

The Ising model is used in lots of aspects of human lives, mostly in material engineering, chemical engineering, polymer technology and physics. The modifications of the Ising model are used to explain phase transition in materials, for example, order-disorder transition of a quantum magnet at a concrete temperature [82], order-disorder transition of adsorbates at a metal surfaces [83], temperature-induced phase transition of Si is also order-disorder transition due to the thermal fluctuation of two types of tetramer [84], ordered phases of Sr and Mo and their phase transitions up to one physical monolayer [85], the effect of surface coupling J on the dependency of the layering transition temperature as a function of film thickness is studied [86], etc.

The evolution of a magnetic transition in ultra thin Fe film and Cu(100) surface with increasing film thickness is described by two-dimensional Ising model [87], as well as a thin ferromagnetic bi-layer structure with interface magnetic moment and different exchange interactions is studied in terms of a mixed Ising model [88]. The semi-infinite ferroelectric system with a free surface energy is described by transverse Ising model and the surface phase diagrams are examined by three approximations [89].

The model of lattice gas is used to simulate a process of an oxidation [90].

The process of particle migration is simulated using the Monte Carlo scheme is based on Ising model [91], a model of PVA hydrogels was developed on the bases of the Ising model, which was used to immobilize the catalyst and reduce the diffusivity of the ions [92]. The fractalization on the Si(111) surface covered by a monolayer of silicon is explain by the simple conservative Ising model, where the diffusion of a single atom is simulated by a single spin flip [93]. The equilibrium shapes of single crystals islands on surface are determined with high accuracy as a function of temperature for different surfaces [94].

Ising model and statistical mechanics show that in thin crystal films achiral molecules undergo spontaneous polar order under conditions of thermal equilibrium [95].

The one-dimensional Ising model is used to study protein folding of a protein consist of N contacts [96]. Other authors map the version of protein DNA interaction problem, the simulation reveals the possibility of biased diffusion in one direction followed by sequence viruses have been interpreted by Ising model [97]. The dynamics of a simple matrix model for identification and binding [98], the population dynamics of tRNA-like macromolecules and stiff polymers, a spatial conformation of single chain, is discussed using one-dimensional Ising model configuration [99]. The same authors investigate properties of polymer models where the chain conformation can be described solely by an Ising – like parameterization and a set of independent, predetermined bond direction vectors [100]. Chromatin can be model by Ising model to illustrate a potential mechanism how the gene regulatory DNA sequences can effect the chromatin structure over a long distance in cis [101].

The big field of interest to use Ising model is to investigate structure of alloys, for example, to compute the electric structure, surface composition in binary alloys and to show that the surface segregation is driven by the point of interaction [102].

In medicine, biotechnology and agriculture areas Ising models are used to describe some attempts to exploit these inversion relation to solve the susceptibility, to find analogenous results for polygon generating function for square lattice polygons [103], to study in detail many important binding phenomena the ligand binding problems on two-dimensional ladders [104], to model the *Escherichia coli* chemotaxis pathway [105], the quenching of monomer fluorescence is accounted using Ising model for energy transfer to weakly fluorescent aggregates [106], the district transition of triplex DNA to duplex as well as duplex to single strands are analysed using the Ising model [107]. The simulations predict epithelial cell detachment in nephrotic glomerulus under normal conditions and detachment at lower binding affinity [108].

In civil engineering the Ising model is used to predict the relation between the volume of fraction of zirconia particles, temperature and external load, during the phase transformation in ceramics [109], to model traffic congestion formation on highways and roads by recognising the centrality of dynamical system, and the increase in air pollution caused by vehicle exhaust emission can be traced to traffic congestion [110].

Ising model is one from the model of statistical mechanics which can be applied in theory of large deviations in psychology and social science [111]. The theoretical study of Hebb synapse was done using Ising model [112]. Consideration of contextual guidance role in learning and processing within multi-stream neural network is done using the model as well [113].

4.1 The Ising model and Its Modifications

The primary model was build by Wilhelm Lenz in 1920. It was used for a simulation of paramagnetic properties of solids [114]. The concept of a microscopic magnetic model is based on the elementary magnetic moments fixed at their positions. There is a constant number N_m of magnetic moments in the model. They are oriented in two positions characterised by an angle $\alpha = 0$ and $\alpha = \pi$. The energy of the model is constant, a flip process occurs very rarely. The flip is always realized by two magnets. One changes its orientation from 0 to π , and the second in the opposite sense, to keep the energy constant. All magnets are in average in each position equally long.

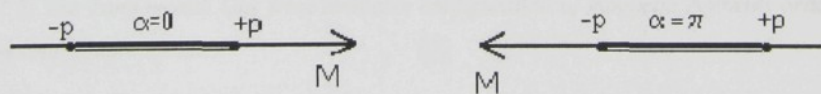


Figure 4.1.1: The magnetic moment oriented in two directions.

In the presence of the external magnetic field, where the intensity M has its orientation, the sense of $\alpha = 0$, the equivalence of the two positions disappears. The system can be ordered in different configurations with different values of energy. The system occurs for each energy level with a concrete probability according to Boltzman principle [115].

Ising found that one-dimensional model is not able to describe a phase transition of solid to ferromagnetic ordered state. He composed a model with more complicated interactions between elementary magnets [116]. The final result of his aspiration was two-dimensional Ising model. The model is constructed from final number N of elementary magnets ordered into two-dimensional regular lattice. The magnets are able to be oriented into two directions „up“ and „down“, as shown in Figure 4.1.2. To describe the model, the each magnet is noted by the Ising variable σ . The magnets oriented „up“ is $\sigma = +1$, and for magnets oriented down is $\sigma = -1$. The energy of the model in the presence of external magnetic field is determined by Hamiltonian

$$H = -\sum_{i,j} U_{ij} \cdot \sigma_i \cdot \sigma_j + \mu \cdot H \cdot \sum_i \sigma_i, \quad (4.1.1)$$

The value σ_i is Ising variable of elementary magnet, σ_j is the Ising variable of a magnet j from the nearest neighbouring of magnet i . U_{ij} is exchange energy, which characterises the nature of magnets i and j interaction. U_{ij} has different value for pairs of magnets $\sigma_i = +1$ and $\sigma_j = +1$, $\sigma_i = +1$ and $\sigma_j = -1$, $\sigma_i = -1$ and $\sigma_j = 1$. The value μ is elementary magnetic charge.

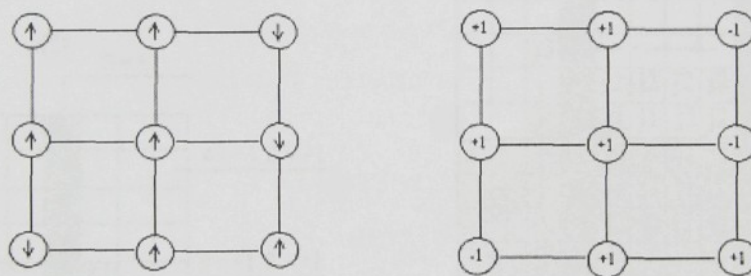


Figure 4.1.2: The Ising model. One from available configuration of magnetic moments ordering in two dimensional square lattice.

4.2 Models for Wetting and Wickin Phenomena Simulation

In the phenomena of wetting and wicking processes, the dynamic behaviour of liquid in a contact with solid material is investigated. The same principle described above in Chapter 4.1, where the Ising model is used for simulation of ferromagnetic solids behaviour is used. It means that each elementary unit of a model can acquire only one from two values of Ising variables.

Lukas and Glazyrina [117] used a modification of two-dimensional Ising model to simulate behaviour of a liquid in contact with a solid representing a textile material. The two-dimensional lattice is built from final number N of square cells of unit square area. An each cell is occupied by the Ising variables σ or S . The different values of σ correspond with different environments present in the simulated system. One example of the air – liquid – fibres system is shown in Figure 4.2.1. The air cells have $\sigma = -1$, the liquid cells have $\sigma = +1$. The fibre cells have $S = +1$ and the non-fibre cells have $S = -1$. The surface tension is simulated as a result of attractive forces between cells i and j with the equal values of Ising variables σ_i and σ_j . It is expressed as cohesion energy (4.1.2) of the system. Every cell i has attractive forces with the cells j of equal Ising variable value in its three levels of nearest neighbours as shown in Figure 4.2.2. Characteristic of the attractive forces are expressed by exchange energies C_{c1} , C_{c2} , C_{c3} , for first nearest neighbour, second nearest neighbours and third nearest neighbour respectively. Values of the exchange energies for concrete example of a model are in Table 4.2.1.

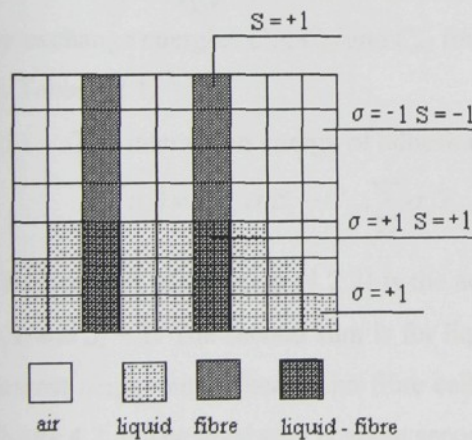


Figure 4.2.2: The energy of cell i is determined according to neighboring cells from 3 levels of nearest neighbours.

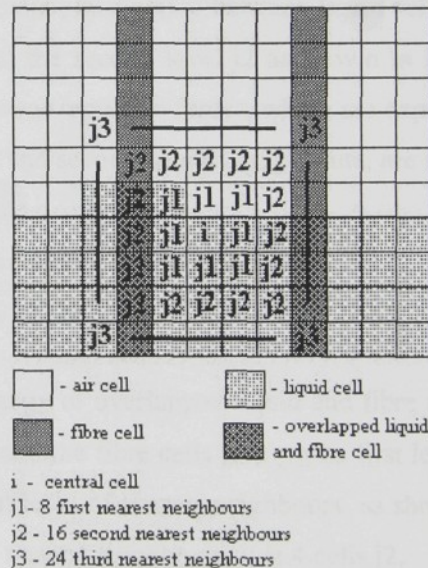


Figure 4.2.3: The example of modification of two-dimensional Ising model. The model contents three kinds of environment. Air - $\sigma = -1$, liquid $\sigma = +1$, solid fibres $S = +1$ and non-fibre cells $S = -1$.

Table 4.2.1: Values of exchange energies characterising intensity of attraction forces between liquid cells i and j.

	$S_{j0} = 1$	$\sigma_{j1} = -1$	$\sigma_{j1} = 1$	$S_{j1} = 1$	$\sigma_{j2} = -1$	$\sigma_{j2} = 1$	$S_{j2} = 1$	$\sigma_{j3} = -1$	$\sigma_{j3} = 1$
$\sigma_i = -1$									
$\sigma_i = 1$	$C_{a0} = -45$		$C_{c1} = -15$	$C_{a1} = -35$		$C_{c1} = -15$	$C_{a2} = -5$		$C_{c1} = -5$

The interaction energy of cohesion action of a liquid related to one cell i is H_C :

$$H_c(\sigma_i) = C_{c1} \cdot \sum_{nn} \sigma_i \sigma_{j1} - C_{c2} \cdot \sum_{nnn} \sigma_i \sigma_{j2} - C_{c3} \cdot \sum_{nnn} \sigma_i \sigma_{j3}. \quad (4.2.1)$$

The first sum in Equation (4.2.1.) is the cohesion energy between the central liquid cell i, and the liquid cells from the first level of nearest neighbours, it is 6 liquid cells j1 as shown in Figure 4.2.3. The second sum is for cell i and the liquid cells from its second level of nearest neighbours, it is 10 cells j2. The third sum is belongs to third level of nearest neighbours, then 14 cells j3.

The interaction between liquid cells and fibre cells is expressed as adhesion energy H_a . In to the account is taken mutual acting overlapped liquid cell $\sigma_i = 1$ and fibre cell $S_i = 1$ of the cell i is considered, so called zero nearest neighbours, then acting between liquid cell i and its nearest fibre neighbours in the first level j1 and the second level j2 as shown in Figure 4.2.3. The examples of characteristic of the attractive or repulsive forces, which are expressed by exchange energies C_{a0} , C_{a1} and C_{a2} for zero, first and second nearest neighbours, are shown in Table 4.2.1.

The interaction energy of adhesion related to one cell i $H_a(\sigma_i)$ is:

$$H_a(\sigma_i) = C_{a0} \cdot \sigma_i S_i - C_{a1} \cdot \sum_{nn} \sigma_i S_{j1} - C_{a2} \cdot \sum_{nnn} \sigma_i S_{j2}. \quad (4.2.2)$$

The first part of equation (4.2.2) is the adhesion energy of overlapped liquid and fibre cell $\sigma_i = 1$ and $S_i = 1$. The second sum is for liquid cell i, and the fibre cells j1 from its first level of nearest neighbours. There is no fibre cell in the first level of nearest neighbours, as shown in Figure 4.2.3. The third sum is about second level of nearest neighbours, it is 4 cells j2.

In the presence of the external gravitational field, it is characterised by gravitational constant C_g . The gravitational energy of a liquid cell $H_g(\sigma_i)$ is proportional to its location along vertical y - axis

$$H_g(\sigma_i) = C_g \cdot y_i. \quad (4.2.3)$$

The co-ordinate y_i is the vertical co-ordinate of the cell i in two-dimensional lattice.

The total energy of the system is the Hamiltonian H calculated over all cells in the lattice, where each has above mentioned three parts of energy.

$$H = \sum_{i=1}^N H_g(\sigma_i) + \sum_{i=1}^N H_c(\sigma_i) + \sum_{i=1}^N H_a(\sigma_i) \quad (4.2.4)$$

The next two-dimensional modification of the Ising model, which follows the above described model [117], was proposed by Yhong [118]. The model simulates liquid wicking into a fibre material. The modification of the system is shown in the Figure 4.2.4. There are air cells, liquid cells, fibre cells, and cells where two environments coexist, air – liquid cells and liquid – fibre cells.

The total energy of the simulated system is the Hamiltonian (4.2.5). The equation describes the interactions between neighbouring cells. The interaction has different characteristic according to the existence of cells with two coexisting environments and according to the pairs of neighbouring cells i and j (liquid – liquid, liquid – fibre, etc.) and for liquid cell i also the influence of gravitational field.

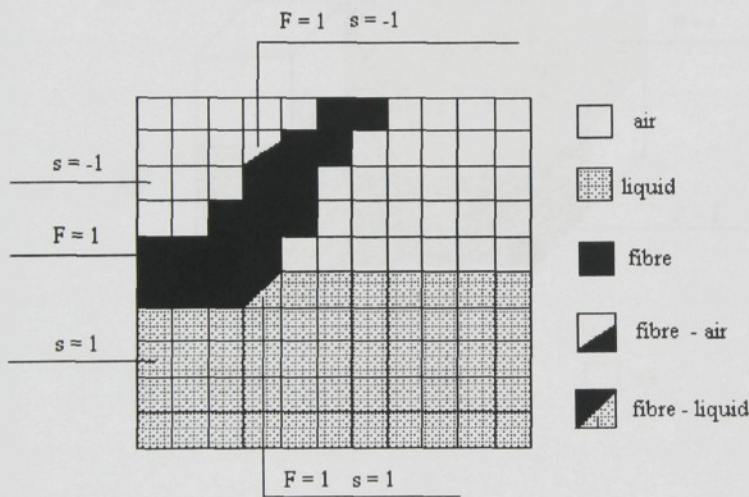


Figure 4.2.4: Two-dimensional Ising model modification.

The intensity of interactions is expressed by values of exchange energies B_0 , C_{ij} .

$$H = - \left(B_0 \cdot \sum_i s_i F_i + \sum_{i,j} s_i F_j \right) - C_{ij} \cdot \sum_{i,j} s_i s_j + G \cdot \sum_i s_i y_i. \quad (4.2.5)$$

The first sum in the bracket describes the interaction energy between liquid and fibre coexisting in one cell. The second sum in the bracket represents neighbouring liquid cell and fibre cell interaction. The next sum behind the bracket belongs to cohesion energy expression between two liquid cells. The last sum is the gravitational contribution of gravitational field,

characterised by intensity C_g , acting at liquid cells and it is proportional to the vertical position of the cell i in the lattice y_i .

Lukáš a Pan [39] designed three-dimensional modification of the Ising model to simulate fibrous assemble wetted by liquid. The model of such system is ordered into three-dimensional lattice built from elementary cubic cells of unit volume. Each cell is occupied by Ising variable σ or S . Different values of σ correspond with the different environments presented in the simulated system. The air cells have $\sigma = -1$, the liquid cells have $\sigma = +1$. The fibre cells have $S = +1$ and the non-fibre cells have $S = -1$. Each cell interacts only with cells from its nearest neighbours, it is 26 closest cells in tree-dimensional lattice, as shown in Figure 4.2.5.

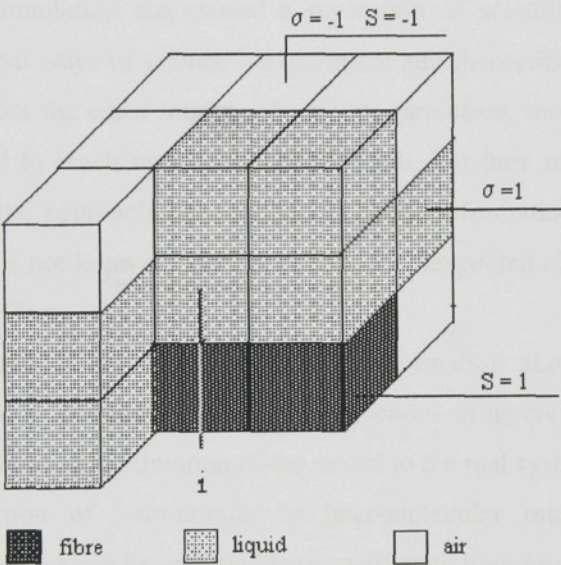


Figure 4.2.5: The central cell i surrounded by 26 cells in three-dimensional lattice.

Three types of interaction occur in the model. The interactions express cohesion acting between liquid cells, it is characterised by exchange constant C_c . The adhesion acting between liquid cell and fibre cell is characterised by exchange energy C_a . The Hamiltonian describing total energy of the system (4.2.6) also contents the gravitational part in the case of presence of the gravitational field.

$$H = \sum_i \sum_j C_c \sigma_i \sigma_j + \sum_i \sum_j C_a \sigma_i S_j + \sum_i C_g z(i) \cdot \delta(\sigma_i - 1). \tag{4.2.6}$$

The last sum in Equation (4.2.6.) expresses the gravitational energy. The intensity of the gravitational field is C_g , z_i is the vertical co-ordinate of liquid cell i in the lattice. δ_i is the Dirac function.

The three-dimensional lattice model designed for computer simulations in this thesis is described in Chapter 5.2.1 and it is followed by constant settings for particular simulation processes.

4.3 Monte Carlo Method

The computer simulation has started a revolution of scientific approaches. It has completed two traditional ways of science – experiment and theoretical description [81]. An analytical theory provides the exact results only in very rare cases, more often the simplified approximation are used to reach useful theoretical result, but they result only for an ideal model. The experimental approach does not get sufficient information. If some unexpected results are occurred, it is not known if their reason is an unexpected character of the sample, influence of unknown effects.

The computer simulation allows find exact information about a model of a real system, and it is possible to describe the model more accurate using computer simulation [81]. The simulation allows close approximation of the model to the real system. The big advantage is the arbitrary selection of inter-atomic or inter-molecular interactions. The model configurations and properties can be modified very easily with high variability.

One of the most popular simulation methods and recently used in a lot of fields of applications are the Monte Carlo methods.

The Monte Carlo method was chosen for simulation of wetting and wicking processes due to its ability to simulate dynamic processes in models of statistical mechanics.

4.3.1 History of Monte Carlo Method

The Monte Carlo Method (MC) has more than 50 years of history. The method was born by solving the problem of behaviour of neutrons and its penetration through materials. This task was insoluble theoretically and experimentally then Neuman and Ulam used for

prediction of “history of a neutron live” using known roulette technique. The degree of the MC method is that reliability is determined by mathematical – statistical methods of the theory of reflection. Generally, the quality of results depends on the number of realised attempts.

The Monte Carlo method has two characteristic features [120]. Firstly, it is a numeric method used in mathematical tasks simulating of random variables. Secondly, it bears on its growth and using as a universal numerical method has connection to rapid expansion of computer technology.

The mathematical theory of Monte Carlo arises from concrete demands on a solution of difficult issues of many fields, scientific, technical, economics, etc. The method comes out from the probability theory and mathematical statistics, which create conditions to solve issues, insoluble using traditional mathematical methods. The knowledge of bulk random event laws and processes leads to solving of tasks with no relation to random situations.

4.3.2 Monte Carlo Method and Statistical Mechanics

The primary idea of Monte Carlo method is based on a relation between probability characteristics of different random processes and variables, which are the solutions of different mathematical fields (mathematical analyse). The method is understood as a result of a combination of different approaches, like numerical solution of mathematics, physics and other tasks. It is realised by using multiplied random attempts.

The model in statistical physics usual has a lot of degrees of freedom. The task of statistical physics is to determine a mean value of a quantity of the model which characterises the model over all its configurations, which describe the real system. The model has to be described by initial configuration setting and initial value of its energy calculated as a Hamiltonian H . The Hamiltonian for three dimensional model is calculated in equation (4.2.6).

The normalised Boltzman factor gives a failure probability $P(x_i)$ of the x configuration presence [115]:

$$P(x_i) = \frac{1}{Z} \cdot \exp\left(\frac{-H(x_i)}{k_B \cdot T}\right), \quad (4.3.1)$$

where k_B is Boltzman constant, T is temperature, and $H(x_i)$ is the Hamiltonian of the system in x_i configuration. The Z is so called particular function of the system with constant number of particles N and for constant temperature T .

$$Z_{N,T} = \int dx \cdot \exp\left(\frac{H(x_i)}{k_B \cdot T}\right). \quad (4.3.2)$$

The integration is done over Boltzman factors for all configurations x of the model with N particles. Generally the partition function is the proportionality factor between the probability $P(x_i)$ and Boltzman factor $\exp(H(x_i)/k_B \cdot T)$.

The task of Monte Carlo method used in equilibrium statistical physics is to replace the integration over all configurations $\{x\}$ and their proper weights $p(x)$ to the sum over a characteristic subset of configurations $\{x_1, x_2, \dots, x_m\}$ of the model which is used as a statistical sample. The number of configurations in the statistical sample m [81] is much smaller then the number of all configurations of the investigated system. The question is how to choose the right subset of configurations which characterizes the system properly? For the investigation of systems in equilibrium, the simple sampling Monte Carlo method is used. Random walks in two dimensional lattice are used for modelling of properties of long flexible macromolecules in solution. The variations in simple sapling techniques are shown in [81] with examples of unrestricted random walks, non-reversal random walks, self – avoiding random walks, etc.

The fibrous structures wetted by liquid or liquid absorption into fibrous material represent systems in non-equilibrium state. For non-equilibrium systems, the importance sampling Monte Carlo method is used to simulate unstable behaviour of a system. The importance sampling realises the statistical sample as, so called, Markov process where each configuration x_{i+1} is constructed from previous configuration x_i with a suitable transition probability $W(x_i \rightarrow x_{i+1})$. Then the principle of a detailed balance valid for transition from $x_i \rightarrow x_{i+1}$ and inverse transition $x_i \leftarrow x_{i+1}$ is:

$$p(x_i) \cdot W(x_i \rightarrow x_{i+1}) = p(x_{i+1}) \cdot W(x_{i+1} \rightarrow x_i). \quad (4.3.3)$$

It is clear from Equation (4.2.3) that the ration of transition probabilities for move $x_i \rightarrow x_{i+1}$ and inverse move $x_i \leftarrow x_{i+1}$ depend only on the energy change (4.2.1) $\Delta H = H(x_{i+1}) - H(x_i)$,

$$\frac{W(x_i \rightarrow x_{i+1})}{W(x_{i+1} \rightarrow x_i)} = \exp\left(-\frac{\Delta H}{k_B \cdot T}\right) = P_{TR}. \quad (4.3.4)$$

The Equation (4.3.4) describes the probability of transition. In the real simulation process, two situations are distinguished. One is the transition from the configuration with higher

energy $H(x_i)$ to configuration with lower energy $H(x_{i+1})$, what means negative energy difference of change ΔH . From the graph of exponential function shown in Figure 4.3.1, the portion from Equation (4.3.4) is in this case higher than 1. The probability of transition from configuration x_i to x_{i+1} is higher than the reverse transition probability and the system comes into new configuration x_{i+1} . The different situation is occurred in the case when the following configuration $H(x_{i+1})$ has higher energy than the initial configuration $H(x_i)$, then the difference in energies ΔH has positive value and the probability of transition from configuration x_i to x_{i+1} is lower than the reverse transition probability.

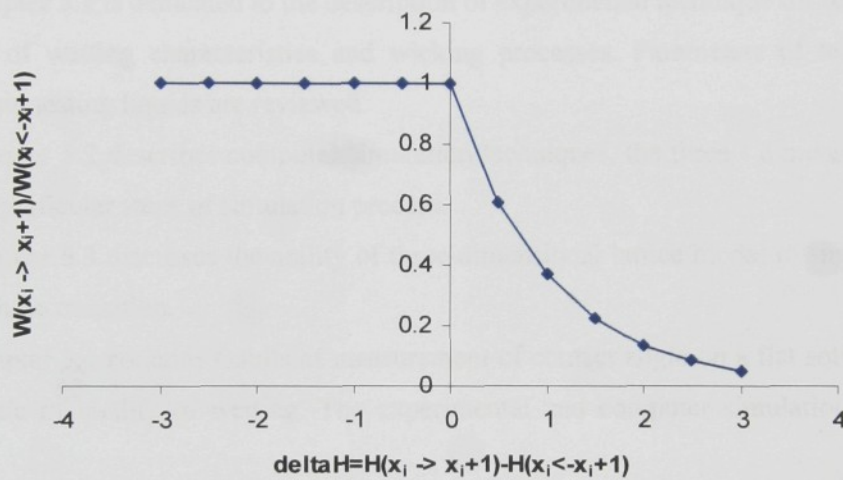


Fig. 4.3.1: The function of the transition probabilities from Equation (4.2.4).

The transition from configuration x_i to configuration x_{i+1} is realized with the probability given by the portion from Equation (4.3.4).

5. EXPERIMENTAL WORK AND COMPUTER SIMULATION PROCESS

The chapter 5 concentrates on experimental measuring of wetting and wicking characteristics of fibrous materials and their evaluation related to analytical theories described in Chapter 2. The configurations of models for computer simulations are designed to follow experimental setting. The experimental results and computer simulation outputs together with the ability of computer simulation processes to simulate real processes are discussed, and advantages of the computer simulation outputs are described in following chapters.

Chapter 5.1 is dedicated to the description of experimental technique for recording and evaluation of wetting characteristics and wicking processes. Parameters of tested fibrous materials and testing liquids are reviewed.

Chapter 5.2 describes computer simulation techniques, the three - dimensional lattice model and particular steps of simulation process.

Chapter 5.3 discusses the ability of three-dimensional lattice model to simulate liquid – vapour phase transition.

Chapter 5.4 contains results of measurement of contact angle on a flat solid as a basic characteristic of quality of wetting. The experimental and computer simulation results are reviewed.

Chapter 5.5 studies the computer simulation of instability of liquid drop placed on heterogeneous surface is studied.

Chapter 5.6 discusses results of computer simulation of a liquid drop behaviour of a single fibre according to theoretical prediction from Chapter 3.3.1 and 3.3.2, and experimental results from chapter 5.4.

Chapter 5.7 describes the behaviour of liquid drop on fibrous assemblies in dependence on number of fibres and fibre geometry in assemble. The experimental results are accompanied by outputs from computer simulation.

Chapter 5.8 evaluates liquid penetration into fibrous layer with different fibrous orientation and the liquid transport inside these layers. The computer simulation results are used to describe the behaviour inside the structures and it is used to predict the behaviour of composite material pleated from those layers.

5.1 Experimental Techniques

The experimental techniques for the investigation of air - liquid – solid mutual behaviour are similar for all experiments described within Chapters 5.4 – 5.8.

Several experimental configurations were used for investigation of behaviour of liquids in contact with solid materials. These examples are shown in Figure 5.1.1. A liquid drop placed on a solid flat surface, as shown in Figure 5.1.1A, a liquid drop placed on a single fibre stretched over the plastic frame, as shown in Figure 5.1.1B, or on a fibre bundle stretched over the plastic frame, shown in Figure 5.1.1C. A liquid drop placed on a complex fibre structure, as shown in Figure 5.1.1D.

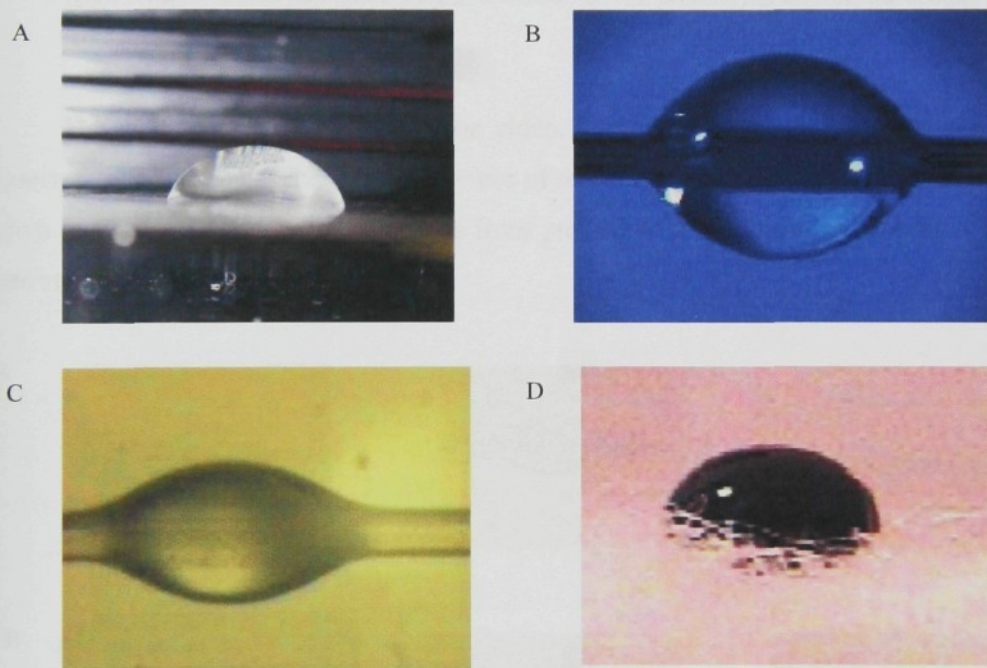


Figure 5.1.1: A – drop of distilled water on a PP flat surface. B – drop of distilled water drop on a single boron fibre. C – oil drop on parallel PP fibres ordered in a bundle. D – coloured liquid drop on nonwoven fabric structure.

The experimental samples were captured by digital camera connected to a computer. The recorded images were interpreted using image analyser LUCIA G [121]. The program allows quantification of some parameters if the calibration is known. A length characteristic is marked on the coloured picture as shown in Figure 5.1.2A as marked

diameters of a fibre. The program gives the mean value of the diameters and standard deviation, the maximum and minimum values of diameters in the measuring area. Length and height of a drop can be measured. The program measures automatically a contact angle on the coloured picture, as shown in Figure 5.1.2 B.

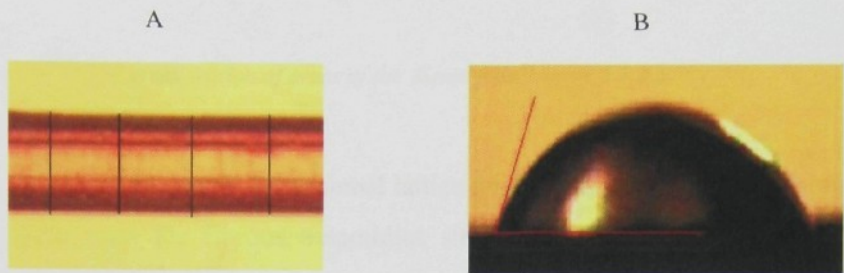


Figure 5.1.2 A – liquid film on PP fibrous assemble; B – oil drop on flat surface, the contact angle is marked. .

The wetting process is captured on video. Particular images are selected according to requested time intervals. The three sequences of the wetting process of a fibrous assemble are shown in Figure 5.1.3 A. The sequences from process of a liquid drop penetration into fibre mass are shown in Figure 5.1.3. B.

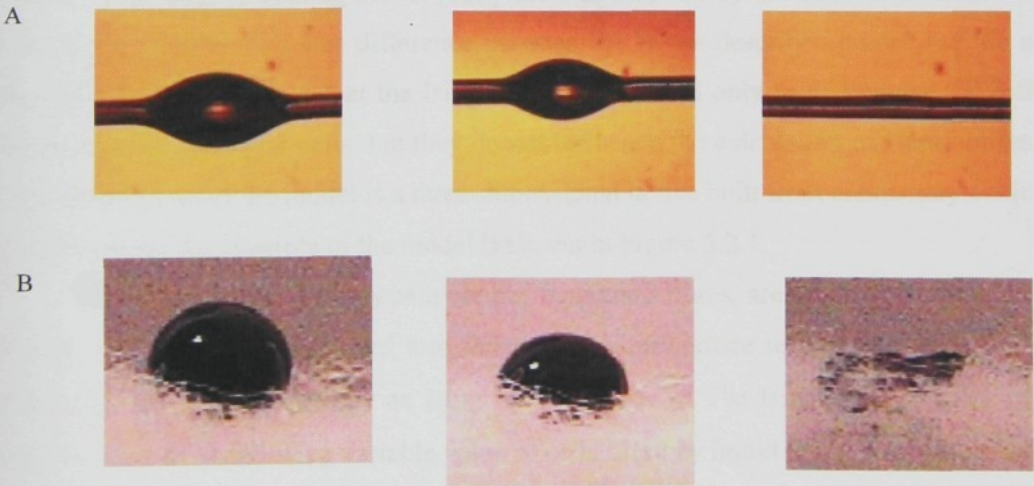
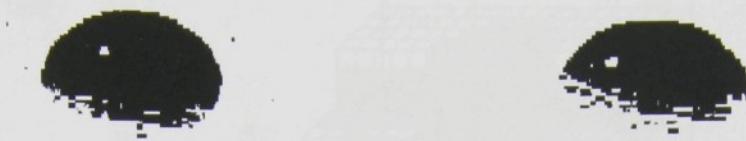


Figure 5.1.3: A – spreading of a drop into fibrous assemble; B – penetration of a drop into fibre mass.

The area in cross-section of the liquid drop was evaluated in experiments, as shown in Figure 5.1.4. The software LUCIA G gives direct value of the surface area.



5.2 *Figure 5.1.4: The cross section of areas of the liquid from Figure 5.1.3 B.*

The design of the three-dimensional lattice model was inspired by the Ising Model and its modification used for fibrous assemblies simulation described in Chapter 4.1.1. The simulation process is driven by principles of Monte Carlo simulation method and statistical mechanics mentioned in Chapter 4.3.

5.2.1 Three Dimensional Lattice Model

The three-dimensional lattice model is used for simulation of wetting processes on solid substrates and for liquid wicking into fibrous materials in the doctoral thesis. The model is based on principles of Ising model [122] and was inspired by the three-dimensional model described in Chapter 4.2. The difference between the below described model and the model presented in Chapter 4.2 is that the Ising variables are used only to distinguish the different environment in particular cells, but they do not influence the calculation of Hamiltonian. The basic composition of the model is a three-dimensional lattice built from elementary cubic cells of unit volume. An example of the model is shown in Figure 5.2.1.

The components of the system are air, liquid and fibres, are present in total number N of cells. The system is organised into three-dimensional lattice using Ising variables. Each elementary cell i is occupied by an Ising variable value σ . The Ising variable value of cells filled by air is $\sigma=0$, the Ising variable value of cells filled by liquid is $\sigma=1$ and Ising variable value for fibre cells is $\sigma=2$.

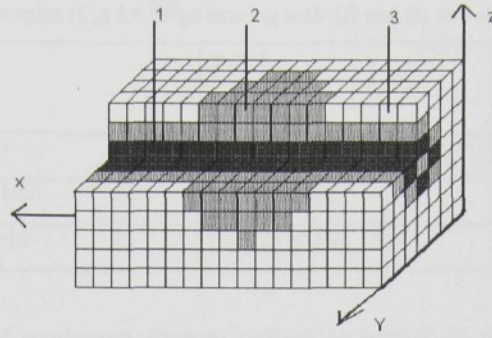


Figure 5.2.1: Three dimensional Ising model modification of system composed of fibrous assembly in contact with liquid. The fibrous assembly 1 is surrounded by liquid 2. The air 3 is present in other lattice cubes.

The total energy H of the system is the sum of energies E_i of all elementary cells in the lattice. The energy of one elementary cell i depends on the interactions between the cell i and the cells in its nearest vicinity. Each cell has twenty six nearest neighbours in the three dimensional lattice. The cell i can be air, liquid or fibre component. Also the neighbouring cells can represent one from of these three environments. The characteristics of mutual cohesion and adhesion influence the behaviour of the model. The quality of the interactions are characterised by values of exchange energies C_{ij} between the central cell i and a particular cell j in its nearest vicinity. The liquid cells are also under the influence of gravitational field. The energy of elementary cube E_i has two parts

$$E_i = C_g \cdot z_i + \sum_{j=1}^{26} C_{ij}, \quad (5.2.1)$$

where C_g is gravitational constant and the vertical position of cube i in the lattice is characterised by z_i co-ordinate. The second term is the sum of exchange energies between cell i and 26 cells in its vicinity.

The Hamiltonian H expresses the total energy of the system. It is the sum over all elementary cells in the model

$$H = \sum_{i=1}^N E_i = C_g \cdot \sum_{i=1}^N z_i + \sum_{i=1}^N \sum_{j=1}^{26} C_{ij}. \quad (5.2.2)$$

Example of values of C_{ij} for each interaction of a pair of cells i and j are shown in Table 5.2.1.

Table 5.2.1: Values of exchange energies (C_{ij}) for neighbouring cells (i) and (j) in a simulation process.

Central cell $i \rightarrow$	$\sigma_i = 0$	$\sigma_i = 1$	$\sigma_i = 2$
Neighbour cell $j \downarrow$			
$\sigma_j = 0$	$C_{ij}(0,0) = -1$	$C_{ij}(0,1) = +10$	$C_{ij}(0,2) = +10$
$\sigma_j = 1$	$C_{ij}(0,1) = +10$	$C_{ij}(1,1) = -92$	$C_{ij}(1,2) = -102$
$\sigma_j = 2$	$C_{ij}(0,2) = +10$	$C_{ij}(1,2) = -102$	$C_{ij}(2,2) = -59$

The determination of exchange energy values is based of the definition of liquid surface tension on the definition of surface tension [123]. The exchange energies determination is shown on an example of one air and one liquid cell. A liquid cell inside the volume of liquid phase is surrounded in three-dimensional lattice by twenty six liquid cells, as shown in Figure 5.2.2A, and an air cell inside the volume of air phase is surrounded in three-dimensional lattice by twenty six air cell, as shown in Figure 5.2.2B.

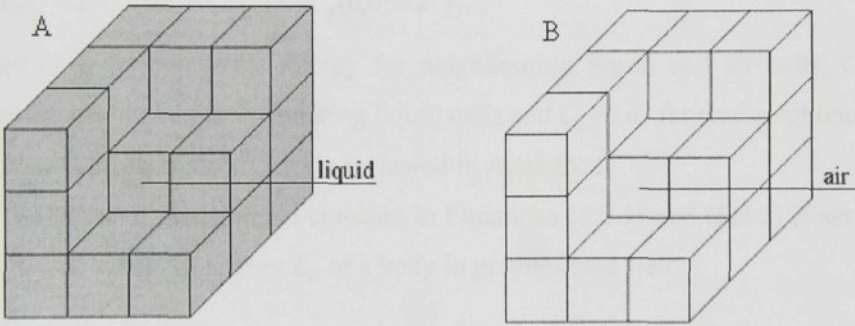


Figure 5.2.2: A – a liquid cell inside volme of liquid phase in 3D lattice, B – an air cell inside volume of air phase in three-dimensional lattice.

If the liquid cell is replaced from inside liquid volume at the liquid – air interface, at least one air cell is present in its nearest vicinity, as shown in Figure 5.2.3A. If the air cell is replaced from inside air volume at the liquid – air interface, at least one liquid cell is present in its nearest vicinity, as shown in Figure 5.2.3B

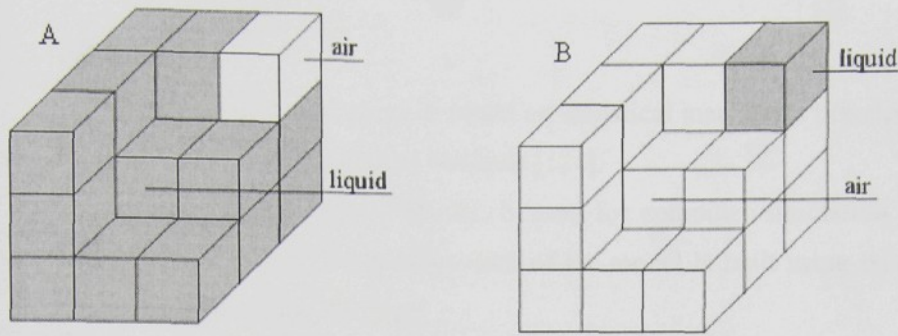


Figure 5.2.3: A – a liquid cell at the liquid – air interface in 3D lattice, B – an air cell at liquid – air interface in 3D lattice.

The difference of the energies of those two cells inside the phase volumes and at the interface is:

$$\Delta E_c = 2 \cdot C_{ij}(0,1) - C_{ij}(1,1) - C_{ij}(0,0) = 2 \cdot \gamma_l. \quad (5.2.3)$$

The $C_{ij}(0,1)$ is the exchange energy for neighbouring liquid and air cells, $C_{ij}(1,1)$ is the exchange energy for two neighbouring liquid cells and $C_{ij}(0,0)$ for two neighbouring air cells. The derivation of equation (5.2.3) is reviewed in Appendix 1.

The value of gravitaional constant in Equations (5.2.1) and (5.2.2) is set up according to definition of potential energy E_p of a body in gravitaional field:

$$E_p = m_b \cdot g \cdot h_p, \quad (5.2.4)$$

where m_b is the body mass, g is gravitaional acceleration, h_p is the high of the body in gravitational field. In the gravitational part of Equation (5.2.1) is the high h_g equivalent to vertical z-coordinate of the cell, and the cell has unit volume then unit mass also. The constant C_g is equivalent to the value of gravitational acceleration $g = 9.81 \text{ m} \cdot \text{s}^{-1}$. The value of gravitaional constant C_g in simulation processes is 10.

5.2.2 Computer Simulation Process

The computer simulation process is based on statistical mechanics principles and it is realised using the Monte Carlo simulation methods [124].

The three - dimensional lattice model, is used for computer simulation. Before the simulation process starts, the initial configuration of the model is built using Ising variables and the characteristic constant are defined.

Several conditions are preserved during simulation process.

1. The temperature is constant during simulation process.
2. The number of liquid cells is constant during the simulation process. The evaporation of liquid is neglected.
3. The cells presenting solid environment are fixed in their positions during simulation process.

The dynamics in the simulation process is controlled by Kawasaki spin exchange dynamics on long range distances. In the present process, the cells characterised by values of Ising variables σ are randomly selected from any position at liquid – air interface. The interface positions are a condition for simulation process to preserve the natural liquid behaviour and move the liquid cells from liquid surface only, and not from the inner liquid volume.

The probability of liquid and air cells positions exchange depends on the value of system energy before and after exchange ΔH . One Monte Carlo step (MCS) involves following operations [124]:

- one liquid cell and one air cell are randomly chosen from liquid – air interface
- the sum of energies E_1 of air and liquid is calculated from Equation (5.2.1)
- the positions of the Ising variables of these two cells are changed in the lattice
- the sum of energies E_2 of air and liquid after position exchange is calculated from Equation (5.2.1)
- the difference between energy before and after exchange is calculated as $\Delta H = E_1 - E_2$
- if the exchange decreases the energy below zero $\Delta H < 0$, the Ising variables stay in their new positions and the energy of the systems changes to ΔH
- if the exchange increases the energy above zero $\Delta H > 0$, the decision process about system behaviour is more complicated. The probability of transition P_{TR} from Equation (4.3.4) of the system is calculated.

- the number P is randomly generated from interval $(0,1)$
- if $P > P_{TR}$, the system returns to initial configuration and its energy remains constant. If $P < P_{TR}$, the system stays in the new configuration and the energy of the systems is changes to ΔH .

The next simulation step starts the same process with another two cells.

The simulation process finishes when the system reaches the equilibrium state, it is when the energy of the system varies around a constant value during simulation.

The values of thermodynamic temperature $k_B T$ are set up in computer simulation between values $k_B T = 0$ and $k_B T = 40$. The influence of different values of thermodynamic temperature $k_B T$ on behaviour of system during simulation processes is discussed in following Chapter 5.3.

5.3 Computer Simulation of Two Phase System

The Ising Model is frequently used for simulation of phase transition [125,126,127]. To simulate processes on the liquid – vapour interface using the above mentioned three - dimensional model was inspired by the Helmholtz definition of surface tension and his prediction about existence of so called sphere of phase interface.

Several different phases of one component can be found in one component system under specific conditions. The different structural constitution of each phase of the component, and the different character of interactions in inert volume of each phase, cause the creation of sphere of phase interface between two neighbouring phases [124]. According to Gibbs, the phase interface has a final thickness, where the thermodynamic characteristics are different from the thermodynamic characteristics in the inert volume of each phase.

5.3.1 Thermodynamic Relations in the Sphere of Phase Interface

Two phases can coexist in one component system in balance. The stability of phase interface depends on the increase of Helmholtz energy F_S during increasing surface area A of

the phase interface. So long as Helmholtz energy increases with increasing surface area $dF/dA > 0$, an increase of Helmholtz surface energy F_S belongs to emergent surface area [128]:

$$F_s = \frac{dF}{dA} \cdot A = \gamma \cdot A, \quad (5.3.1)$$

where γ is Helmholtz surface energy related unit surface area of phase interface.

The Helmholtz surface energy F_S can also be defined as a force preventing the surface area increase, as described in the Dupre attempt for surface tension definition in Chapter 3.1.

The presence of Helmholtz surface energy F_S and then surface tension γ is explained by the presence of unsaturated interactions on the phase interface. To establish a new surface means to expend work necessary to release molecules from the inert volume of a phase and bring them to the surface [128].

The sphere of phase interface is a layer of infinite thickness, which is comparable with the size of molecules [128]. The characteristic properties for one phase are step by step changed to the characteristics of the other phase inside this transition layer. Because the composition and properties are inhomogeneous in transition layer, Gibbs also called this layer as a physical surface of homogeneity disturbance.

The characteristics of interphase are studied on the bases of changes of the Helmholtz surface energy F_S in the transition layer between two phases. The density of Helmholtz energy f for a system of one phase in the state of constant values of pressure p , temperature T and volume V and the number of moles is:

$$f = \mu \cdot c - p, \quad (5.3.2)$$

where chemical potential $\mu = \partial G / \partial N$ is equal to change of Gibbs energy ∂G related to the change of number of moles ∂N , concentration $c = \partial N / \partial V$ is equal to the change of number of moles ∂N related to the change of volume ∂V .

For two phases in balance, the values of chemical potential μ and pressure p are equal. Then from Equation (5.3.2), the change of density of Helmholtz energy is influenced by the difference of concentrations in both phases only. Generally, Helmholtz energy is then higher for liquids than for gases.

The character of change of Helmholtz energy is presented in an example of one component system containing two phases – liquid and vapour [128]. This system is closed in a prism. The prism contains liquid of volume V_l and vapour of volume V_v , as shown in Figure 5.3.1.

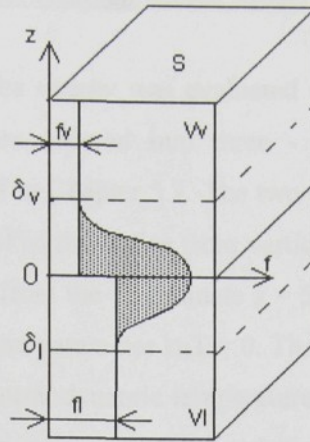


Figure 5.3.1: The change of Helmholtz energy on the sphere of phase transition.

There are marked two lines δ_l and δ_v in the volume of the prism. From the lower plane of the prism to the line δ_l is the density of Helmholtz energy constant and equal to the density of Helmholtz energy in the liquid phase $f=f_l=\text{const}$. From the top plane of the prism to the line δ_v is the density of Helmholtz energy constant and equal to the density of Helmholtz energy in the vapour phase $f=f_v=\text{const}$. The layer between lines δ_l and δ_v is sphere of phase transition and its thickness is $\delta_l + \delta_v$. In the ideal system, the Helmholtz energy jumps from the value F_l in liquid volume to value F_v in vapour volume on the phase interphase line. The total Helmholtz energy of the whole system is sum of energies in particular phases $F_l + F_v$. In the real system, the sphere of phase transition has its own characteristics and cause a higher value of total Helmholtz energy F_S for real system than for ideal system $F_l + F_v$. The increase of the total Helmholtz energy F_S in real system over the ideal system is:

$$F_s = F - (F_l + F_v) = F - (f_l \cdot V_l + f_v \cdot V_v) = \gamma \cdot A,$$

This surplus F_S is related to a surface area S expresses value of surface tension γ .

$$\gamma = \int_{-\delta}^0 [f(z) - f_l] \cdot dz + \int_0^{+\delta} [f(z) - f_v] \cdot dz. \quad (5.3.4)$$

The boundaries of integrals in Equation (5.3.4) are set from δ_l to δ_v . From the geometrical expression, the value of surface tension γ is equal to designated area in Figure 5.3.1, which is restrain by a curve of function $f(z)$, and by lines $f=f_l$ and $f=f_v$, and by a section of line $z=0$, as shown in Figure 5.3.1. The Equation (5.3.4) is equal to value of γ for this concrete position of the interphase line $z=0$.

5.3.2 Two Phase System in Three Dimensional Lattice Model

The density of the Helmholtz energy was evaluated using computer simulation. The two phases of one component are ordered into three - dimensional lattice built from elementary cubic cells, as described in Chapter 5.2. The two phases were strictly separated in two halves of volume. The lower part of the lattice from vertical co-ordinate $z = 0$ to $z = 50$ is filled in by water, and the top half from the co-ordinate $z = 51$ to $z = 99$ is filled in by air, as shown in Figure 5.3.2 for temperature parameter $k_B T = 0$. The temperature parameter includes Boltzman constant value k_B and thermodynamic temperature T [129]. There is no sphere of phase transition in the initial configuration, the phase volumes are separated and the dividing line $z = 50$. The simulation process is based on position exchange of liquid and air cells, the principle is described in Chapter 5.4. The behaviour of the model was simulated for different values of temperatures and the existence of sphere of phase transition was observed and its thickness was evaluated.

The configurations of the model after 500000 simulation steps for different temperature parameters are shown in Figure 5.3.2.

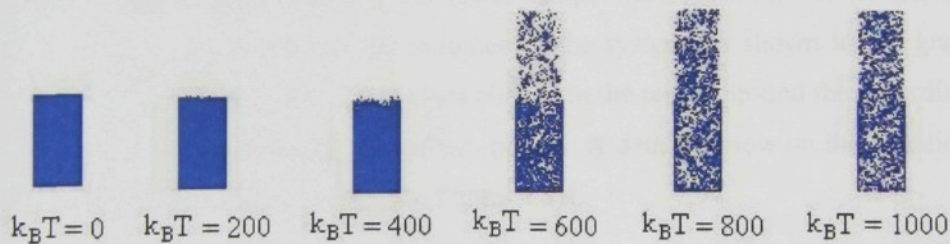


Figure 5.3.2: Configurations of two phase system after 500 000 simulation steps for different temperature parameters from $k_B T = 0$ to $k_B T = 1000$.

It is visible that for temperature parameter $k_B T = 1000, 800$ and 600 , liquid cells are dispersed in the whole volume of the system. For lower temperature parameter $k_B T = 400, 200$ and 0 , the liquid and air cells exchanged their positions only in a part of the whole volume. The exact results are derived from graphs of density of energy of the system in the horizontal levels.

The energies of particular levels were calculated as Hamiltonians (5.2.2) for cells in each horizontal level of the model. The density of energy is the energy of particular horizontal level related to the number of the cells in the level.

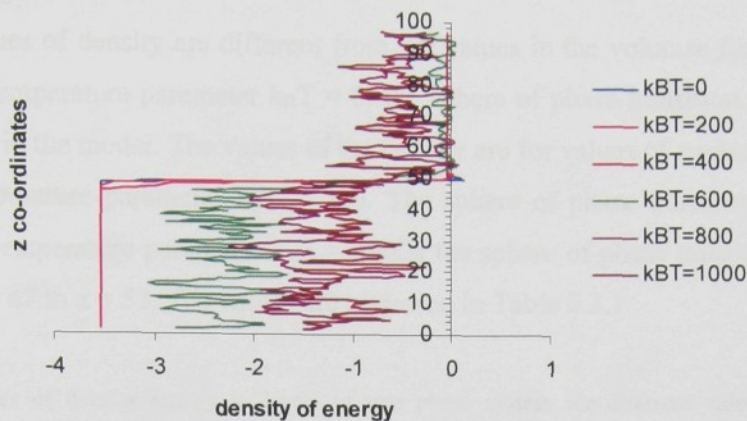


Figure 5.3.3: The density of energy in horizontal levels of the model of one component system containing liquid and air phase. The change of energy is observed for different temperature parameter $k_B T$.

The change in the behaviour of the system between values $k_B T$ 400 and 600 is visible in the graph above. For $k_B T = 600, 800$ and 1000 the values of density vary in the whole volume due to the liquid and air cells being dispersed. There is no sphere of phase transition for these temperatures. The situation is different for lower temperatures. The values of density of energy are constant in the liquid and air volumes of the system, as shown in the graph in Figure 5.3.3 for $k_B T = 0, 200$ and 400 . The values change in the region around the co-ordination $z = 50$, what was the initial dividing line of two phases. A detailed view on the situation the temperatures under 400 is shown in graph in Figure 5.3.4.

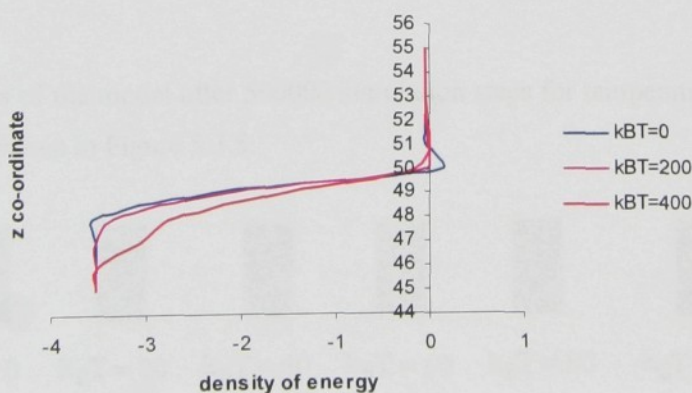


Figure 5.3.4: The density of energy between horizontal levels $z = 45$ and $z = 55$ of the model for one component system containing liquid and air phase. The change of energy is observed for different values of $k_B T$.

The line where the constant value of density of energy is disturbed is different for different temperatures.

The values of density are different from the values in the volumes for z co-ordinates 49 and 50 for temperature parameter $k_B T = 0$, the sphere of phase transition is very narrow, only two layers in the model. The values of the density are for values of z co-ordinates 49, 50, 51, 52 for temperature parameter $k_B T = 200$. The sphere of phase transition is five layers thick. And for temperature parameter $k_B T = 400$ is the sphere of phase transition thick seven layers, from $z = 47$ to $z = 53$. The values are reviewed in Table 5.3.1.

Table 5.3.1: Values of density energy in levels of two phase system for different values of temperature parameters $k_B T$.

z co-ordinate	$k_B T = 0$	$k_B T = 200$	$k_B T = 400$
44	-3.53846	-3.53846	-3.53846
45	-3.53846	-3.53846	-3.53846
46	-3.53846	-3.53846	-3.51124
47	-3.53846	-3.53846	-3.06775
48	-3.53846	-3.53846	-2.68994
49	-2.31361	-2.16391	-1.52027
50	0.107988	-0.05518	-0.14985
51	-0.03846	-0.0287	0.008728
52	-0.03846	-0.3521	-0.0287
53	-0.03846	-0.03846	-0.3683
54	-0.03846	-0.03846	-0.03846
55	-0.03846	-0.03846	-0.03846

The configurations of the model after 500000 simulation steps for temperatures from $k_B T = 0$ to $k_B T = 100$ are shown in Figure 5.3.5.

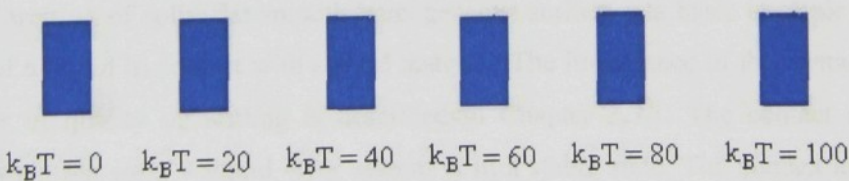


Figure 5.3.5: Configurations of two phase system after 500 000 simulation steps for different values $k_B T = 0$ to $k_B T = 100$.

The differences in distribution of values of density if energy for temperatures from $k_B T = 0$ to $k_B T = 100$ is not possible to recognize from graph, the curves are overlapped. The values are shown in Table 5.3.2. The values of the density are different from the values in the volumes for z co-ordinates 49 and 50 for $k_B T = 0$ and $k_B T = 20$, where the sphere of phase transition is very narrow, only two layers in the model.

Table 5.3.2: Values of density of energy in levels of the two phase system for different values of temperature parameter $k_B T$.

z co-ordinate	$k_B T = 0$	$k_B T = 20$	$k_B T = 40$	$k_B T = 60$	$k_B T = 80$	$k_B T = 100$
46	-3.53846	-3.53846	-3.53846	-3.53846	-3.53846	-3.53846
47	-3.53846	-3.53846	-3.53846	-3.53846	-3.53846	-3.53846
48	-3.53846	-3.53846	-3.53846	-3.52485	-3.51124	-3.52485
49	-2.31361	-2.31361	-2.34083	-2.3	-2.28639	-2.31361
50	0.107988	0.107988	0.111243	0.106361	0.0104734	0.02692
51	-0.03846	-0.03846	-0.03521	-0.03846	-0.03846	-0.03683
52	-0.03846	-0.03846	-0.03846	-0.03846	-0.03846	-0.03846
53	-0.03846	-0.03846	-0.03846	-0.03846	-0.03846	-0.03846

The values of the density are different from volume phases in z co-ordinates 49, 50 and 51 for temperature $k_B T = 40$, and in z co-ordinates 48, 49 and 50 for temperature parameter $k_B T = 60$, $k_B T = 80$ and $k_B T = 100$.

The simulation processes in the following chapters use chosen values between $k_B T = 0$ and $k_B T = 40$. The layer of transition is very low and the behaviour of liquids is appropriate to the behaviour of real liquids used in experimental works in laboratory conditions where the temperatures are between 20°C and 25°C.

5.4 Wetting of Homogeneous Surface

The wetting of solid flat smooth homogeneous surface is a basic example of mutual behaviour of a liquid in contact with a solid material. The importance of the contact angle as an indicator of quality of wetting is described in Chapter 3.3.1. The contact angle θ is measured when the solid – liquid – air system is in a stable state. The contact angle is the angle between the tangent to liquid – air interface and liquid - solid interface, as shown in Figure 3.3.1. The contact angle, as important characteristic for particular solid material and

concrete liquid, is used as a material parameter in Lucas – Washburn equation for study of liquid dynamics in single capillary (3.3.15).

5.4.1 Experimental Results of Contact Angle Measurement

The theses deals with the study of wetting and wicking characteristics of fibrous structures and one part of the experimental work and computer simulation is focused on dynamics of liquid motion on assemblies of propylene (PP) fibres, describe within Chapter 5.7. The dynamics is evaluated using Lucas – Washburn equation (3.3.15), where contact angle between PP fibre and testing liquid is used. The variant of contact angle measurement on flat surface from the equal material was chosen.

PP filaments from the company Mitop Mimon a.s. were used in experimental work [130]. The filaments of fineness 11 dtex were taken out from the spinning process straight after spinning and cooling process, before the application of surface agents or lubricants. It assures clear surface of filaments. The filaments were cut to the form of staple fibres and fibrous web was prepared using carding machine. The web was moulded on laboratory hydraulic press applying melting temperature of PP polymer, and PP foil was prepared. The foil was cleaned using inorganic solution to remove the surface contamination caused during foil preparation.

Pharmaceutical oil was used as testing liquid for experimental work. This kind of oil was chosen because of its excellent affinity to PP fibres and its low viscosity. These characteristics assure good wetting and fast transport of oil on the fibrous assemble, what is suitable for time effective experimental work and it eliminates the liquid evaporation, what could influence the quality of results. The parameters of pharmaceutivcal oil are in Table 5.4.1.

Table 5.4.1: Density, viscosity and surface tension of testing liquid.

	Density	Viscosity	Surface Tension
Pharmaceutical oil	$\rho = 884 \text{ kgm}^{-3}$	$\nu = 0.6392\text{St}$ $\eta = 0.0565 \text{ kgm}^{-1}\text{s}^{-1}$	$\gamma = 32.88 \text{ mNm}^{-1}$
Liquid drop volume	$0.0010 \text{ g} \pm 0.0001 \text{ g}$		

The suitable pipette was used to place finite oil volume, shown in Table 5.4.1, on horizontal foil surface. The drop in balance shape was captured and the contact angle was measured

using image analysis software LUCIA M, as shown in Figure 5.2.1B. Two values of contact angles are measured on each image, as shown in Figure 5.4.1. The results are shown in Table 5.4.2.

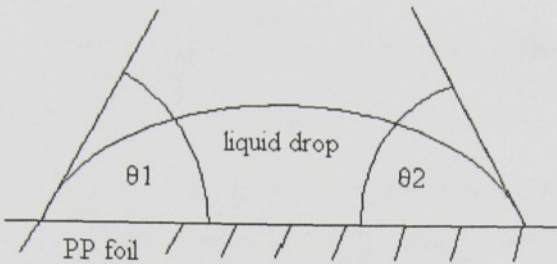


Figure 5.4.1: Two values of contact angle θ_1 and θ_2 are measured on a oil drop placed on surface of PP foil.

Table 5.4.2: Results of contact angle θ measured between pharmaceutical oil and PP foil.

	1	2	3	4	5	6	7	8	9	10	Average value [°]	Standard deviation [°]	Coefficient of variation [%]
θ_1 [°]	43	38	45	56	49	48	43	52	52	39			
θ_2 [°]	52	41	46	52	50	48	39	44	45	42	46.2	5.1	11.12

The value of contact angle between pharmaceutical oil and surface of PP foil is approximately 46°.

5.4.2 Computer Simulation of Wetting Process on Homogeneous Surface

The simulation process follows the results of the above mentioned experimental work. A hemispherical liquid drop was placed on a horizontal flat smooth surface and its behavior was recorded till the system reached an equilibrium state. The contact angle as a characteristic of wetting quality was evaluated [130].

The setting of values of exchange energies for simulation process was derived from real values of surface energy and liquid surface tension and liquid – solid interface tension. The value of oil surface tension is taken from Table 5.4.1. The surface energy of solid surface is taken from literature [131]. The value of contact angle is taken from experimental results

within Chapter 5.4.1 and the liquid – solid interface tension is calculated from Young equation (3.3.3).

Table 5.4.3: Values of surface tension and surface energies used for calculation of computer simulation constants.

Liquid surface tension	Solis surface energy	Contact angle	Liquid – solid interface tension
$\gamma = 32.88 \text{ mNm}^{-1}$	$\gamma_s = (29 - 30) \text{ J}\cdot\text{m}^{-2}$	46.2°	$\gamma_{sl} = (5.5 - 7.5) \text{ mNm}^{-1}$

The initial configuration of the model is shown in two cross sections in Figure 5.4.2. The contact angle between liquid surface and solids surface is 90° in initial configuration.

From the figures in Table 5.4.3, the values of exchange energies were calculated according to Equation (5.2.3). The values of constants for computer simulation are reviewed in Table 5.4.4.

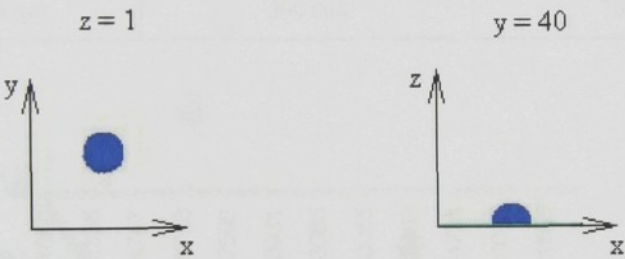


Figure 4.4.2: Initial configuration of the model in two sections.

The model of liquid drop with radius 6 lattice unit length achieved the equilibrium state after 300 000 simulation steps, the model of liquid drop with radius 10 lattice unit length achieved the equilibrium state after 700 000 simulation steps. The graph of energy thereafter plotted as shown in Figure 5.4.3.

Table 5.4.4: Values of computer simulation constants: dimensions of 3D lattice model, liquid drop radius, $k_B T$ – thermodynamic temperature parameter, C_g – gravitational constant, C_{aa} – exchange energy between two air cells, C_{al} – exchange energy between air cell and liquid cell, C_{as} – exchange energy between air cell and solid cell, C_{ll} – exchange energy between two liquid cells, C_{ls} – exchange energy between liquid cell and solid cell, C_{ss} – exchange energy between two solid cells.

3D lattice dimensions (x×y×z) [number of cells]	80×80×30	80×80×30
Drop radius [lattice unit length]	6	10
$k_B T$	30	30
C_g	10	10
C_{aa}	-10	-10
C_{al}	4	4
C_{as}	10	10
C_{ll}	-47	-47
C_{ls}	-31	-31
C_{ss}	-30	-30
Number of simulation steps	300 000	700 000

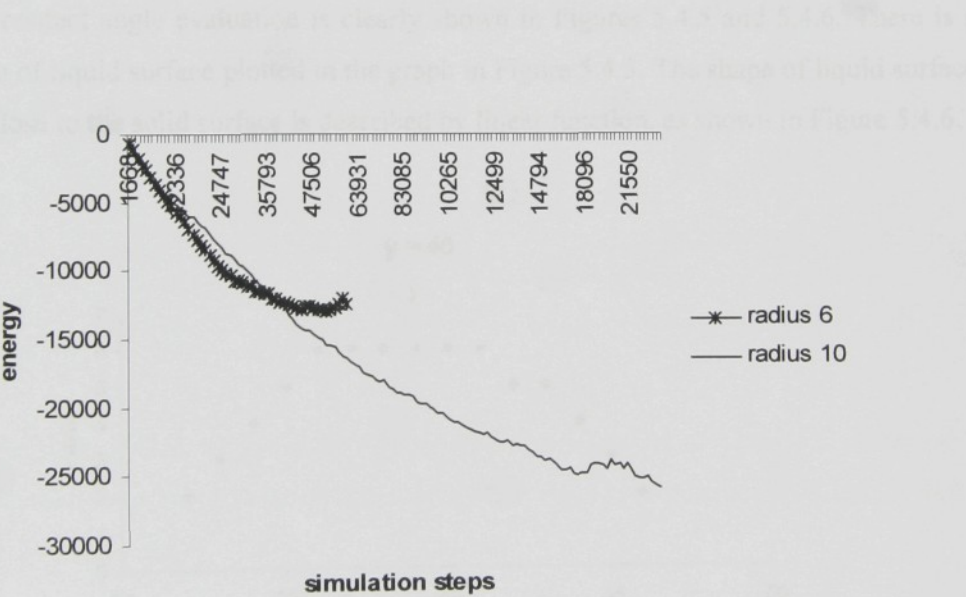


Figure 5.4.3: Decrease of energy during simulation process.

The final configurations of liquid drops are shown in figure 5.4.4.

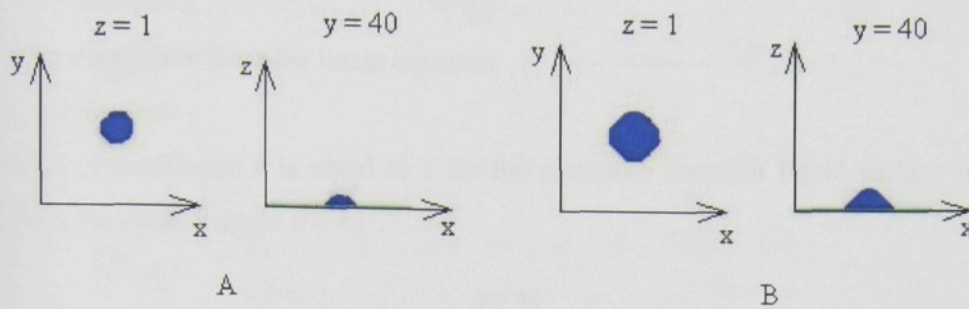


Figure 5.4.4: The final configuration of system. A – drop with initial radius 6 after 300 000 simulation steps, B – drop of initial radius 10 after 700 000 simulation steps.

From the comparison of Figure 5.4.2 and Figure 5.4.4 is clear that the liquid drop changed its shape, it means that the contact angle was changed.

5.4.2.1 Contact Angle Evaluation

The contact angle evaluation is clearly shown in Figures 5.4.5 and 5.4.6. There is a cross section of liquid surface plotted in the graph in Figure 5.4.5. The shape of liquid surface in the area close to the solid surface is described by linear function, as shown in Figure 5.4.6.

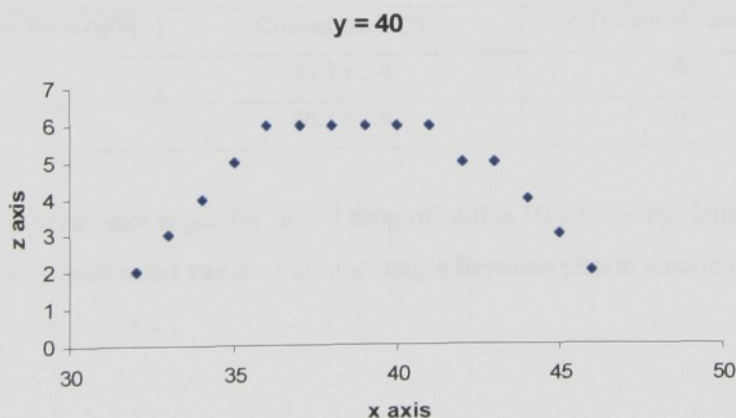


Figure 5.4.5: The shape of liquid surface in cross section.

The angle between the tangent of liquid surface and x – axis corresponds with the contact angle and it is calculated as

$$\theta = \arctan(k),$$

where k is coefficient from the linear equation

$$y = k \cdot x + l.$$

The value of coefficient k is equal to 1 for the particular shape of liquid surface in Figure 5.4.6, then the contact angle $\theta = 45^\circ$.

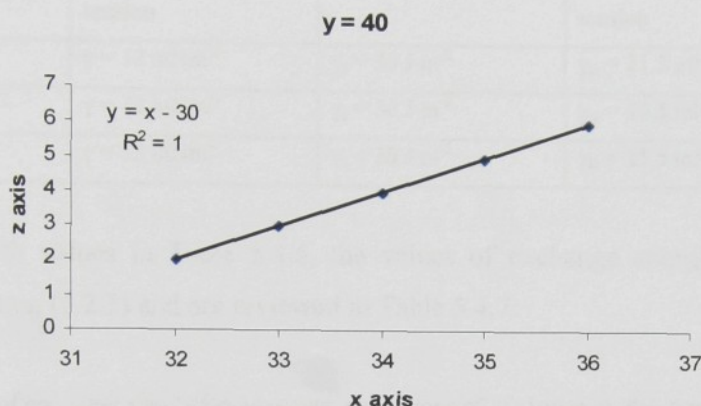


Figure 5.4.6: The shape of liquid surface in the vicinity of the horizontal solid surface.

The results of contact angle values for drops of two different diameters are in Table 5.4.5.

Table 5.4.5: Results of contact angle investigation from computer simulation.

Drop radius [lattice unit length]	Contact angle [°]	Coefficient of variation [%]
6	43.0 ± 3.6	8.3
10	46.3 ± 3.0	6.5

The value of contact angle for liquid drop of radius 10 lattice unit length is comparable with experimentally measured value of contact angle between pharmaceutical oil and PP solid surface shown in Table 5.4.2.

5.4.3 Influence of Interface Energy on Wetting of Homogeneous Surface

The influence of values of solid – liquid interface tension on the quality of wetting process are investigated using 3D lattice model. The values of solid - gas energy and liquid

surface tension are kept constant. Only the value of solid – liquid interface tension is changed, as shown in Table 5.4.6.

Table 5.4.6: Values of surface tension and surface energies used for calculation of computer simulation constants.

Sample	Liquid surface tension	Solis surface energy	Liquid – solid interface tension
A	$\gamma = 12 \text{ mNm}^{-1}$	$\gamma_s = 30 \text{ J}\cdot\text{m}^{-2}$	$\gamma_{sl} = 21.5 \text{ mNm}^{-1}$
B	$\gamma = 12 \text{ mNm}^{-1}$	$\gamma_s = 30 \text{ J}\cdot\text{m}^{-2}$	$\gamma_{sl} = 19.5 \text{ mNm}^{-1}$
C	$\gamma = 12 \text{ mNm}^{-1}$	$\gamma_s = 30 \text{ J}\cdot\text{m}^{-2}$	$\gamma_{sl} = 15.5 \text{ mNm}^{-1}$

In agreement with values in Table 5.4.6, the values of exchange energies are calculated according to relation (5.2.3) and are reviewed in Table 5.4.7.

Table 5.4.7: Values of computer simulation constants: dimensions of 3D lattice model, liquid drop radius, $k_B T$ – thermodynamic temperature parameter, C_g – gravitational constant, C_{aa} – exchange energy between two air cells, C_{al} – exchange energy between air cell and liquid cell, C_{as} – exchange energy between air cell and solid cell, C_{ll} – exchange energy between two liquid cells, C_{ls} – exchange energy between liquid cell and solid cell, C_{ss} – exchange energy between two solid cells.

Sample	A	B	C
3D lattice dimensions (x×y×z) [number of cells]	80×80×30	80×80×30	80×80×30
Drop radius [lattice unit length]	6	10	10
$k_B T$	30	30	30
C_g	10	10	10
C_{aa}	-2	-2	-2
C_{al}	1	1	1
C_{as}	14	14	14
C_{ll}	-21	-21	-21
C_{ls}	-4	-6	-10
C_{ss}	-30	-30	-30
Number of simul. steps	1 500 000	1 500 000	1 500 000

The initial configuration of the model is the same as in Figure 5.4.2. The system reaches the equilibrium state in 1.5 million simulation steps, as shown in the Figure 5.4.7.

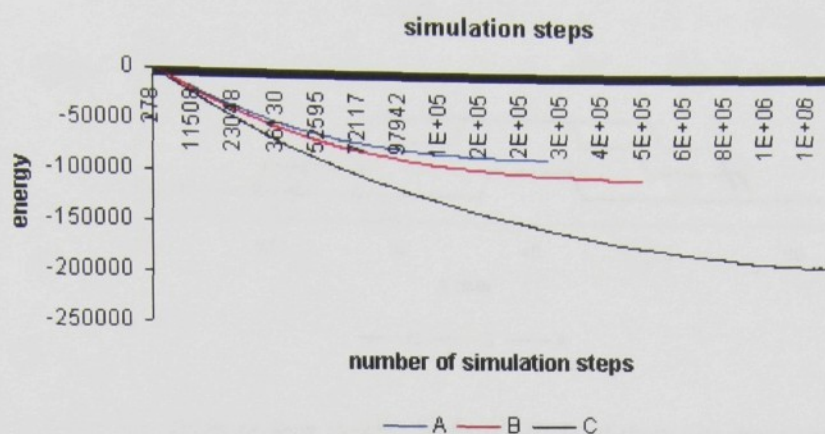


Figure 5.4.7: The energy of the model during the simulation process.

The final configurations in two cross-sections after 1.5 million simulation steps are shown in Figure 5.4.8, and the cross-sections of the surface curves of the drops in the final state are shown in Figure 5.4.9.

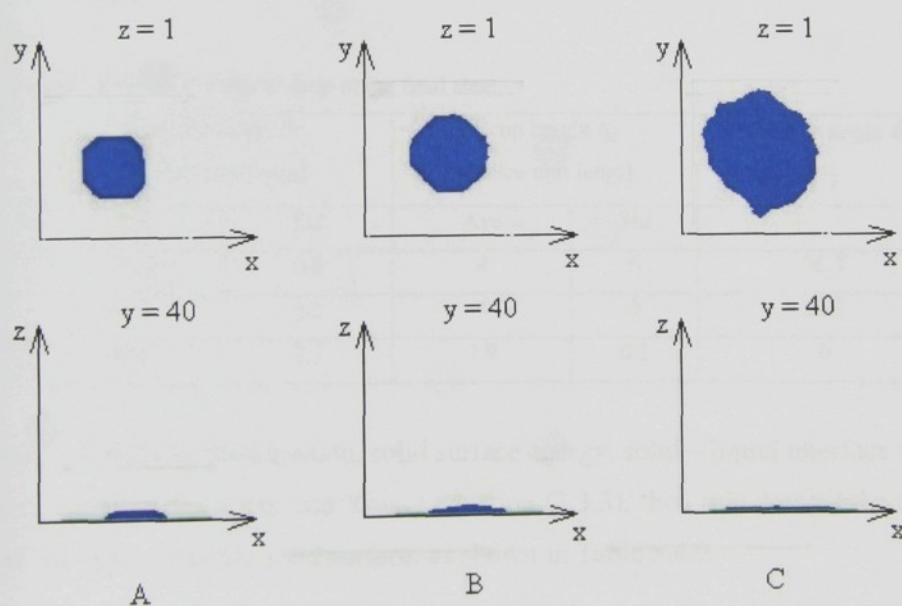


Figure 5.4.8: A – cross sections of the final shape of liquid drop on solid surface with solid – liquid interface tension $\gamma_{sl} = 21.5 \text{ mNm}^{-1}$, B – cross sections of final shape of liquid drop on solid surface with solid – liquid interface tension $\gamma_{sl} = 19.5 \text{ mNm}^{-1}$, C – cross sections of final shape of liquid drop on solid surface with solid – liquid interface tension $\gamma_{sl} = 15.5 \text{ mNm}^{-1}$.

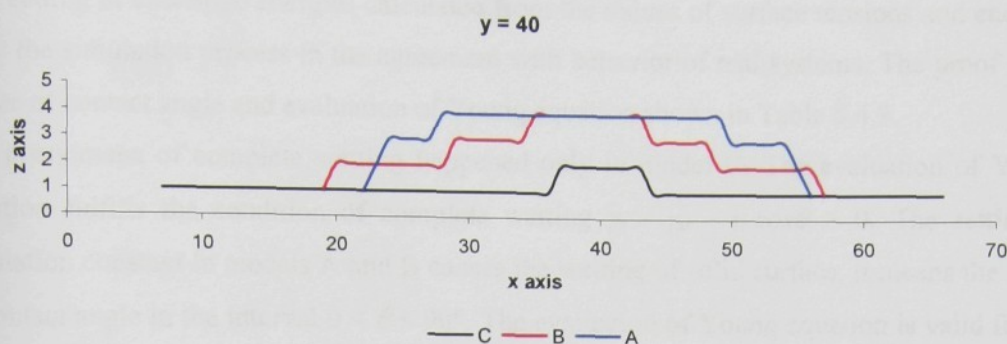


Figure 5.4.9: The curves of drop surfaces in cross section of drop. The drops are in final stable position after 1.5 million simulation steps.

The geometrical parameters of the shape of the drops were evaluated from the graph in Figure 5.4.9. The diameter $2r$ of the drop was measured in the bottom level, the height of the drop h , shown in Figure 3.3.2 in Chapter 3. The contact angle is calculated from the arctangent function of liquid surface and x – axis corresponds with the contact angle and it is calculated as shown in Chapter 5.4.2.1. The results are reviewed in Table 5.4.8.

Table 5.4.8: The parameters of liquid drop in the final state.

Sample	Drop diameter $2r$ [lattice unit length]		Drop height h_d [lattice unit length]		Contact angle θ [°]
	Ave	Std	Ave	Std	
A	32.6	0.8	4	0	36.7
B	41.3	2.2	4	0	24.3
C	60.6	2.7	1.9	0.3	0

If the values of liquid surface tension, solid surface energy, solid – liquid interface tension and the contact angle are institutes into Young equation (3.3.3), then it is derived the equation of balance of the liquid drop on solid surface, as shown in Table 5.4.9.

Table 5.4.9: The values of surface energy γ_s , solid – liquid surface tension γ_{sl} , liquid surface tension γ_l , contact angle θ and evaluation of Young equation $\gamma_s - \gamma_{sl} - \gamma_l \cdot \theta$.

	γ_s	γ_{sl}	γ_l	θ	$\gamma_s - \gamma_{sl} - \gamma_l \cdot \theta$
A	30	21.5	12	36.7	-1.37
B	30	19.5	12	24.3	-0.44
C	30	15.5	12	0	2.5

The setting of exchange energies calculated from the values of surface tensions and energies drive the simulation process in the agreement with behavior of real systems. The proof is the values of contact angle and evaluation of Young equation shown in Table 5.4.9.

The phenomena of complete wetting happened only in model C. The evaluation of Young equation fulfills the condition of complete wetting $\gamma_s - \gamma_{sl} - \gamma_l \cos \theta > 0$. The setting of simulation constant in models A and B causes the wetting of solid surface, it means the value of contact angle in the interval $0 < \theta < 90^\circ$. The evaluation of Young equation is valid for the case of incomplete wetting $\gamma_s - \gamma_{sl} - \gamma_l \cos \theta < 0$.

The results confirm the behavior of the model following the theoretically described phenomena of liquid drop placed on horizontal homogeneous substrate. The different values of solid – liquid interface tension cause the different shapes of liquid drops and then the different values of contact angles. The higher value of solid – liquid interface tension causes the higher value of contact angle and then the lower value of $\cos \theta$. This influences the total decrease of the left site of Young equation, what means the worse wetting of solid surface. The higher value of solid – liquid interface tension decreases the spreading ability of liquid on the solid surface.

5.5 Computer Simulation of Droplet Motion on a Heterogeneous Substrate

Experimental work investigating the behaviour of a liquid drop placed on a heterogeneous substrate is described in [132]. This behaviour is investigated using computer simulation is described within this chapter [133].

The simulation process described below presents a liquid drop motion on a heterogeneous horizontal flat solid surface. The liquid drop has hemispherical shape in the initial configuration. The substrate is composed from two different materials - hydrophilic primary flat surface and hydrophobic cross on the surface. In the beginning of simulation, the liquid drop is in an unstable state and it starts its motion on the substrate. It is completed when the liquid reaches the stable position on the substrate [131]. The results of this experiment will be achieved by computer simulation.

The initial configuration of the simulation model is shown in Figure 5.5.1. The basic solid plate has dimensions $114 \times 114 \times 1$. In the middle of the flat square is the centre of the cross. The cross divides the plate into four parts (I, II, III and IV) as marked in Figure 5.5.1. The wide of each cross stripe is given as one-third of droplet radius R , as shown in Figure 5.5.1A. The drop has hemispherical shape and its radius is $r = 21$ lattice unit. It is placed in position distanced $0.2 \cdot r$ upward and $0.1 \cdot r$ to the

right from the centre of the cross, as shown in Figure 5.5.1B. The smallest drop volume is placed in the part III of the solid plate, the biggest drop volume is placed in the part II of the solid substrate.

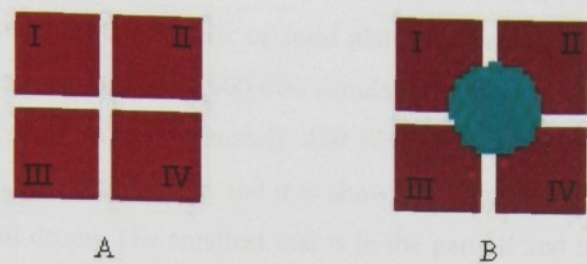


Figure 5.5.1: A - heterogeneous solid substrate, B – the initial track of drop on the substrate.

The parameters of computer simulation are reviewed in Table 5.5.1. The simulation ends after the model reaches stable state, which is after 500 000 simulation steps.

Table 5.5.1: Values of computer simulation constants: dimensions of 3D lattice model, liquid drop radius, $k_B T$ – thermodynamic temperature, C_g – gravitational constant, C_{aa} – exchange energy between two air cells, C_{a1} – exchange energy between air cell and liquid cell, C_{as1} – exchange energy between air cell and solid plate cell, C_{as2} – exchange energy between air cell and solid cross cell, C_{11} – exchange energy between two liquid cells, C_{1s1} – exchange energy between liquid cell and solid plate cell, C_{1s2} – exchange energy between liquid cell and solid cross cell, C_{s1s1} , C_{s2s2} – exchange energy between two solid cells.

3D lattice dimensions (x×y×z) [number of units]	115×115×22
Drop radius [lattice unit length]	21
$k_B T$	30
C_g	100
C_{aa}	-40
C_{a1}	26
C_{as1}	20
C_{as2}	-40
C_{11}	-26
C_{1s1}	-30
C_{1s2}	+120
C_{s1s1} , C_{s2s2}	0
Number of simulation steps	500 000

The track of the drop on the solid plate in the different simulation times is shown in Figure 5.5.2. The drop contracts inward along the hydrophobic cross and spreads on the hydrophilic plate, as shown in Figure 5.5.2A. The first part of drop volume is separated after 300 000 simulation steps on the part III of solid plate, shown in Figure 5.5.2B. The second part of drop volume is separated after 400 000 simulation steps, shown in Figure 5.5.2C. The last two parts are divided in approximately 450 000 simulation steps. The stable state is reached after 500 000 simulation steps and it is shown in Figure 5.5.2D. The drop volume is divided into four small drops. The smallest one is in the part III and the biggest one is in the part II.

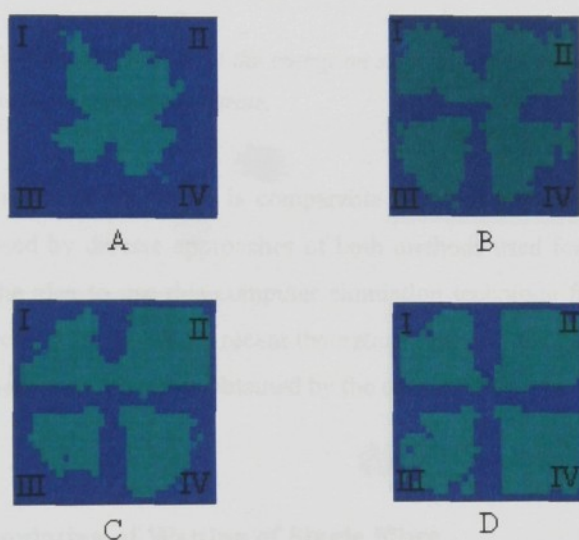


Figure 5.5.2: A - the drop contracting along the hydrophobic cross, B - the first part of the drop is separated after 300 000 simulation steps, C - the second part of drop is separated after 400 000 simulation steps, D - the drop is divided into four parts after 500 000 simulation steps.

The energy of system plotted versus the simulation time is shown in Figure 5.5.3. The drop spreads and the curve of energy decreases slowly. The fluctuations of the curve are caused by introduction of temperature in simulation process. After 300000 simulation steps, the drop starts to divide and the curve decreases more rapid. The liquid spreading stops after the state with minimal energy of system is achieved. The liquid drop is divided into four particles on the parts of the hydrophilic solid plate, as shown in Figure 5.5.3.

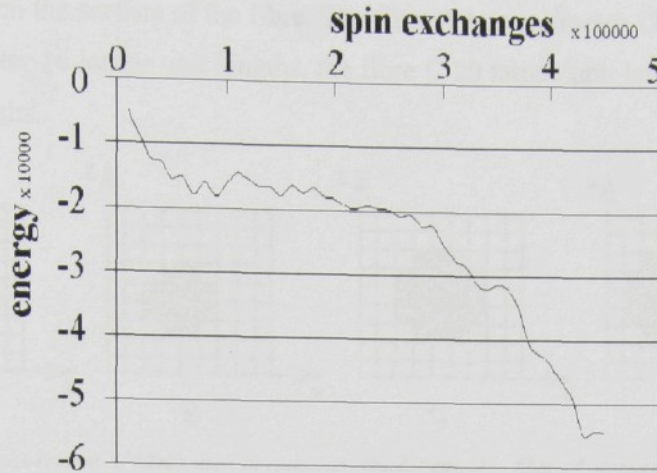


Figure 5.5.3: Graph of the dependence of the energy on simulation time during the simulation of the droplet motion on the heterogeneous substrate.

Monte Carlo simulation technique is comparable with the experimental results from [131]. The differences are caused by diverse approaches of both methods used for solving of this problem. These results support the idea to use this computer simulation technique for solution liquid contact with more complex fibrous systems, where recent theoretical descriptions do not exist. We can expect reliable accurate results of these processes obtained by the computer simulation.

5.6 Computer Simulation of Wetting of Single Fibre

The wetting of single fibre is theoretically described in Chapter 3.3.2. From the comparison of conditions for complete wetting of a flat surface (3.3.4) and a single fibre (3.3.7) is concluded following: if the flat surface is wetted by concrete liquid, the single fibre could not discharge condition of complete wetting [45]. The shape of surface influences the ability of the surface to be wet by a liquid.

The conclusion was not possible to establish experimentally. The computer simulation was used to investigate behaviour of a liquid drop placed on a single fibre. The condition of complete wetting (3.3.7) depends only on the geometrical parameters of fibre and liquid body, and on the liquid surface tension. The fibre cross-section was chosen as a variable for the computer simulation. The computer simulation was done on fibres of four different cross sections, as shown in Figure 5.6.1. The surface area of the fibre is the parameter influencing the wetting quality. The perimeter of the fibres in computer simulation is done as a sum of the

lattice unit length on the surface of the fibre. The fibre A has perimeter 12 lattice unit lengths, fibre B has perimeter 16 lattice unit lengths, the fibre C 20 lattice unit lengths and the fibre D 28 lattice unit lengths.

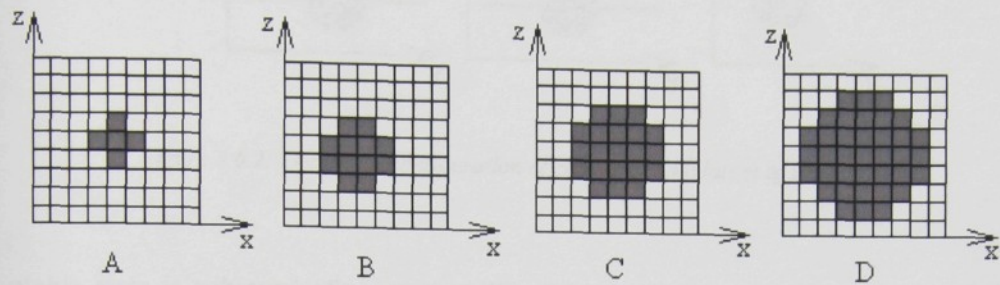


Figure 5.6.1: The cross-section of fibres used in computer simulations. A – fibre of perimeter 12, B – fibre of perimeter 16, C – fibre of perimeter 20 and D – fibre with perimeter 28.

The compute simulation constants were set up as in computer simulation in Chapter 5.4 for simulation of liquid drop on flat surface, as shown in Table 5.6.1.

Table 5.6.1: Values of computer simulation constants: dimensions of 3D lattice model, liquid drop radius, $k_B T$ – thermodynamic temperature parameter, C_g – gravitational constant, C_{aa} – exchange energy between two air cells, C_{al} – exchange energy between air cell and liquid cell, C_{as} – exchange energy between air cell and solid cell, C_{ll} – exchange energy between two liquid cells, C_{ls} – exchange energy between liquid cell and solid cell, C_{ss} – exchange energy between two solid cells.

3D lattice dimensions (x×y×z)	40×100×40	40×100×40	40×100×40	40×100×40
[number of cells]				
Fibre perimeter [lattice unit length]	12	16	20	28
Drop radius	15	15	15	15
$k_B T$	30	30	30	30
C_g	10	10	10	10
C_{aa}	-10	-10	-10	-10
C_{al}	4	4	4	4
C_{as}	10	10	10	10
C_{ll}	-47	-47	-47	-47
C_{ls}	-31	-31	-31	-31
C_{ss}	-30	-30	-30	-30
Number of simulation steps	7 000 000	7 000 000	7 000 000	7 000 000

The contact angle between liquid surface as a indicator of the quality of wetting of single fibre. The spherical drop was placed on a single horizontal fibre in the beginning of computer simulations. The initial configuration is shown in Figure 5.6.2.

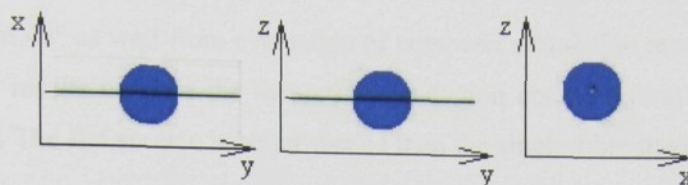


Figure 5.6.2: The initial configuration of computed simulation of fibre A.

The stable state is achieved after seven million simulation steps and the contact angle was measured as described in Chapter 5.4.2.1. The final configurations are shown in Figure 5.6.3.

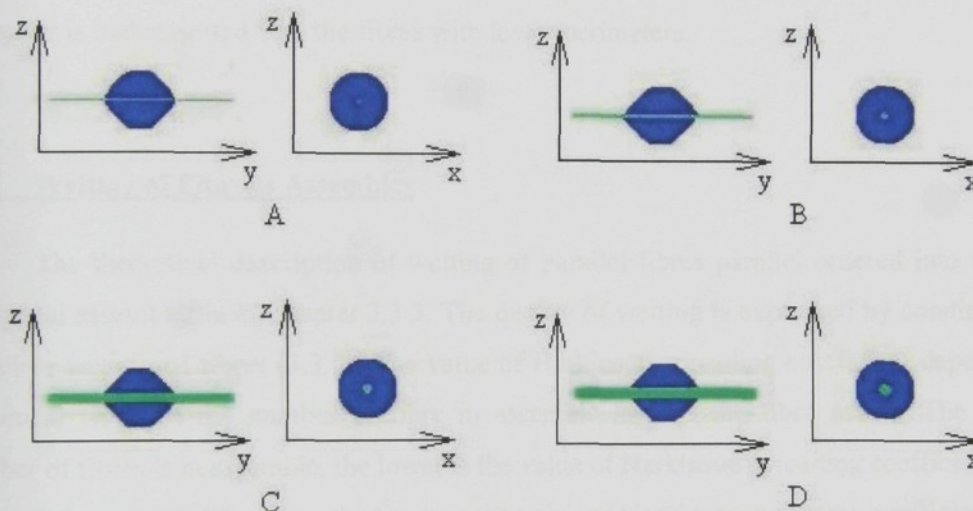


Figure 5.6.3: The final configurations of fibres with different cross section after 7 million simulation steps.

The results of contact angle measurement are reviewed in tabulated 5.6.2.

Table 5.6.2: The values of contact angle for fibres of different cross section, as shown in Figure 5.6.1.

	A	B	C	D
Contact angle [°]	61.3	57.4	54.9	55.5
St dev	2.7	3.4	3.9	4.0

The values of contact angle for all four types of fibres A, B, C, D are higher than the values of contact angle investigated in Chapter 5.4 on the flat surface from the same polymer.

The value of contact angle measured in experimental work is about 46° , as shown in Table 5.4.1, and it is about 46° as well from evaluation of computer simulation results, as shown in Table 5.4.5. These results confirm the theoretical prediction about wetting of single fibres from Chapter 3.3.2. The flat surface is better wetted than the single fibre made from the same polymer.

The results are in agreement with the condition of complete wetting of a single fibre (3.3.7). The quality of wetting is expressed using Harkinson spreading coefficient S_c . Harkinson spreading coefficient S_c depends on the reciprocal value of fibre radius. The higher is the fibre radius, the lower is S_c , it means better wetting of fibres of higher radius and then higher perimeter in cross section. From the results reviewed in Table 5.6.2 is apparent the decreasing contact angle with increasing perimeter of cross section. The fibre D with highest perimeter is better wetted than the fibres with lower perimeters.

5.7 Wetting of Fibrous Assemblies

The theoretical description of wetting of parallel fibres parallel ordered into fibrous horizontal assemblies is in Chapter 3.3.3. The quality of wetting is expressed by condition for complete wetting of fibres (3.3.9). The value of Harkinson spreading coefficient depends on reciprocal value of the number of fibre in assemble and on the fibre radius. The higher number of fibres is in assemble, the lower is the value of Harkinson spreading coefficient. The bigger is the radius of the fibre, the lower is the value of Harkinson spreading coefficient. The lower coefficient is, the better a liquid wetting of the fibrous assemble.

5.7.1 Wetting of Assemblies from Parallel Filaments

The experimental work [134] was done on PP filaments of parameters mentioned in the Chapter 5.4. The filaments of different fineness were used as shown in Table 5.7.1. The filaments were taken out from spinning process straight after spinning and cooling process, before application of surface agents or lubricants. It assures clear surface of filaments.

Table 5.7.1: Parameters of PP filaments.

PP filaments	Fineness [dtex]	Fibre diameter [μm]
1	6.7	30.6
2	11	39.3
3	17	48.8

The used testing liquid is pharmaceutical oil of characteristic reviewed in Table 5.4.1.

Assembles of 13 fibres were stretched over a plastic frame with scale for length measurement.

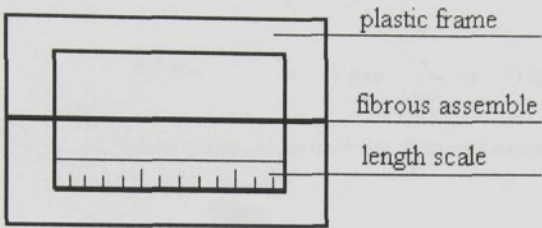


Figure 5.7.1: The parallel filaments in assemble stretched over plastic frame.

The testament was placed in the microscope connected to digital camera and computer with software for image analysis. The drop of testing liquid was placed on fibrous assemble and the liquid motion was recorded using digital camera.

The speed of liquid motion on fibrous assemble was evaluated as distance h_a between liquid drop and the liquid front moving on assemble against square root of time according to Lucas – Washburn equation (3.3.15). The graph is plotted in Figure 5.7.2.

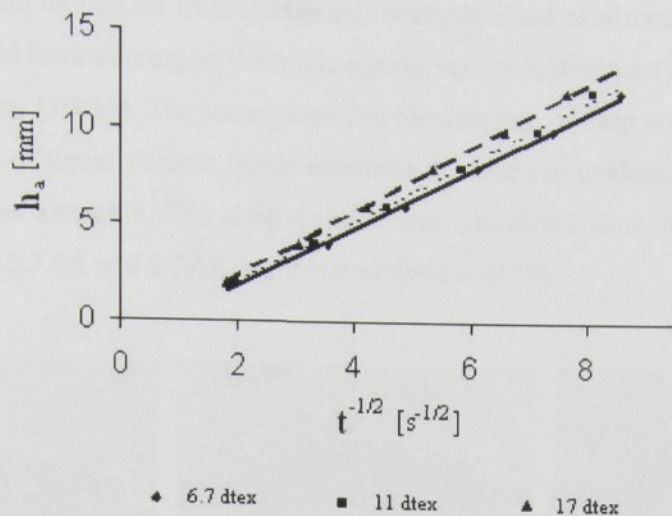


Figure 5.7.2: The speed of liquid transport on horizontal fibrous assemblies from fibres of different fineness.

From the graph in Figure 5.7.2 is clear that the liquid moves fastest on assemblies from coarse fibres of 17 dtex and slowest on assemblies from fine fibres of 6.7 dtex.

The filaments of 11 dtex were used in experimental work where the influence of number of fibres in assemblies was investigated [135]. Assemblies of 5, 7, 10 and 15 filaments were stretched over plastic frames and the equal experimental technique was used for recording of the wetting process. The different method was used for liquid transport speed on assemblies. After the liquid drop was placed on assemble, the decreasing drop volume was recorded till the drop completely penetrated into assemble. The sequences of drop on assemble in five different times are shown in Figure 5.7.3. The method of drop volume evaluation using image analysis is described in [135].

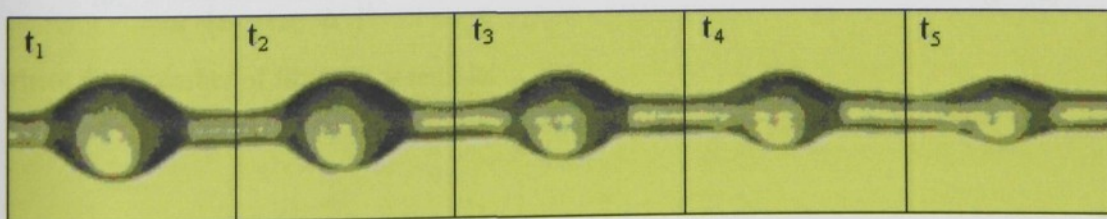


Figure 5.7.3: The sequences of liquid drop on fibrous assemble recorded in five different times from t_1 to t_5 .

The speed of liquid motion on fibrous assemble was evaluated as distance h_v between liquid drop and the liquid front moving on assemble against square root of time according to Lucas – Washburn equation (3.3.15). The assumption that the decrease of drop volume on assemble is equal to increase of liquid volume inside assemble was used to evaluate the speed of liquid motion on fibrous assemble. The drop volume was calculated from the drop dimensions marked in Figure 5.7.4A and 5.7.4B and it is described in [123].

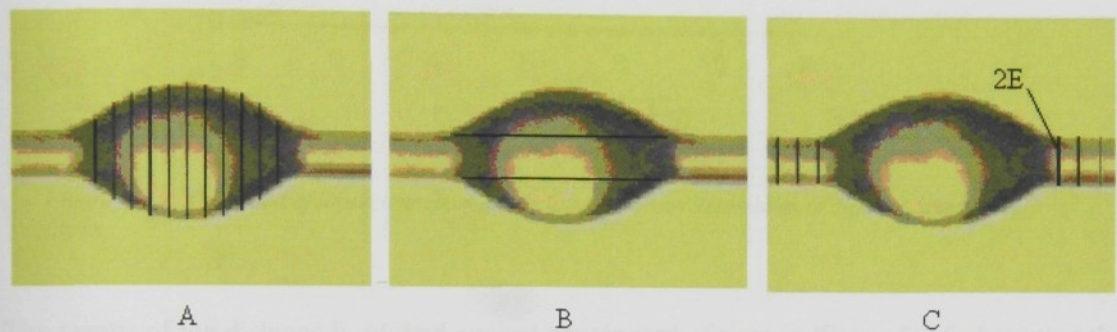


Figure 5.7.4: The parameters of liquid drop on fibrous assemblies measured using image analysis.

The increase of distance of moving liquid front on the assemble dh_v was calculated from the decrease of drop volume dV_d :

$$dh_v = \frac{dV_d}{A_p}, \tag{5.7.1}$$

where A_p is the total pore area in cross section of assemble, and it is calculated from Equation (3.4.2). The radius E of assumed cylindrical liquid body around an assemble is measured from the experimental picture using image analysis as shown in Figure 5.7.4.C, and the fibre radius b is the half of fibre diameter from Table 5.7.1. Then the distance of moving on assemble is

$$dh_v = \frac{dV_d}{\pi \cdot (E^2 - n_v \cdot b^2)}, \tag{5.7.2}$$

where n_v is number of fibres in assemble.

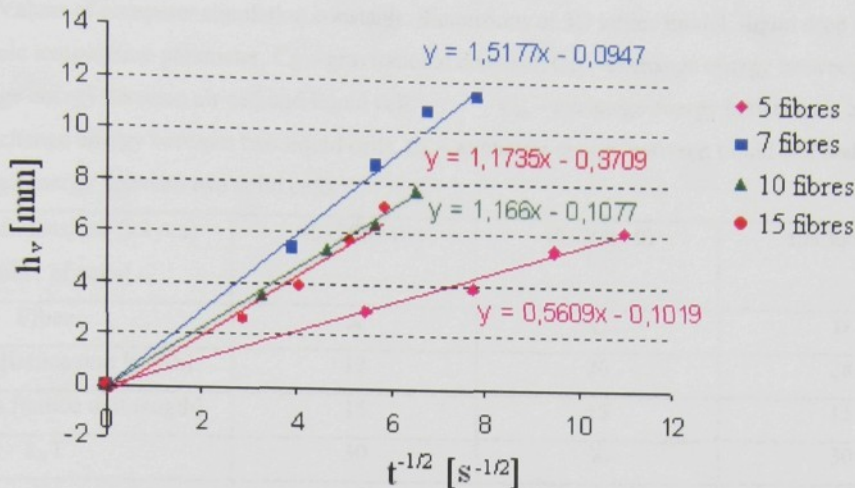


Figure 5.7.5: The speed of liquid transport on horizontal fibrous assemblies of different number of fibres.

The results of the distance h_v plotted against square root of time in Figure 5.7.5 show that the higher is number of fibres in an assemble the faster is liquid motion.

The both conclusions from above mentioned experimental works are in agreement with the condition of complete wetting of fibre assemblies (3.3.9), it means that the higher fibre radius and the higher number of fibres in the assemble improve the wetting of the assembles.

Any detailed analysis of liquid motion on fibrous assemble is not possible from available experimental techniques. The computer simulation has been used to investigate liquid motion inside porous space of fibrous assemblies in Chapter 5.7.2.

5.7.2 Computer Simulation of Wetting of Fibrous Assemblies

Fibres of three different fibre cross sections were chosen for computer simulation. Fibre A is shown in Figure 5.6.1A, fibre C is shown in Figure 5.6.1C and fibre D is shown in Figure 5.6.1D. The computer simulation constants were set up as in computer simulation in Chapter 5.4 and 5.6, as shown in Table 5.7.2. The fibres were ordered in assemblies of two, three and seven fibres, as shown in Figures 5.7.7, 5.7.8 and 5.7.9.

Table 5.7.2: Values of computer simulation constants: dimensions of 3D lattice model, liquid drop radius, $k_B T$ – thermodynamic temperature parameter, C_g – gravitational constant, C_{aa} – exchange energy between two air cells, C_{al} – exchange energy between air cell and liquid cell, C_{as} – exchange energy between air cell and solid cell, C_{ll} – exchange energy between two liquid cells, C_{ls} – exchange energy between liquid cell and solid cell, C_{ss} – exchange energy between two solid cells.

3D lattice dimensions (x×y×z) [number of cells]	40×300×40	40×300×40	40×300×40
Fiber	A	C	D
Perimeter [lattice unit length]	12	20	28
Drop radius [lattice unit length]	15	15	15
$k_B T$	30	30	30
C_g	10	10	10
C_{aa}	-10	-10	-10
C_{al}	4	4	4
C_{as}	10	10	10
C_{ll}	-47	-47	-47
C_{ls}	-31	-31	-31
C_{ss}	-30	-30	-30
Number of simulation steps	3 000 000	3 000 000	3 000 000

The spherical drop was placed on horizontal fibrous assemblies is shown in an initial configuration of assemble designed from seven fibres of shape D in Figure 5.7.6.

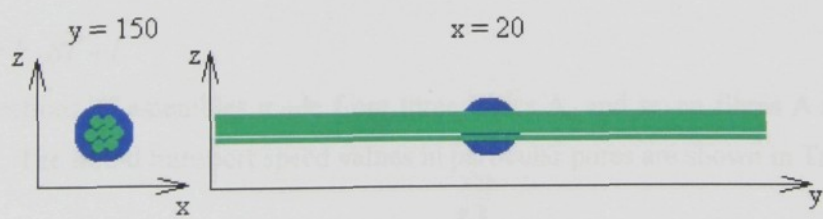


Figure 5.7.6: Initial configuration of computer simulation of liquid motion on fibrous assemble.

The contact angle was evaluated as a indicator of quality of wetting described in Chapter 5.4 and shown in Figure 5.4.7. The results are reviewed in Table 5.7.3. The values of contact angle on single fibres are taken from Table 5.6.2 in Chapter 5.6.

Table 5.7.3: Results of contact angle investigation from computer simulation on fibres of different cross section.

Contact Angle	A		B		C	
	Ave	Std	Ave	Std	Ave	Std
1 fibre	61.3°	2.7°	54.9°	3.9°	55.5°	4.0°
2 fibres	54.9°	5.2°	47.5°	5.6°	45.6°	5.7°
3 fibres	51.1°	7.8°	45.5°	4.5°	39.2°	6.7°
7 fibres	50.6°	8.5°	48.4°	11.4°	0°	0°

The values of contact angle decrease with bigger fibre diameter and with higher number of fibres in assemble. This dependency is in agreement with the condition of complete wetting of fibre assembles (3.3.9), it means that the higher fibre radius and the higher number of fibres in assemble improve the wetting of the assembles.

The computer simulation was also oriented on the evaluation of speed of liquid transport on fibrous assembles. The advantage of computer simulation in comparison with experimental investigation is the evaluation of the liquid motion inside structure of assemble, inside the pore space, which is not observable using microscopic technique. The assembles of three and seven fibres of fibres A, C and D are shown in Figure 5.7.7, 5.7.8, 5.7.9, respectively. The pores where the liquid motion was investigated are marked in the Figures. The liquid transport was evaluated according to Lucas – Washburn equation (3.3.15). The square value y^2 of y co-ordinate of moving liquid inside the pore was plotted against simulation time ST . The speed of liquid motion is equal to the coefficient k from linear function

$$y^2 = k \cdot ST + l. \tag{5.7.3}$$

The cross-sections of assembles made from three fibres A, and seven fibres A are shown in Figure 5.7.7. The liquid transport speed values in particular pores are shown in Table 5.7.4

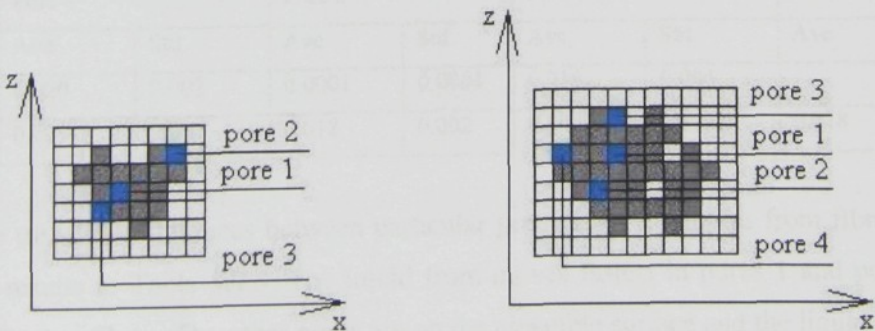


Figure 5.7.7: The cross-section of fibrous assembles from three and seven fibres A.

Table 5.7.4: Values of speed of liquid motion if assemblies from fibres A.

Fibre A	Pore 1		Pore 2		Pore 3		Pore 4	
	Ave	Std	Ave	Std	Ave	Std	Ave	Std
3 fibres	0.010	0.001	0.0006	0.0003	0.0003	0.0002		
7 fibres	0.014	0.001	0.011	0.001	0.0003	0.0001	$3 \cdot 10^{-5}$	$8 \cdot 10^{-5}$

The liquid front moves fastest in pore 1 on assemblies of three and seven fibres as well, and in pore 2 in assemble of seven fibres. In these pores, the liquid is surrounded mostly by fibres. The pores 3 and pore 4 are on the surface of assemble, surrounded by air also. Presence of air cells in the vicinity of liquid cells decreases the ability of liquid movement.

The assemblies designed from fibres C are shown in Figure 5.7.8.

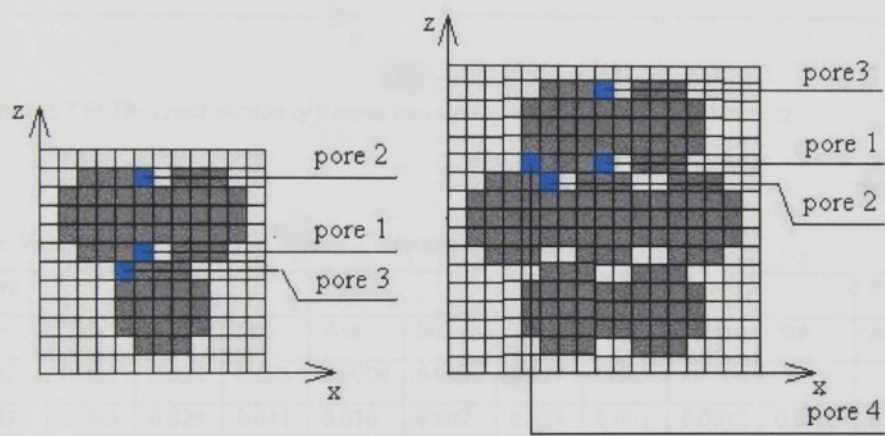


Figure 5.7.8: The cross- section of fibrous assemblies from three and seven fibres C.

Table 5.7.5: Values of speed of liquid motion if assemblies from fibres C.

Fibre C	Pore 1		Pore 2		Pore 3		Pore 4	
	Ave	Std	Ave	Std	Ave	Std	Ave	Std
3 fibres	0.020	0.002	0.0001	0.0001	0.016	0.004		
7 fibres	0.029	0.004	0.018	0.002	0.0003	0.0002	0.018	0.002

The same trend of differences between particular pores as in assemblies from fibre C is clear from the results in Table 5.7.5. The liquid front moves fastest in pores 1 and pore 2 in the bundle of seven fibres. The other pores are on the assemble surface and the liquid moves very slowly. Generally, the liquid moves faster on assemblies designed from coarser fibre C.

The assemblies designed from fibres D are shown in Figure 5.7.9.

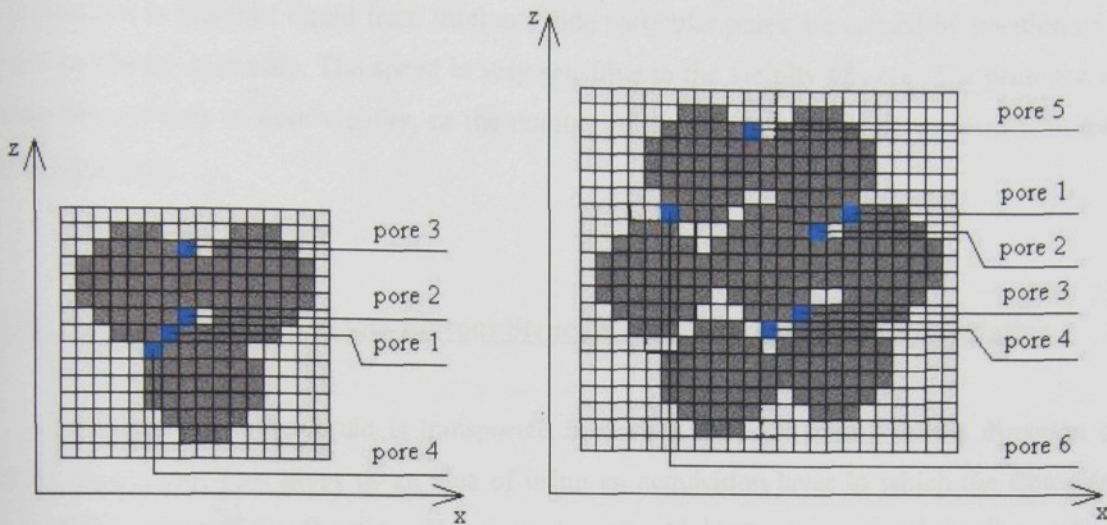


Figure 5.7.9: The cross-section of fibrous assemblies from three and seven fibres D.

Table 5.7.6: Values of speed of liquid motion if assemblies from fibres D.

Fibre D	Pore 1		Pore 2		Pore 3		Pore 4		Pore 5		Pore 6	
	Ave	Std	Ave	Std	Ave	Std	Ave	Std	Ave	Std	Ave	Std
3 fibr	0.025	0.003	0.024	0.003	0.0009	0.0004	0.017	0.005				
7 fibr	0.027	0.003	0.029	0.011	0.030	0.002	0.029	0.002	0.0012	0.0003	0.026	0.003

The fastest liquid motion is in the pores 1 and 2, and pore 3 in the assemble of seven fibres. Again, these are pore inside the assemble structure. The trend is same as in above mentioned assemblies from finer fibres. The assemble from coarse fibres D transport liquid slightly faster than finer fibres C and A.

The conclusions from above mentioned experimental works are in agreement with the condition of complete wetting of fibre assemblies (3.3.9), it means that the higher fibre radius and the higher number of fibres in the assemble improve the wetting of the assemblies.

The computer simulation shows the advantage of computer simulation for investigation of liquid behaviour inside fibrous structure, where the phenomena is not observable using recently available methods. The computer simulation shows that whilst the

liquid keeps the drop shape on assemble, it seems like the liquid does not wet the fibrous structure, the liquid motion inside the pores of the assemble is present and very fast. The differences in speed of liquid front motion inside particular pores are caused by position of a pore in fibrous assemble. The speed is very sensitive to the vicinity of pore. The presence of only fibrous cells in pore vicinity, or the number of air cells present in pore vicinity, makes the difference.

5.8 Liquid Penetration into Fibrous Structures of Different Fibrous Orientation

It is known that the liquid is transported in fibrous structure mainly in the direction of fibre orientation. This gives us an idea of using an acquisition layer in which the fibres are oriented in the vertical direction. The technology for highloft nonwoven production, where vertical folds from fibre web are created and thermally bonded, was developed about 15 years ago at the Technical University of Liberec [136] which is commercially known as Struto®. This structure was compared with cross laid thermally bonded fibre web of the same composition. Both structures were compared in their abilities of liquid acquisition in the vertical direction and liquid distribution in the horizontal direction.

5.8.1 Liquid acquisition and Liquid Distribution

The density of samples was 40 kg.m⁻³ [137]. This value corresponds with the density of commercially used acquisition/distribution layers. Two different base fibres were used in samples, as shown in Table 5.8.1 and four different compositions of fabric were produced, as shown in Table 5.8.2.

Table 5.8.1: Parameters of fibres used in nonwoven structures.

	Fibre	Finesses [dtex]	Length [mm]	Metling point [°C]
Base fibre	PET	11	60	256
	PET	17	80	256
Bonding fibre	PET/coPET	5.2	50	130-140

Table 5.8.2: Characteristics of tested samples.

Finesses of base fibres	Base fibres / bonding fibres [%]	Predominant fibre orientation
11 dtex	80/20	Cross direction
	80/20	Vertical direction
17 dtex	80/20	Cross direction
	80/20	Vertical direction

The 0.9 % aqueous solution of NaCl of surface tension $\gamma = 52.158 \pm 0.666 \cdot 10^{-3} \text{N/m}$ was chosen according to EDANA standards for testing hygiene products [138]. The solution was dyed. The liquid surface tension γ of baby urine is $45 \cdot 10^{-3} \text{N/m}$, and of adult urine is $69 - 70 \cdot 10^{-3} \text{N/m}$ at temperature 20°C .

The liquid acquisition, transport in the vertical direction from the top to the bottom of the sample, was measured according to EDANA standard method of Liquid strike – through time [136]. The experimental set up is shown in Figure 5.8.1.

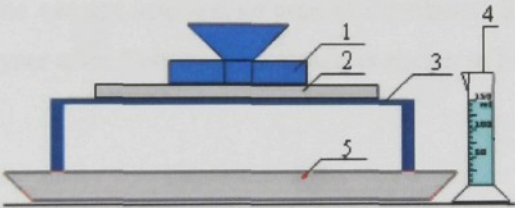


Figure 5.8.1: The experimental set up for measuring acquisition speed. Dosing device (1) is placed onto sample of fabric (2) laying on supporting grate (3). The liquid volume (4), 150 ml of 0.9% NaCl is poured into dosing device in the beginning of the measurement. The liquid goes through the sample and supporting grate and is collected in a vessel (5).

The sample of width 100 mm, length 200 mm and height 13.6 mm was placed on supporting grille. On the top of sample was placed the dosing perspex vessel weighing 512.9 g. The dosed testing liquid volume was 150 ml. The decreasing height of liquid level, calculated from decreasing level of volume of liquid in the vessel, was plotted against time and evaluated as a liquid acquisition speed [m/sec], as shown in Figure 5.8.2.

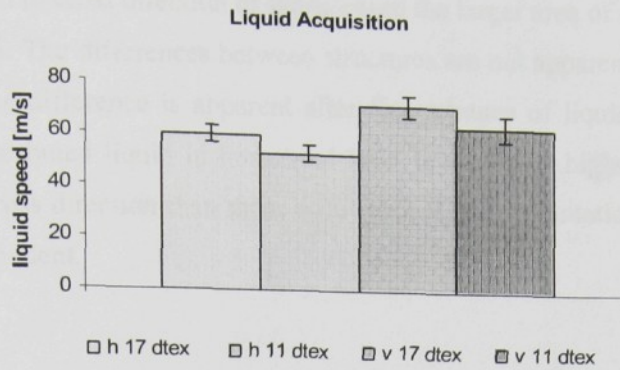


Figure 5.8.2: Liquid acquisition speed into different fibrous structures. The acquisition speed [m/sec] is calculated from the decreasing height of liquid level in the dosing vessel in given time of experimental observations.

The sample of width 100mm, length 200mm and height 13.6 mm was placed on the glass board. The video camera was placed under the board. The calibration scale was fixed on the board in the camera side. 10ml of testing liquid was dosed on the top of the sample from the pipette of flow 0.8 ml/s. The camera scanned an area of distributed liquid. The results were evaluated using image analyser after 5 sec and 5 minutes as shown in Figure 5.8.3.

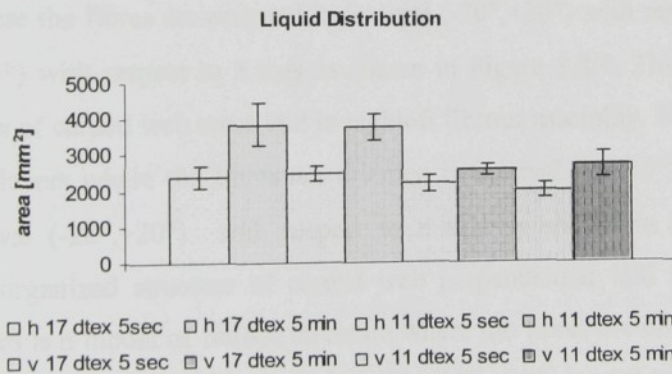


Figure 5.8.3: The graph of distributed liquid in horizontal direction of different fibrous structures measured in 5 seconds and 5 minutes after liquid dosing.

The vertical orientation of fibrous web in nonwoven structure causes the faster liquid acquisition through the fabric in the vertical direction. The fabrics of the same volume density and produced from fibres of different fineness have different pore size distribution.

The fibres oriented in cross direction of fabric cause the larger area of distributed liquid as shown in Figure 5.8.3. The differences between structures are not apparent after 5 seconds of the measurement. The difference is apparent after five minutes of liquid transport process, when the area of distributed liquid in horizontal level is 1.2 times higher for samples with fibre orientation in cross direction than those with vertical fibre orientation. The influence of fibre fineness is not evident.

5.8.2 Computer Simulation of Liquid Penetratin Process

The configuration of simulation process was set up similar to the real system in experimental work [139]. The fabric structure is idealized but preserves the main differences in parameters of experimental samples. The volume of fibres in the unit volume corresponds to the density of fabric 40 kg/m^{-3} , the ratio of a fibre diameter to fibre length is set up close to real fibre diameters and lengths. The different shapes of fibre in experiment and computer simulation cause the difference in surface area of fibres. The quotient of surface area between 17dtex and 11 dtex fibres is 1.25 in experiment. This ratio is 1.5 in the model. The orientation of fibres in the three dimensional lattice is organized in three ways. The first is a model of fibrous layers where the fibres are oriented in interval $(-20^\circ, +20^\circ)$ with respect to x axis and in interval $(-5^\circ, +5^\circ)$ with respect to z axis as shown in Figure 5.8.4. This simulates highly organized structure of carded web cross laid in highloft fibrous assembly. The second way is a model of fibrous layers where the fibres are oriented in interval $(-5^\circ, +5^\circ)$ with respect to y axis and in interval $(-20^\circ, +20^\circ)$ with respect to z axis as shown in Figure 5.8.5. This simulates highly organized structure of carded web perpendicular laid in highloft fibrous assembly. The third is a model of fibrous structure where the fibres are oriented in interval $(-45^\circ, +45^\circ)$ with respect to y axis and in interval $(-45^\circ, +45^\circ)$ with respect to z axis as shown in Figure 5.8.6. This simulates randomly organized structure of fibrous assembly. This structure is used only in computer simulation. The weight of the perspex vessel placed on the sample in experimental measurement can change the density of fabric, however, it was not taken into account in simulation. The defined volume of liquid was placed on fabric and was surrounded by "glass" cells, since these cells do not affect calculation of Hamiltonian (5.2.2).

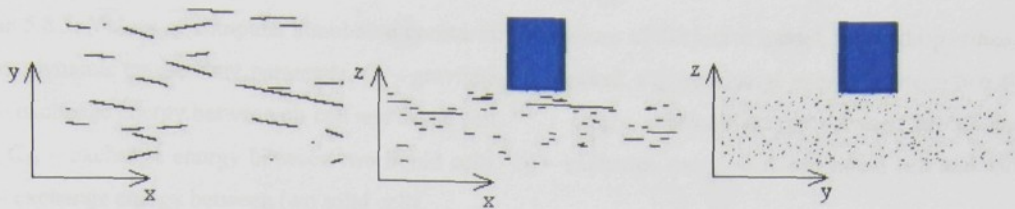


Figure 5.8.4: The initial configuration of 3D lattice model for simulation of cross-laid highloft fibrous structure. The liquid volume is closed in a "glass vessel" and placed up to the fibre structure.

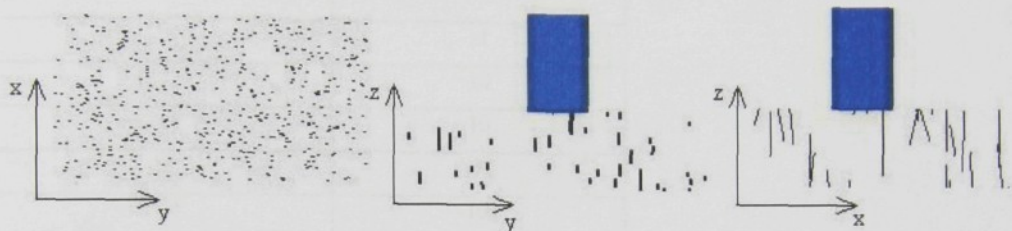


Figure 5.8.5: The initial configuration of 3D lattice model for simulation of vertically laid highloft fibrous structure. The liquid body is closed in a "glass vessel" and placed on to the fibre structure.

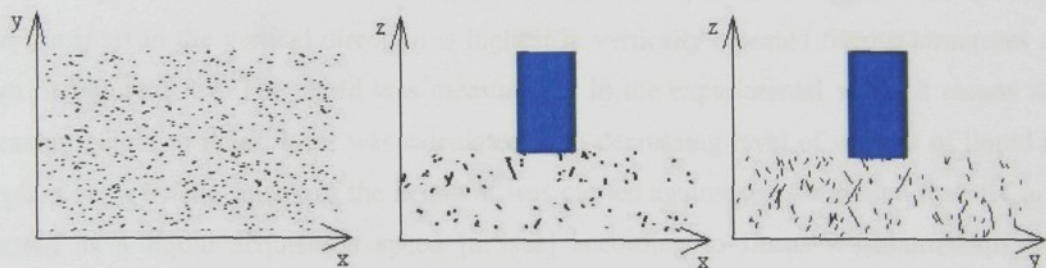


Figure 5.8.6: The initial configuration of 3D lattice model for simulation of randomly laid fibrous structure. The liquid body is closed in a "glass vessel" and placed on to the fibre structure.

The simulation constants C_{ij} were set to reach proportional values of liquid surface tension and surface energies of PET fibre. The constants C_g , k_B and T were chosen according to results from Chapter 5.3, where the influence of temperature in two-phase system behaviour was observed, shown in Table 5.8.3.

Table 5.8.3: Values of computer simulation constants: dimensions of 3D lattice model, liquid drop radius, $k_B T$ – thermodynamic temperature parameter, C_g – gravitational constant, C_{aa} – exchange energy between two air cells, C_{al} – exchange energy between air cell and liquid cell, C_{as} – exchange energy between air cell and solid cell, C_{ll} – exchange energy between two liquid cells, C_{ls} – exchange energy between liquid cell and solid cell, C_{ss} – exchange energy between two solid cells.

3D lattice dimensions (x×y×z)	200×200×200
[number of cells]	
$k_B T$	50
C_g	10
C_{aa}	-1
C_{al}	10
C_{as}	10
C_{ll}	-92
C_{ls}	-102
C_{ss}	-59
Number of simulation steps	1 000 000; 4 000 000

The computer simulation results are consistent with the experimental results. The speed of liquid transport in the vertical direction is highest in vertically oriented fibrous structures as shown in Figure 5.8.7. The speed was measured as in the experimental work, it means the decreasing height of liquid level was calculated from decreasing level of volume of liquid in the “glass vessel”. The square of the height h^2 was plotted against the simulation time ST and evaluated as a liquid acquisition speed [m^2/sec] according to Lucas-Washburn Equation (3.3.15).

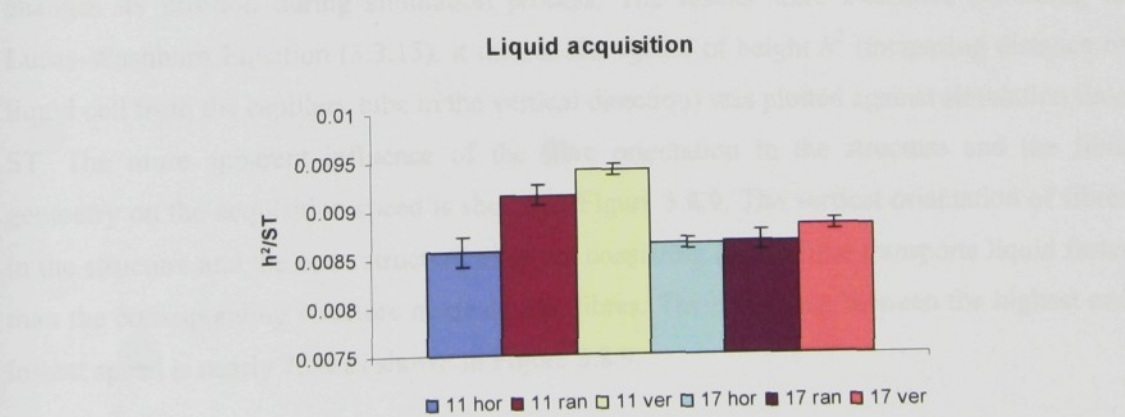


Figure 5.8.7: Liquid acquisition speed measured in vertical direction from the top of the fabrics into fabric from computer simulation. The acquisition speed h^2/ST is calculated from the decreasing height h of liquid level in the dosing vessel during simulation process.

The lower speed was measured on structures with cross-laid oriented fibres. The influence of the fineness of the fibres is not evident from the computer simulation. For random and vertical oriented fibres, the finer fibres absorb liquid faster than the coarse fibres. The fastest absorption was evaluated for vertical oriented structure of finer fibres.

This evaluation shows how fast the liquid is absorbed into the sample, but not how fast it is transported in vertical direction. The shapes of liquid volumes in Figure 5.8.8 characterise the difference in liquid transport in different structures.

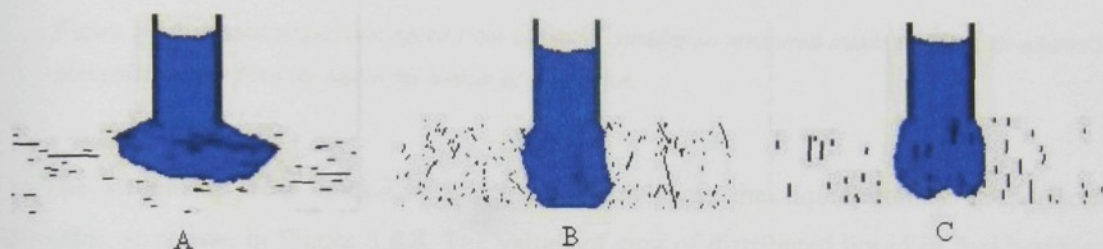


Figure 5.8.8: The configuration of the models after 4 million simulation steps. The difference of the shapes of liquid bodies inside the three types of highloft fibrous structures is apparent. A – cross-laid fibrous structure, B – randomly oriented fibres in structure, C – vertically laid fibrous structure.

The more accurate results of liquid transport in the vertical direction inside the fibrous structure are obtained from the computer simulation [139]. The liquid transport inside fibrous structure was recorded as Z co-ordinate of the lowest liquid cell in the structure, which changes its position during simulation process. The results were evaluated according to Lucas-Washburn Equation (3.3.15), it means, the square of height h^2 (increasing distance of liquid cell from the capillary tube in the vertical direction) was plotted against simulation time ST. The more apparent influence of the fibre orientation in the structure and the fibre geometry on the acquisition speed is shown in Figure 5.8.9. The vertical orientation of fibres in the structure and the open structure of fabric consisting coarse fibre transports liquid faster than the corresponding structure made of fine fibres. The difference between the highest and lowest speed is nearly 75% as shown in Figure 5.8.9.

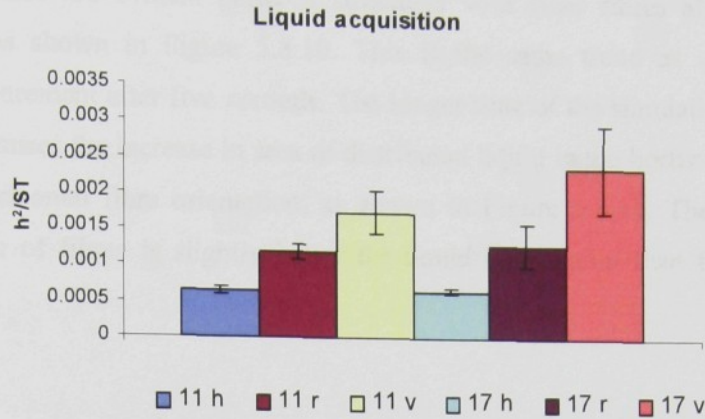


Figure 5.8.9: Liquid acquisition speed from computer simulation measured inside the fibre structures in vertical direction from the top to the bottom of the fabrics.

The structures with cross-laid fibrous web transport the liquid mainly in horizontal direction as shown in Figure 5.8.8. The values of area of distributed liquid in five horizontal layers of the fibrous structures are in Table 5.8.4 after 1 million simulation steps and in Table 5.8.5 after 4 million simulation steps. The area is evaluated as a number of liquid cells in particular horizontal layers.

Table 5.8.4: The average values and standard deviations of area of distributed liquid in horizontal layers of different z co-ordinates after 1 million simulation steps.

1 mill	11 cross-laid		11 random		11 vertical-laid		17 cross-laid		17random		17 vertical-laid	
	ave	std	ave	std	ave	std	ave	std	ave	std	ave	std
z = 45	2079	44	1864	30	1654	85	2039	48	1685	49	1466	32
z = 35	1352	69	1272	99	1229	53	1472	62	1061	81	995	29
z = 25	0	0	459	69	634	65	7	11	579	92	669	74
z = 15	0	0	45	27	191	68	0	0	150	41	346	62
z = 5	0	0	0	0	98	101	0	0	40	47	132	35

Table 5.8.5: The average values and standard deviations of area of distributed liquid in horizontal layers of different z co-ordinates after 4 million simulation steps.

4 mill	11 cross-laid		11 random		11 vertical-laid		17 cross-laid		17random		17 vertical-laid	
	ave	std	ave	std	ave	std	ave	std	ave	std	ave	std
z = 45	2398	107	1352	74	1300	217	2362	74	1492	50	1142	52
z = 35	2859	66	1663	166	1418	263	3062	152	1453	133	1281	71
z = 25	1682	50	1724	109	1565	220	1647	123	1570	93	1465	43
z = 15	250	198	1792	56	1713	357	42	92	1648	150	1853	42
z = 5	0	0	1440	178	1949	468	0	0	1227	200	1969	63

No big differences are evident between structures with finer fibres after one million simulation steps as shown in Figure 5.8.10. This is the same trend as observed in the experimental measurement after five seconds. The longer time of the simulation, four million simulation steps, causes the increase in area of distributed liquid in the horizontal direction in structures with horizontal fibre orientation, as shown in Figure 5.8.11. The structure with random orientation of fibres is slightly better for liquid distribution than the vertical laid fibrous structure.

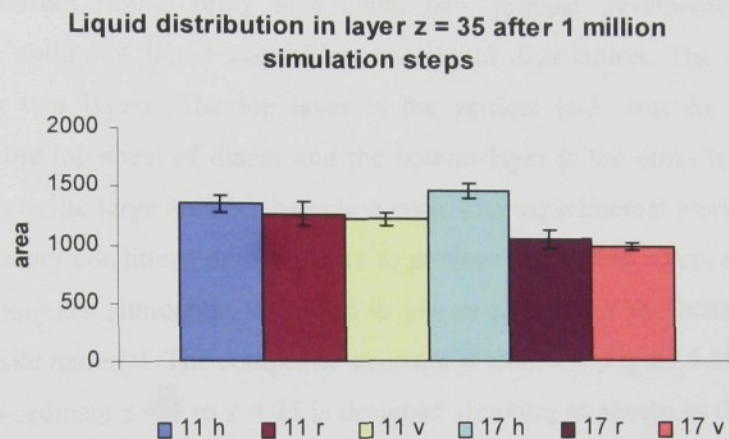


Figure 5.8.10: Area of distributed liquid in horizontal direction for different fibrous structures from computer simulation measured after 1 million simulation steps.

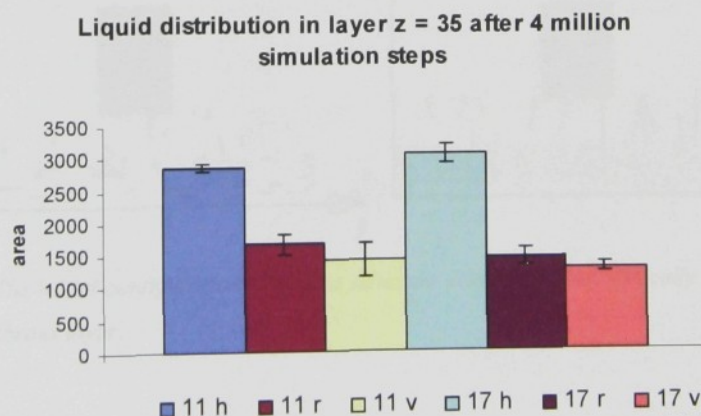


Figure 5.8.11: Area of distributed liquid in horizontal direction for different fibrous structures from computer simulation measured after 4 millions simulation steps.

From the results of liquid acquisition in Figure 5.8.9 and liquid distribution in Figure 5.8.11 is clear that horizontal laid structure is suitable for liquid distribution in horizontal direction and it is not good for liquid transport in vertical direction. The vertical laid fibrous structure is excellent for liquid transport in vertical direction and it is not suitable for laid distribution. The structure with random orientation of fibres in the structure is the optimal material for the application as acquisition/distribution layer in baby diaper due to the combination of its acquisition and distribution abilities. The fine fibres are better than the coarser fibres.

The above present results bring idea about new product development of material improve the ability of liquid acquisition and liquid distribution. The new composite material contains two layers. The top layer is the vertical laid structure for fast liquid acquisition from the top sheet of diaper and the bottom layer is the cross laid structure for liquid distribution to the large area of absorption core. The experimental work was not done, because the laboratory conditions do not allow to produce 2 mm thin layers of the requested materials. The computer simulation was used to get an idea about the behaviour of liquid inside the composite material. The composite structure is shown in Figure 5.8.11. The bottom layer from the co-ordinate $z = 1$ to $z = 25$ is designed structure as shown in the Figure 5.8.4. The top layer from the co-ordinate $z = 26$ to $z = 50$ is designed structure as shown in the Figure 5.8.5.

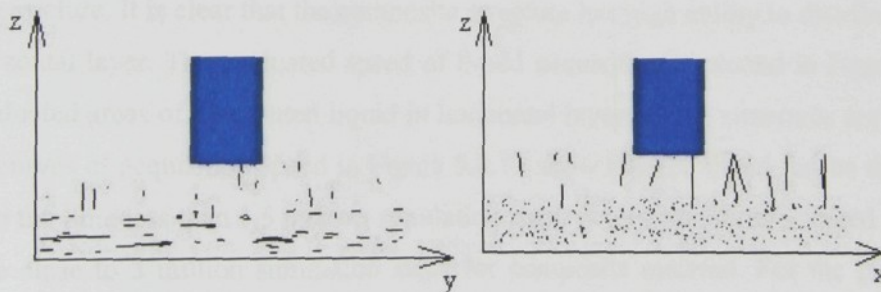


Figure 5.8.11: The initial configuration of fibrous structure composed from vertically laid fibrous layers and cross laid fibrous layer.

The results of liquid acquisition and liquid distribution are compared with the structure of random fibre orientation, shown in Figure 5.8.6.

The final configuration after four million simulation steps is shown in Figure 5.8.12.

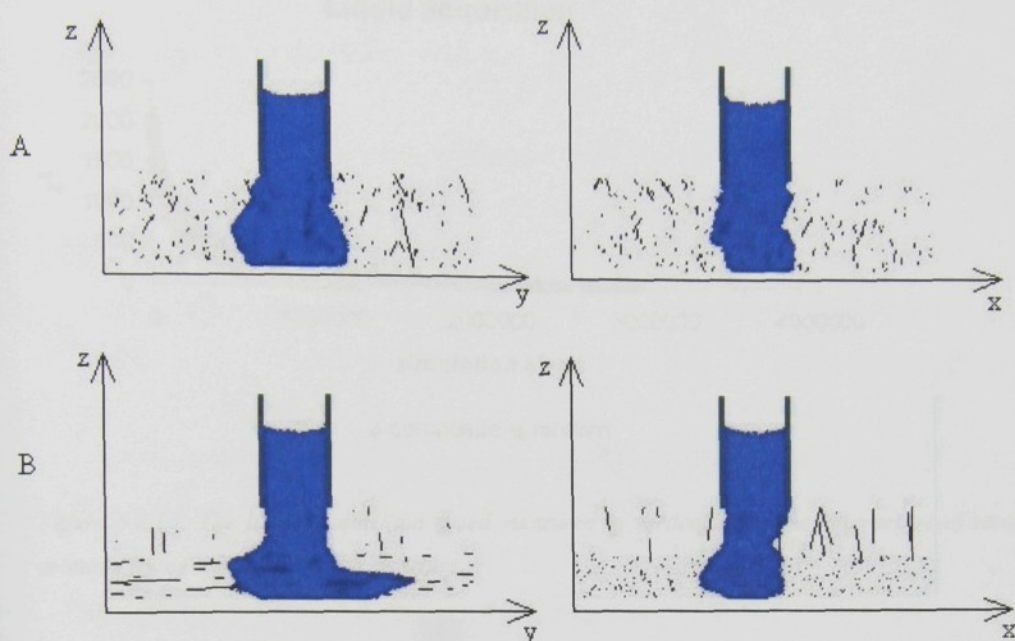


Figure 5.8.12: A – final configuration after 4 million simulation steps of liquid acquisition and distribution in the structure of randomly oriented fibres. B – final configuration after 4 million simulation steps of liquid acquisition and distribution in the composite structure.

The shape of liquid volume inside the fibrous structure in Figure 5.8.12 expresses the differences of liquid distribution of the structure of random fibre orientation and the composite structure. It is clear that the composite structure has high ability to distribute liquid in low horizontal layer. The evaluated speed of liquid acquisition is plotted in Figure 5.8.13 and the evaluated areas of distributed liquid in horizontal layers of the structures are in Table 5.8.6. The curves of acquisition speed in Figure 5.8.13 show that the liquid reaches the lowest layer $z=1$ in the time less than 1,5 million simulation steps in random fibres oriented structure and in time close to 3 million simulation steps for composite material. For the purpose of acquisition function is important the liquid transport in the top half of the structure, then from the $z = 50$ to $z = 25$. This distance is equal to the $z^2 = 2500$ to $z^2 = 625$ in the Figure 5.8.13. In this part of the graph is the difference of liquid acquisition speed very small and shows slightly higher speed for random fibres oriented structure.

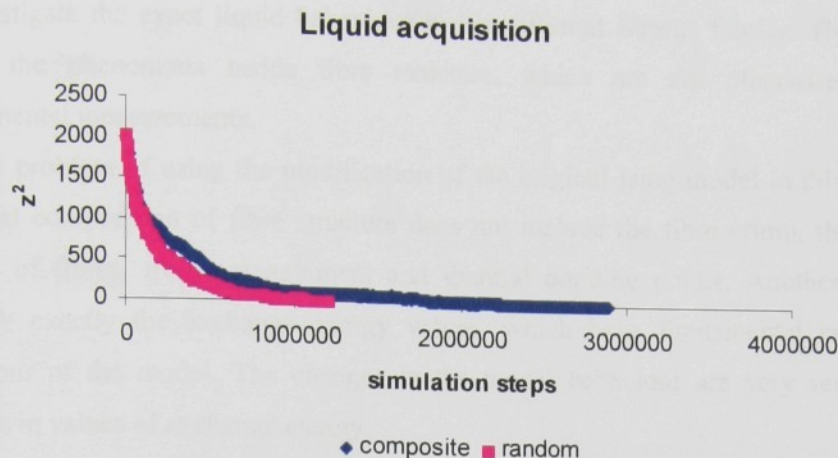


Figure 5.8.13: The liquid acquisition speed measured in vertical direction in structure of randomly oriented fibres and in composite structure.

The areas of distributed liquid in horizontal layers of fibrous structures shows the different trend of liquid distribution in these structures. For the purpose of liquid distribution to the area of absorption core under the acquisition/distribution layer are important results in lower layers of the structures $z = 15$ and $z = 5$. The liquid distribution is significantly better in cross-laid fibrous web structure than the structure of random oriented fibres as shown in Table 5.8.6.

Table 5.8.6 The average values and standard deviations of area of distributed liquid in horizontal layers of different z co-ordinates after 4 million simulation steps.

4 mill	11 composite		11 random	
	ave	Std	ave	std
$z = 45$	1105	121	1352	74
$z = 35$	1265	164	1663	166
$z = 25$	1807	164	1724	109
$z = 15$	2180	180	1792	56
$Z = 5$	1718	383	1440	178

The composite material achieves requests of the function of acquisition/distribution layer for fast liquid transport in vertical direction from in the top part of the layer, and liquid distribution in the bottom part of the layers.

The results show the ability of the three dimensional model to simulate real liquid behaviour in a fibrous system which is in good agreement with the experimental results. The advantage of the computer simulation in comparison to experimental work is that it allows us

to investigate the exact liquid behaviour inside different fibrous fabrics. This investigation shows the phenomena inside fibre structure, which are not otherwise evident from experimental measurements.

The problem of using the modification of the original Ising model in this chapter is that the ideal composition of fibre structure does not include the fibre crimp, the circular cross section of fibres, fibre entanglement and thermal bonding points. Another problem is to quantify exactly the exchange energy values, which have fundamental influence on the behaviour of the model. The changes in the model behaviour are very sensitive to small changes in values of exchange energy.

The differences between liquid behaviour in particular fibrous structures lead to design of composite material with better ability of liquid transport from the top-sheet of baby diaper by using fabric with vertical fibre orientation, and liquid distribution to the higher area of absorption core using fabric with horizontal fibre orientation.

6. DISCUSSION

The dissertation thesis is concerned with the problematic of wetting and wicking phenomena present in situations when liquid and fibre structure come into a contact. The objective of the thesis is to establish computer simulation as a tool of investigation for the mentioned phenomena. There are two aspects for the computer simulation process. Firstly, it is composition of a model for a system of three components – solid, liquid and air, which is similar to a real system (a liquid drop on a heterogeneous solid flat surface, a liquid in contact with a textile fibre, a liquid in contact with a textile structure, etc.). Secondly, it is the setting of simulation process variables consistent with wetting and wicking phenomena in real systems known from experimental measurement.

The three-dimensional lattice model was chosen for simulation of real systems. The difference between the investigated model described in Chapter 5.2.1 and the previous model presented in Chapter 4.2 is that the Ising variables are used in simulation program only to distinguish the different environment in particular cells, but the values of Ising variables do not influence the calculation of Hamiltonian (5.2.2).

The composition of models used for simulation is easy and quite accurate for simple systems as a liquid drop placed on a homogeneous surface and a liquid drop placed on a heterogeneous substrate in Chapters 5.4.2 and 5.5.

The composition of model is different from real system in simulation of synthetic fibres of circular cross-section. The design of fibres in the models as similar as possible to real fibres is shown in Figure 5.6.1. From the cross-section of fibres is derived design of assemblies of parallel fibres. The ideal structure of real fibrous assemble of seven fibres is shown in cross-section in Figure 3.3.5. The ability to design models of very close structure is clear from cross-section of design fibrous assemblies in Figures 5.7.8 and 5.7.9.

The design of highloft fibrous structure in Chapter 5.8 follows real systems by setting of the accurate value of volume density, geometrical parameters of fibre and fibre orientation in particular structures. The models do not take into account the crimp of real fibres, fibre entanglement in structure, and presence of bonding points in thermal bonded structures.

The ability of the mentioned idealised models of real systems to simulate real process of wetting and wicking is discussed below.

The above-mentioned simplification of calculation of Hamiltonian excluding the Ising variable values allows more precise determination of exchange energies. The exchange energies values are the indicators of intensity of two neighbouring cell interaction in the three-dimensional lattice. The idea of exchange energy values determination is based on difference of energy of a cell inside volume phase and the energy of the cell on the interface with other phase present in the system. The derivation of setting for values of exchange energy according to values of real surface energies of solids and surface tension values of real liquid is presented in Appendix 1.

The value of gravitational constant was set up very close to value of real gravitational acceleration as described in Chapter 5.2.1.

The setting of constant related to temperature was determined from the computer simulation of two-phase system in Chapter 5.3. The simulation processes in the thesis use chosen values between $k_B T = 0$ and $k_B T = 40$. For these temperatures, the layer of phase transition is very low and the behaviour of liquids is appropriate to the behaviour of real liquids used in experimental works in laboratory conditions where the temperatures are between 20°C and 25°C.

The ability of the three-dimensional lattice model to simulate the real behaviour of liquid in contact with a solid was proven using easy method. The contact angle between surface of a liquid drop and horizontal homogeneous surface was evaluated by experimental way and from computer simulation as well in Chapter 5.4. The values of contact angle from computer simulation 43.6° and 46.3° are in very close agreement with the experimental value of contact angle 46.2°.

The computer simulation of liquid drop placed on heterogeneous substrate follows the trends of behaviour observed in experimental work as shown in Chapter 5.5. The liquid drop, places eccentrically on heterogeneous cross, is divided into four parts of different sizes indifferent times of simulation process.

The computer simulation was used to investigate behaviour of a liquid drop placed on a single fibre in Chapter 5.6. The condition of complete wetting (3.3.7) depends only on the geometrical parameters of fibre and liquid body, and on the liquid surface tension. The fibre cross-section was chosen as a variable for the computer simulation. The computer

simulation was done on fibres of four different cross sections, as shown in Figure 5.6.1. The surface area of the fibre is the parameter influencing the wetting quality. The perimeter of the fibres in computer simulation is done as a sum of the lattice unit lengths on the surface of the fibre. The fibre A has perimeter 12, fibre B has perimeter 16, the fibre C 20 and the fibre D 28. The fibre length is equal. The results are in agreement with the condition of complete wetting of a single fibre (3.3.7). Harkinson spreading coefficient S_c depends on the reciprocal value of fibre radius. The higher is the fibre radius, the lower is S_c , it means better wetting of fibres of higher radius and higher perimeter in cross section. From the results reviewed in Table 5.6.2 is apparent the decreasing contact angle with increasing perimeter of cross section, shown in Table 5.6.1. The fibre D with highest perimeter is better wetted than the fibres with lower perimeters.

Experimental work and computer simulation on assemblies of parallel filaments was done in Chapter 5.7. The conclusions from experimental work are in agreement with the condition of complete wetting of fibre assemblies (3.3.9).

The values of contact angle from computer simulation decrease with bigger fibre diameter and with higher number of fibres in assemble. This dependency is in agreement with the condition of complete wetting of fibre assemblies (3.3.9), it means that the higher fibre radius and the higher number of fibres in assemble improve the wetting of assemblies. The computer simulation shows the advantage of computer simulation for investigation of liquid behaviour inside fibrous structure, where the phenomena is not observable using recently available experimental methods.

All value of contact angle in Table 5.6.2 is higher than contact angle value of liquid drop on homogeneous surface in Chapter 5.4. This fact confirms the theoretical conclusion from Chapter 3.3.2 that whilst the flat surface is wetted by concrete liquid, the single fibre could not discharge condition of complete wetting. The values of contact angle on assemblies are in Table 5.7.3 show what is the critical number of fibres and fibre diameter for better wetting of assemble than the flat surface. Liquid drop placed on seven fibres A in assemble has higher contact angle value than on flat surface. At least three fibres C and two fibres D in the assemble cause the lower value of contact angle.

The computer simulation shows that whilst the liquid keeps the drop shape on assemble, what seems like the liquid does not wet the fibrous structure, the liquid motion inside the pores of the assemble is present and very fast.

The computer simulation of liquid penetration into complex fibrous structure is presented in Chapter 5.8. The results show the ability of the three dimensional model to simulate real liquid behaviour in a fibrous system which is in good agreement with the experimental results. The advantage of the computer simulation in comparison to experimental work is that it allows us to investigate the exact liquid behaviour inside different fibrous fabrics. This investigation shows the phenomena inside fibre structure, which are not otherwise evident from experimental measurements.

The differences between liquid behaviour in particular fibrous structures lead to design of composite material with better ability of liquid transport from the top-sheet of baby diaper by using fabric with vertical fibre orientation, and liquid distribution to the higher area of absorption core using fabric with horizontal fibre orientation.

7. CONCLUSION

The results show the ability of the three dimensional lattice model to simulate real liquid behaviour in a fibrous system which is in good agreement with the experimental results despite simplifications of design of fibrous structures and approximation of simulation constants.

The advantage of the computer simulation in comparison to experimental work is that it allows us to investigate the exact liquid behaviour inside different fibrous fabrics. This investigation shows the phenomena inside fibre structure which are not otherwise evident from experimental measurements.

The advantage the computer simulation is possibility to design structures of specific properties, exactly defined parameters, structures from diverse materials, etc. The simulation gives a basic idea about the differences of systems behaviour influenced by those diverse conditions. The computer simulation procedure is faster and cheaper than experimental work.

The above mentioned facts show the reason to continue with improvement of three dimensional lattice model and computer simulation process for the computer modeling of wetting and wicking phenomena.

The work is oriented on the accuracy of design of fibrous structure according to real systems. The exact quantification of fiber orientation in real fabrics was not a part of the thesis. The evaluation of this structural parameter will help to define the model configuration of fibrous structure very close to real fabric.

The main features, dependencies and rules of wetting and wicking phenomena are involved into thesis and accomplish the ability of the model to simulate real behavior. The following work is oriented on detailed analysis the processes, inside fibrous structure with respect to exact definition of internal structure, material parameters, liquid parameters and external conditions. The results are evaluated using different theoretical tools based on principles of hydrodynamics, capillary forces, Laplace pressure, etc. and should show which theoretical tool is the most precise for evaluation in the particular model.

The computer simulation results should bring us the idea about liquid behavior inside complex fibrous structure and find out the reasons for deviation of experimental results from theoretical description. The identification of the differences could improve the theory of wetting and wicking processes and helps to better understanding of the phenomena.

8. REFERENCES

- [1] Wietz, P.: Past and Future of European Nonwovens Growth, *Nonwovens World*, Decembre 2002 – January 2003.
- [2] EDANA 10.1-72, Nonwovens Absorption.
- [3] INDA 10.1-92 Nonwoven Absorption.
- [4] KRUSS GmbH, Hamburg User Manual of K12.
- [5] An Overview of MTS Service, Kalmazoo, MI, USA.
- [6] Eurofin ATS, Baby Hygiene, Z.I des Milles, France.
- [7] S. L. Goren, The Shape of Thread of Liquid Undergoing Break-up, *J. of Coll. Sci.* 19, 81-86 (1964).
- [8] R - J. Roe, Wetting of Fine Wires and Fibres by a Liquid Film, *J. of Coll. and Interf. Sci.* Vol. 50, No. 1, January 1975.
- [9] F. Brochard, Spreading of Liquid Drops on Thin Cylindres: The “manchon /droplet” Transition, *J. Chem. Phys.* 84 (8), 15 April, 1986.
- [10] G. McHale, N. A. Kab, L. Newton, S. M. Rowan, Wetting of High Energy Fibre Surface, *J. of Col. and Interf. Sci.* 186, 453-461 (1997).
- [11] B. Song, A. Bismarc, R. Tahhan, J. Springer, A Generalized Drop Length – Height Method for Determination of Contact Angle in Drop – on – Fibre System, *J. of Col. and Interf. Sci.* 197, 68-77 (1998).
- [12] S. Barsberg, I. G. Thygesen, nonequilibrium Phenomena Influencing the Wetting Behaviour of Plant Fibres, *J. of Col. and Interf. Sci.* 234, 59-67 (2001).
- [13] Q. Wei, R. R. Mather, A. F. Fotheringham, R. D. Yang, Observation of Wetting Behaviour of PP Microfibres by Environmental Scanning Electron Microscope, *Aerosol Sci.* 33, 1589-1593 (2002).
- [14] D. Lukas, N. Pan, Wicking of Liquids into a Fibre Bank: 3d IM Simulation, *Euromech 367 “Fluid Mechnaics of Coating Process”*, July 1997, Strasbourg, France.
- [15] L. Barci, F. Brochard – Wyart, Droplet Suction on Porous Media, *Eur. Phys. J. E* 3, 87-97 (2002).
- [16] V.M. Starov, S.R. Kosvinstev, V.D. Sobolev, M.G. Velarde, S.A. Zhdanov, Spreading of Liquid Drops over Saturated Porous Layers, *J. of Coll. and Interf. Sci.* 246, 372-379 (2002).
- [17] V.M. Starov, S.R. Kosvinstev, V.D. Sobolev, M.G. Velarde, S.A. Zhdanov, Spreading of Liquid Drops over Dry Porous Layers: Complete Wetting Case, *J. of Coll. and Interf. Sci.* 252, 397-408 (2002).
- [18] R.K. Holman, M.J. Cima, S.A. Uhland, E. Sachs, Spreading and Infiltratin of Injet – Printed Polymer Solusion Droplets on a Porous Substrate, *J. of Coll. and Interf. Sci.* 249, 432 – 440 (2002).
- [19] G. Martic, J. De Coninck, T.D. Blake, Influence of the Dynamic Contact Angle on the Characterization of Porous Media, *J. of Coll. and Interf. Sci.* 263 (2003) 213-216.
- [20] A. Marmur, Contact Angle Hysteresis on Heterogeneous Smooth Surfaces, *J. of Col. and Interf. Sci.* 168, 40-46 (1994).
- [21] S. Brandon, A. Marmur, Simulation of Contact Angle Hysteresis on Chemically Heterogeneous Surfaces, *J. of Col. and Inter. Sci.* 183, 351-355 (1996).
- [22] S. Brandon, A. Wachs, A. Marmur, Simulated Contact Angle Hysteresis of a Three-Dimensional Drop on a Chemically Heterogeneous Surface: A Numerical Example, *J. of Col. and Inter. Sci.* 183, 351-355 (1996).

- [23] L. W. Schwartz, R. R. Eley, Simulation of Droplet Motion on Low – Energy and Heterogeneous Surfaces, *J. of Coll. and Inter. Sci.* 202, 173-188 (1998).
- [24] Zhong W., Ding X., Tang ZL, A Statist. Appr. in Studying Wicking beh. of Fibrous Struc., The 6th Asian text.Conference, Hong Kong 2001.
- [25] R. Valéry Roy, A. J. Roberts, M. E. Simpson, A lubrication model of coating flows over a curved substrate in space, *J. Fluid Mech.* (2002), Vol. 454, pp. 235-261.
- [26] L. W. Schwartz, R. R. Eley, Flow of Architecture Coating on Complex Surfaces; Theory and Experiment, *J. of Engineering Mathematics* 43, 153-171, (2002).
- [27] P. R. Gunjal, V. V. Ranade, R. V. Chaundhari, Experimental and Computational Study of Liquid Drop over Flat and Spherical Surface, *Catalysis Today* 79-80 (2003) 267-273.
- [28] V. M. Samson, V. V. Dronnikov, A. A. Volnukhina, S. D. Muravyev, Molecular Dynamical Simulation of Structure Formation after Nanodroplet Spreading over Heterogeneous Surface, *Surface Science* 532-535, (2003) 560-566.
- [29] Osipov, L., I.: *Surface Chemistry*, R.E.Krieger publishing Compant, New York, 1972.
- [30] Noskievic, J.: *Mechanika Tekutin*, SNTL Praha 1987.
- [31] Ramsay, W., Shield., J., *J. Chem. Soc.* 1893, 1089.
- [32] McLeod, D.B., *Trasn Faraday Soc.* 19, 38 (1923).
- [33] Harkins, W.D., Cheng, V.C., *J. Am. Chem. Soc.* 43, 36 (1921).
- [34] Kissa, E.: *Textile Res. J.* 66 (10), 660-668, (1996).
- [35] Harnett, P.R., Mehta, P.N.: *Textile Res. J.* 54, 471 (1984).
- [36] Atkins, P.W. *Physical Chemistry* 3.edition, Oxford University Press 1986.
- [37] Horák, ., Krupka, F.: *Fyzika*, SNL Praha 1966.
- [38] Young, T.: *Philos. Trans. R. Soc. London*, 95 (1805) 65.
- [39] Miller, B., Young, R.A., *Textile Res. J.* 45, 359 (1975).
- [40] Neumann, A.W., Good, R.J.: *Surface and Colloid Science*, vol. II, Plenum Press, New York 1979.
- [41] Tagawa, M., Gotoh, K., Yasukawa, A., Ikuta, .M., *Colloid Polym. Sci.* 268, 589 (1990).
- [42] Brochard, F., *J.Chem. Ohys.* 84, 4664 (1986).
- [43] Heerjes, P.M., Wilwoet, W.C., *Tenside* 8, 248 (1971).
- [44] Lange, H., *Kolloid Z.*, 136, 136 (1954).
- [45] F. Brochard, Spreading of Liquid Drops on Thin Cylindres: The “manchon /droplet” Transition, *J. Chem. Phys.* 84 (8), 15 April, 1986.
- [46] Raleigh, Lord, *Proc. London Math.Soc.* 10,4 (1879).
- [47] Quere, D., di Meglio, J.M., Brochard-Wyart, F., Spreading of Liquids on Highly Curved Surfaces, *Science* vol. 249, 1256-1260 (1990).
- [48] D. Lukas, N. Pan, Wicking of Liquids into a Fibre Bank: 3d IM Simulation, *Euromech* 367 “Fluid Mechnaics of Coating Process”, July 1997, Strasbourg, France.
- [49] Princen, H.M., *Capillary Phenomena in Assemblies of Parallel Cylindres; I. Capillary Rise between Two cylindres*, *J. Colloid and Interface Sci.*, Vol. 30, No. 1, (1969), 69.
- [50] Princen, H.M., *Capillary Phenomena in Assemblies of Parallel Cylindres; II. Capillary Rise in System with More than Two Cylindres*, *J. Colloid and Interface Sci.*, Vol. 30, No. 3, (1969), 359.

- [51] Lord, P.R., Textile Res. J. 44, 516 (1974).
- [52] Lucas, R.: Kolloid - Z., 23, 15 (1918).
- [53] Washburn, E.W.: Phys. Rev., 17, 273 (1921).
- [54] Kvasnica, J.: Mechanika, Academia Praha 1988, 476s.
- [55] Fisher, L.R., Lark, P.D., J. Colloid Interface Sci. 69, 49 (1979).
- [56] Jeje, A.A., J. Colloid Interface Sci. 69, 420 (1979).
- [57] Rowland, S.P. Bertioniere, N.R., Textile Res. J. 46, 770 (1976).
- [58] Hogson, K.T., Berg, J.C., J. Colloid Interface Sci. 121, 22 (1988).
- [59] Gupta, B.: Absorbency – an overview, Betlwide Cotton Conf., 2001.
- [60] Hsieh, Y.L., Bangling, Y., Textile Res. J. 62 (11), 677-685 (1992).
- [61] Tavisto, M., Kuisma, R., Pasila, A., Hautala, M., Wetting and Wicking of fibre plant straw fractions, Industrial Crops and Products 18 (2003) 25-35.
- [62] Guyon, E., hulin, J.P., Petit, L., Hydrodynamic physique, Inter Edition/Edition du CNRS, 1991.
- [63] McLaughlin, J.R., Trounson, M.E., Stewart, R.G., McKinnon, A.J. textile Res. J. 58, 501 (1988).
- [64] EDANA 10.2-02 , Nonwovens Absorption, 1972.
- [65] INDA 10.1-92 Nonwoven Absorption, 1972.
- [66] AATCC Test Method 17-1980.
- [67] Fowkes, F.M., J. Phys. Chem. 57, 98 (1953).
- [68] Lichstein, B.M., 2nd Tech. Symp. Of Intenational Nonw \$ Disposable Assoc., Washington, DC, March 1974.
- [69] Buras, E.M., Goldtwait, C.F., Kraemer, R.M., Textile Res. J. 20, 239 (1950).
- [70] Cary, R.T., Sproles, G.B., textile Res. J. 49, 691 (1979).
- [71] Lord, P.R., Textile Res. J. 44, 516 (1974).
- [72] Gillespie, T., J. Colloid. Interface Sci. 13, 32 (1958).
- [73] Kawase, T., Sekoguchi, S., Fujii, T., Minagava, M., Textile Res. J. 56, 409 (1986).
- [74] Barci, L., Brochard-Wyart, F., Droplet Suction on .Porous Media, The Eur. Phys. J. E 3, 87-97 (2000).
- [75] Kissa, E., J. Colloid Interface Sci. 83, 265 (1981).
- [76] Kissa, E., Pure Appli. Chem. 53, 2255 (1981).
- [77] Kissa, E., Detergency, Theory and Technology, Surface Science Ser., vol. 20, G. Marcel Dekker, NY, 1987.
- [78] Kawase, T., Sekoguchi, S., Fuji, t., Minagawa, M., Spreading of Liquids in Textile Assemblies, Textile Research Journal, 56, 409-414 (1986).
- [79] Neckar, B., Morfologie a strukturni mechanika obecnych vlakennych utvaru, TUL, 1999 Liberec.
- [80] Neckar, B., Sayed, I., Approach for Determining Pore Characteristics Between Fibers, Textile Research Journal, 73(7), 611-619(2003).
- [81] Binder K., Heerman D. W., Monte Carlo Sim. of Stat. Phys., Heidelberg 1997.
- [82] Chatewrjee, I.: Order-disorder transition in one-dimensional quantum magnet, Journal of Magnetism and Magnetic Materials.
- [3] Sakamoto, Y.: Phase transition of 2x2 adsorbates on FCC (111) and HCP (0001) surfaces, Surface Science, 530, (2003), 55-62.

- [84] Hwang, C.C., Kim, K.-J., Kang, T.H., Kim, B., Chung, Y., Park, C.Y.: Temperature -induced phase transitions of the Si (100) and (113) surfaces, *Surface Science*, 514, (2002), 319-326.
- [85] Fedorus, A., Godzik, G., Koval, V., Naumovets, A., Pfnur, H.: Phase transition in two-dimensional anisotropic chain systems: submonolayers of adsorbed on Monolayers (112), *Surface Science*, 460, (2000), 229-242.
- [86] Bahmad, L., Benyoussef, A., Ey-Zahraouy, H.: Surface coupling effect on wetting and layering transition.
- [87] Ma, K.L., Altman, M.S., Poppa, H.: Spin polarized low energy electron microscopy investigations of magnetic transitions in Fe/Cu(100), *Surface Science*, 480, (2001), 163-172.
- [88] Wiatrowski, G., Warda, K., Wojtczak, L., Baldomir, D., Pereiro, M., Arias, J.E.: Magnetic properties of bilayers with a mixed-spi interface, *Surface Science*, 507-510, (2002), 517-521.
- [89] Kaneyoshi, T.: Surface phase diagrams a semi-infinite ferroelectric system described by the transverse Ising model, *Journal of Magnetism and Magnetic Materials*, 264, (2003), 30, 35.
- [90] Chakarova, R., Oner, D. E., Zoire, I., Kasemo, B.: Monte Carlo simulation of initial Al (111) oxidation, *Surface Science*, 472, (2001), 63-79.
- [91] Tarasenko, A.A., Nieto, F., Jastrabik, L., Uebing, C.: Diffusion of particles adsorbed on a triangular lattice: pairwise and three-particle interactions, *Surface Science*, 536, (2003), 1-14.
- [92] Fergg, F., Frerich, J.K.: Diffusion and reaction of multicomponent electrolytes in poly(vinylalcohol) hydrogels – modeling and experiment, *Chemical Engineering Science*, 56, (2001), 1305-1315.
- [93] Olami, Z., Manassen, Y., Rao, N.R., Dana, R.: Fractalization of silicon islands at coverage close to 0,5 monolayers, *Surface Science*, 520, (2002), 35-42.
- [94] Giesen, M., Steimer, Ch., Ibach, H.: What does one learn from equilibrium shapes of two-dimensional islands on surface?, *Surface Science*, 471, (2001), 80-100.
- [95] Hulliger, J., Budde, F., Quintel, A., Bebie, H.: Spontaneous polarity formation in thin crystalline films of host-guest materials, *Surface Science*, 453, (2000), L323-L327.
- [96] Audun, B., Johan, S.H.: One-dimensional Ising model applied to protein folding, *Physics A*, 323, (2003), 504-518.
- [97] Valandro, L., Salvato, B., Caimmi, R., Galzignas, L.: Isomorphism of Quasuspecies and Percolation Models, *J.theor. Biol.* (2000), **202**, 187-194.
- [98] Etcgegoïn, P., Nollmann, M.: A Model for Protein – DNA Interaction Dynamics, *J. theor. Biol.*, (2003), **220**, 233-239.
- [99] Muller-Nedebock, K.K., Frisch, H.L.: Dynamics of stiff polymers mapped from an Ising model, *Polymer* 44, (2003), 2829-2831.
- [100] Muller-Nedebock, K.K., Frisch, H.L.: Matrix models of discretely bending, stiff polymers, *Polymer* 44, (2003), 3151-3164.
- [101] Ishii, H.: A Statistical-Mechanical Model for Regulation of Long-range Chromatin Structure and Gene Expression, *J. theor. Biol.*, (2000), **203**, 215-228.
- [102] Ouannasser, S., Dreyse, H.: Study of surface segregation in $\text{Mo}_{0.75} \text{Re}_{0.25}$ (001) random alloy, *Surface Science*, 523, (2003), 151-156.

- [103] Guttman, A.J.: Inversion Relations, the Ising Model and Polygons, *Math. Comput. Modelling*, Vol. 26, No. 8-10, pp. 315-315, 1997.
- [104] kong, Y.: Ligand binding on ladder lattice, *Biophysical Chemistry*, Volume 81, Issue 1, 13 September 1999, Pages 7-21.
- [105] Shimizu T.S., Aksenov, S.V., Bray, D.: A Spatially Expected Stochastic Model of the Bacterial Chemotaxis Signalling Pathway, *J. Mol. Biol.*, (2003), **329**, 291-309.
- [106] Cellarius, R., Mauzerall, D.: A model for the photosynthetic unit photochemical and spectral on pheophytin a absorbed onto small particles, *Biophysics including Photosynthesis*, Volume 112, Issue 2, 7 February 1966, Pages 235-255.
- [107] Imshik, L., Wenli, D., Linjing, Y., Chen, W., Chunli, B.: Biphasic transition of a hairpin hexanucleotide triplex DNA, *Biophysical Chemistry*, Volume 67, Issues 1-3, 1 September 1997, Pages 159-165.
- [108] Cho, C.R., Lumsden, Ch.J., Whiteside, C.I.: Epithelial Cell Detachment in the Nephrotic Glomerulus: A Receptor Co-operativity Model, *J. theor. Biol.* (1993) **160**, 407-426.
- [109] Liu, Y., Wang, B., Boehler, J-P.: A Statistical Mechanics Model of Phase Transformation of Zirconia Particles in Ceramics, *Engineering Fracture Mechanics*, Vol. 53, No. 3, pp. 311-327, 1996.
- [110] Kukarni, R.G., Stough, R.R., Haynes, K.: Spin Glass and the Interactions of Congestion and Emission: an Exploratory Step, *Transp. Res.-C*, Vol. 4, No. 6, pp. 407-424, 1996.
- [111] Ellis, R.S.: An overview of the theory of large deviations and applications to statistical mechanics, *Mathematics and Economics*, Volume 17, Issue 3, April 1996, Pages 232-233.
- [112] Sejnowski, T.J.: The Once and Future Hebb Synapse, *Canadian Psychology*, Volume 44, Issue 1, February 2003.
- [113] Kay, J., Floreano, D., Philips, W.A.: Contextually Guided Unsupervised Learning using Local Multivariate Binary Processor, *Neural Networks*, Volume 11, Issue 1, 12 January 1998, Pages 117-140.
- [114] W. Leny, *Physic. Y.* 21, 613 (1920).
- [115] Ch. Kittel, *Thermal Physics*, John Wiley & Sons, Inc., USA 1969.
- [116] E. Ising, *Zeitschrift f. Physik* **31**, 253 (1925).
- [117] Lukáš D., Glazyriny E., Phuong T., Stach V., Císařová K., *Transport kapalin vláknennými systémy*, In: STRUTEX 1994, TU- Liberec, 1994, s.97 - 110.
- [118] Zhong W., Ding X., Tang ZL, *A Statist. Appr. in Studying Wicking beh. of Fibrous Struc.*, The 6th Asian text.Conference, Hong Kong 2001.
- [119] Lukas D., Pan N., *Wicking of Liquids into a Fibre-Bank: 3 Ising Model Simulation*, *Euromech 367 „Fluid Mechanics of Coating Process“*, Strasbourg, France.
- [120] Fabian F., Kluiber Y., *Metoda Monte Carlo a možnosti jejího uplatnění*, Praha 19981.
- [121] Lucia M, Version 3, User's Guide, KTM, TUL, Liberec.
- [122] E. Ising, *Zeitschrift f. Physik* **31**, 253 (1925).
- [123] Lukas, D.: *Materialové inženýrství netkaných textilií*, TUL, Liberec 2003.
- [124] Binder K., Heerman D. W., *Monte Carlo Sim. of Stat. Phys.*, Heidelberg 1997.
- [125] Chatewjee, I.: Order-disorder transition in one-dimensional quantum magnet, *Journal of Magnetism and Magnetic Materials*,

- [126] Sakamoto, Y.: Phase transition of 2×2 adsorbates on FCC (111) and HCP (0001) surfaces, Surface Science, 530, (2003), 55-62.
- [127] Hwang, C.C., Kim, K.-J., Kang, T.H., Kim, B., Chung, Y., Park, C.Y.: Temperature –induced phase transitions of the Si (100) and (113) surfaces, Surface Science, 514, (2002), 319-326.
- [128] Scukin, E., D., Percov, A., V., Amelinova, E., A.: Koloidni chemie, Academia, Praha 1990.
- [129] Ch. Kittel, Thermal Physics, John Wiley & Sons, Inc., USA 1969.
- [131] Arthur J.C.: Polymers for Fibres and Elastomers, ACS, Washington D.C., 1984.
- [132] Schwartz, L.W.: Three-dimensional numerical simulation of droplet motion on heterogeneous surfaces. Strasbourg 1997.
- [133] Lukas, D., Soukupova, V., Landeryou, M.: Three-dimensional monte carlo simulation of droplet motion on heterogenous surface, In: Wissenschaftliche abhandulgen, IX, pp. 193-196, 2003.
- [134] Cechova, M.: Diploma Thesis, TUL, Liberec 2002.
- [135] Vochtova, M.: Diploma Thesis, TUL, Liberec 2003.
- [136] Jirsak, O., Wadsworth, L. C.: Nonwoven Textiles. Carolina Academic Press, Durham, NC 1999.
- [137] Roubinkova, L.: Diploma Thesis, TUL, Liberec 2004.
- [138] EDANA 150.3 – 96 Liquid strike – through time, January 1996.
- [139] Soukupova, V., Lukas, D., Roubinkova, L.: Computer Simulation of Liquid Sorption into Textile Structures, II SIENTEX, Natal 2004.

Appendix 1

The determination of exchange energy values for thermodynamic temperature $T=0$

The liquid cell inside liquid volume is surrounded by 26 liquid cells in three-dimensional lattice, as shown in Figure (5.2.2A). The energy of the liquid cell E_{ll} is derived from Equation (5.2.1):

$$E_{ll} = C_g \cdot z_{ll} + 26C_{ll}$$

where C_g is gravitational constant, z_{ll} is the vertical co-ordinate of cube ll in the three dimensional lattice and C_{ll} is exchange energy value between two liquid cells. The second term is the sum of exchange energies between liquid cell ll and 26 liquid cells in its vicinity.

The air cell in side liquid volume is surrounded by 26 air cells in three-dimensional lattice, as shown in Figure (5.2.2B). The energy of the air cell E_{al} is derived from Equation (5.2.1)

$$E_{al} = C_g \cdot z_{al} + 26C_{aa}$$

where C_g is gravitational constant, z_{al} is the vertical co-ordinate of cube al in the three dimensional lattice and C_{aa} is exchange energy value between two air cells. The second term is the sum of exchange energies between liquid cell al and 26 liquid cells in its vicinity. The energy of both cells E_l inside their volumes is

$$E_l = E_{ll} + E_{al} = 2C_g \cdot (z_{ll} + z_{al}) + 26C_{ll} + 26C_{aa}.$$

The energy of liquid cell on the liquid – air interface has at least one air cell in its vicinity, as shown in Figure 5.2.3A. The energy of the liquid cell E_{l2} is

$$E_{l2} = C_g \cdot z_{l2} + 25C_{ll} + C_{al},$$

where z_{l2} is the vertical co-ordinate of cube $l2$ in the three-dimensional lattice and C_{al} is exchange energy value between air cell and liquid cell.

The energy of one air on the liquid – air interface has at least one liquid cell in its vicinity, as shown in Figure 5.2.3. The energy of the liquid cell E_{a2} is

$$E_{a2} = C_g \cdot z_{a2} + 25C_{aa} + C_{al},$$

where z_{a2} is the vertical co-ordinate of cube $a2$ in the three dimensional lattice.

The energy of both cells E_2 on the liquid – air interface is

$$E_2 = E_{l2} + E_{a2} = C_g \cdot (z_{l2} + z_{a2}) + 25C_{ll} + 25C_{aa} + 2C_{al}.$$

The difference of the energies ΔE inside the volume and on the liquid – air interface in the neglected gravitational field

$$\Delta E = E_2 - E_1 = 26C_{ll} + 26C_{aa} - (25C_{ll} + 25C_{aa} + 2C_{al}) = C_{ll} + C_{aa} - 2C_{al}.$$

The relation of the value ΔE and surface tension is clear from the assumption that from liquid inside liquid volume and air inside air volume are established two new liquid – air interfaces, then the difference of energies is equal to

$$\Delta E = E_2 - E_1 = C_{ll} + C_{aa} - 2C_{al} = 2 \cdot \gamma_l,$$

where γ_l is liquid surface tension.

Appendix 2

Microsoft Visual Studio Program for simulation of two phase system

The computer simulation results are mentioned in the Chapter 5.3.1.

```
*3D lattice model for two phase system*/
/*distilled water*/

# include "graphics.h"
# include <stdlib.h>
# include <stdio.h>
# include <conio.h>
# include <math.h>
# include <float.h>
# include <time.h>

# define SMERX 26
# define SMERY 26
# define SMERZ 100

//global variables
int a[SMERX][SMERY][SMERZ];
int q,cas,caskonec=6,krok,pockr=100000,kont;
int x,y,z,cidlo,i,j,l,xk,yk,zk,xv,yv,zv,xb,yb,zb,xp,yp,zp,apomoc,konec,rez1=50,rez2=12;

/* exchange energy C1 liquid - liquid, C2 liquid - air, C3 air - air*/
float xx,yy,zz,xxx,yyy,zzz,b,c,d,energie=0.,deltaE=0.;

//float C[2][2]={ {-1.,+10.},{+10.,-92.}}; //113/2=56 (0.9%NaCl) - surface tension
//float C[2][2]={ {-1.,+5.},{+5.,-50.}} //66/2=33 (oil) - surface tension
float C[16][16]={ {0.,0.,0.,0.,0.,0.,0.,0.,0.,0.,0.,0.,0.,0.,0.,0.},
                  {0.,-50.,0.,0.,0.,0.,0.,0.,0.,0.,0.,0.,0.,0.,+5.},
                  {0.,0.,0.,0.,0.,0.,0.,0.,0.,0.,0.,0.,0.,0.,0.},
                  {0.,0.,0.,0.,0.,0.,0.,0.,0.,0.,0.,0.,0.,0.,0.},
                  {0.,0.,0.,0.,0.,0.,0.,0.,0.,0.,0.,0.,0.,0.,0.},
                  {0.,0.,0.,0.,0.,0.,0.,0.,0.,0.,0.,0.,0.,0.,0.},
                  {0.,0.,0.,0.,0.,0.,0.,0.,0.,0.,0.,0.,0.,0.,0.},
                  {0.,0.,0.,0.,0.,0.,0.,0.,0.,0.,0.,0.,0.,0.,0.},
                  {0.,0.,0.,0.,0.,0.,0.,0.,0.,0.,0.,0.,0.,0.,0.},
                  {0.,0.,0.,0.,0.,0.,0.,0.,0.,0.,0.,0.,0.,0.,0.},
                  {0.,0.,0.,0.,0.,0.,0.,0.,0.,0.,0.,0.,0.,0.,0.},
                  {0.,0.,0.,0.,0.,0.,0.,0.,0.,0.,0.,0.,0.,0.,0.},
                  {0.,0.,0.,0.,0.,0.,0.,0.,0.,0.,0.,0.,0.,0.,0.},
                  {0.,0.,0.,0.,0.,0.,0.,0.,0.,0.,0.,0.,0.,0.,0.},
                  {0.,+5.,0.,0.,0.,0.,0.,0.,0.,0.,0.,0.,0.,0.,-1.}};

float G=0.,kT=30.,P,BF; // G- gravitational constant, kT - temperature parameter, BF - Boltzman factor
int sig=10;
char str[25];

float enkap1,enkap11,envz1,envz11,engpr,enpred, enbun,cenbun;
float enkap2,enkap22,envz2,envz22,engpo,enpo,enpole,cenpole,enepole;
int main(void)
{
FILE *vystup1,*vystup2,*vystup3,*vystup4,*vystup5;
/*request auto detection*/
int gdriver = DETECT, gmode, errorcode;
```



```

        /*initialiye graphics and local variables*/
        initgraph(&gdriver, &gmode, "");

        /*read result of initialization*/
        errorcode =graphresult();

        /*an error occured*/
        if (errorcode != grOk)
        {
            printf("Graphics error: %s/n",grapherrormsg(errorcode));
            printf("Press any key to halt:");
            getch();
            exit(1);
        }
        setfillstyle(1,0);

//a[x][y][z] - initial Ising variables of 3D space
for(x=0;x<SMERX;x++)
    {for(y=0;y<SMERY;y++)
        {for(z=0;z<SMERZ;z++)
            {a[x][y][z]=15;}}
    }

//Ising variables of initial configuration of liquid
for(x=0;x<SMERX;x++)
    {for(y=0;y<SMERY;y++)
        {for(z=0;z<SMERZ/2;z++)
            {a[x][y][z]=1;}}
    }

//grafical output - cross section (x,y)
for(x=0;x<=SMERX-1;x++)
    {for(y=0;y<=SMERY-1;y++)
        {putpixel(x,y,a[x][y][rez1]);}
    }

//grafical outout - cross section (x,z)
for(x=0;x<=SMERX-1;x++)
    {for(z=0;z<=SMERZ-1;z++)
        {putpixel(x+SMERX+100,SMERZ-z,a[x][rez2][z]);}
    }

//open output field 1
//test of opening
if((vystup1=fopen("c:\\energie.cpp","w"))==NULL)
    {printf("output file error\n");getch();return 1;
    }

//open output field 2
//test of opening
if((vystup2=fopen("c:\\konec.cpp","w"))==NULL)
    {printf("output file error\n");getch();return 1;
    }

//open output field 3
//test of opening
if((vystup3=fopen("c:\\hladiny.cpp","w"))==NULL)
    {printf("output file error\n");getch();return 1;
    }

//open output field 4
//test of opening
if((vystup4=fopen("c:\\souradnice.cpp","w"))==NULL)
    {printf("output file error\n");getch();return 1;
    }

//open output field 5

```

```

//test of opening
if((vystup5=fopen("c:\\enepole.cpp","w"))==NULL)
    {printf("output file error\n");getch();return 1;
    }

//energy of the system

for(z=2;z<SMERZ-2;z++)
{for(x=2;x<SMERX-2;x++)
    {for(y=2;y<SMERY-2;y++)
        {xp=x;yp=y;zp=z;
        enpole=0.;cenpole=0.;
        for(i=-1;i<=1;i++)
            {for(j=-1;j<=1;j++)
                {for(l=-1;l<=1;l++)
                    {enpole=enpole+C[a[xp][yp][zp]][a[xp+i][yp+j][zp+l]];}
                } }
            cenpole=enpole-C[a[xp][yp][zp]][a[xp][yp][zp]];
            enepole=enepole+cenpole;
        } } }
}

fprintf(vystup5,"%8.5f\n",enepole);

//beginning of simulation cycle
cas=0;
krok=0;
srand((unsigned)time(NULL));
nav1:

//choose random cell a[x][y][z]

x=random(SMERX-2)+1;
y=random(SMERY-2)+1;
z=random(SMERZ-2)+1;

//look for liquid cell
kont=0;
if(a[x][y][z]==1)
    {for(i=x-1;i<x+2;i++)
        {for(j=y-1;j<y+2;j++)
            {for(l=z-1;l<z+2;l++)
                {if(a[i][j][l]==15)
                    {xk=x;yk=y;zk=z;kont=1;goto nav11;}
                } } } }
    }
//if
else {goto nav1;}
if (kont==0){goto nav1;}

nav11:
//choose random cell a[x][y][z]

x=random(SMERX-2)+1;
y=random(SMERY-2)+1;
z=random(SMERZ-2)+1;

//look for air cell
kont=0;
if(a[x][y][z]==15)
    {for(i=x-1;i<x+2;i++)
        {for(j=y-1;j<y+2;j++)
            {for(l=z-1;l<z+2;l++)
                {if(a[i][j][l]==1)
                    {xk=x;yk=y;zk=z;kont=1;goto nav11;}
                } } } }
    }

```



```

        {xv=x;yv=y;zv=z;kont=1;goto nav111;}

    }}//z,j,i
} //if
else {goto nav111;}
if(kont==0){goto nav111;}

nav111:

krok++;
//calculation of the energy of liquid cell a[xk][yk][zk] and air cell a[xv][yv][zv]
enkap1=0.;envz1=0.;enpred=0.;
for(i=-1;i<=1;i++)
    {for(j=-1;j<=1;j++)
        {for(l=-1;l<=1;l++)
            {enkap1=enkap1+C[a[xk][yk][zk]][a[xk+i][yk+j][zk+l]];
            envz1=envz1+C[a[xv][yv][zv]][a[xv+i][yv+j][zv+l]];}
        }}//l,j,i
    //without central cell
    enkap1=enkap1-C[a[xk][yk][zk]][a[xk][yk][zk]];
    envz1=envz1-C[a[xv][yv][zv]][a[xv][yv][zv]];
    //gravitational energy
    engpr=G*zk;
    //total energy
    enpred=engpr+enkap1+envz1;

//exchange of cell positins.. liquid a[xv][yv][zv]; air a[xk][yk][zk]
apomoc=a[xk][yk][zk];a[xk][yk][zk]=a[xv][yv][zv];a[xv][yv][zv]=apomoc;

//calculaiton of the liquid cell and air cell after exchange of positions

    enkap2=0.;envz2=0.;enpo=0.;
    for(i=-1;i<=1;i++)
        {for(j=-1;j<=1;j++)
            {for(l=-1;l<=1;l++)
                {enkap2=enkap2+C[a[xv][yv][zv]][a[xv+i][yv+j][zv+l]];
                envz2=envz2+C[a[xk][yk][zk]][a[xk+i][yk+j][zk+l]];}
            }}//l,j,i
        //without central cell
        enkap2=enkap2-C[a[xv][yv][zv]][a[xv][yv][zv]];
        envz2=envz2-C[a[xk][yk][zk]][a[xk][yk][zk]];

        //gravitational energy
        engpo=G*zv;
        //total energy
        enpo=engpo+enkap2+envz2;

//energy difference
deltaE=enpo-enpred;

//Boltzmanuv faktor BF, randomly generated number P
P=0.;BF=0.;
if(deltaE>0.){P=(rand()/(float)RAND_MAX);BF=(float)exp(-deltaE/kT);
if(P>BF)}

{//exchange of cell positions - bact to initial positins

    apomoc=a[xk][yk][zk];a[xk][yk][zk]=a[xv][yv][zv];a[xv][yv][zv]=apomoc;

    goto nav1;

} //end position exchange

} //end if(enpred<enpo)

energie=energie+deltaE;
if(fmod(cas,50.)==0.){fprintf(vystup1,"%8d %8.5f\n",cas,energie);}

```

```

if(zk==rez1){putpixel(xk,yk,a[xk][yk][rez1]);}
if(zv==rez1){putpixel(xv,yv,a[xv][yv][rez1]);}
if(yk==rez2){putpixel(xk+SMERX+100,SMERZ-zk,a[xk][rez2][zk]);}
if(yv==rez2){putpixel(xv+SMERX+100,SMERZ-zv,a[xv][rez2][zv]);}

bar(getmaxx()-70,getmaxy()-30,getmaxx(),getmaxy()-10);
outtextxy(getmaxx()-100,getmaxy()-20,"k=");
outtextxy(getmaxx()-70,getmaxy()-20,gcvt(krok,sig,str));
if(krok>pockr){goto konec;}

//output of energy in simulation time intervals

cas++;
outtextxy(getmaxx()-250,getmaxy()-20,"cas=");
bar(getmaxx()-220,getmaxy()-30,getmaxx()-150,getmaxy()-10);
outtextxy(getmaxx()-200,getmaxy()-20,gcvt(cas,sig,str));

goto navl;

konec: //end of simulatin cycle
fprintf(vystup2,"%8d %8d %8.5f\n",cas,krok,energie);

// energy belong z axis
for(z=2;z<SMERZ-2;z++)
{for(x=2;x<SMERX-2;x++)
{for(y=2;y<SMERY-2,y++)
{xb=x,yb=y,zb=z;enbun=0;cenbun=0;
for(i=-1;i<=1;i++)
{for(j=-1;j<=1;j++)
{for(l=-1;l<=1;l++)
{enbun=enbun+C[a[xb][yb][zb]][a[xb+i][yb+j][zb+l]];};
}
}
}
}

}cenbun=enbun-C[a[xb][yb][zb]][a[xb][yb][zb]];
fprintf(vystup3,"%8d %8.5f\n",zb,cenbun);}

//x, y, z co-rdinates of liquid cells
for(z=0;z<SMERZ;z++)
{for(x=0;x<SMERX;x++)
{for(y=0;y<SMERY;y++)
{if(a[x][y][z]==1){fprintf(vystup4,"%8d %8d %8d %8d\n",x,y,z,a[x][y][z]);}

}
}
}

fclose (vystup1);
fclose (vystup2);
fclose (vystup3);
fclose (vystup4);
fclose (vystup5);
getch ();
closegraph();
return 0;
}

```


Appendix 3

Microsoft Visual Studio Program for simulation of liquid drop on homogeneous surface

The computer simulation results are mentioned in the Chapter 5.4.2 and 5.4.3.

```
/*3D lattice model - liquid drop on homogeneous flat surface*/
/*distilled water*/

# include "graphics.h"
# include <stdlib.h>
# include <stdio.h>
# include <conio.h>
# include <math.h>
# include <float.h>
# include <time.h>
//dimensions of 3D lattice
# define SMERX 80
# define SMERY 80
# define SMERZ 30

//global variables
int a[SMERX][SMERY][SMERZ];
int q,cas,caskonec=6,krok,pockr=1500000,kont;
int x,y,z,cidlo,i,j,l,xk,yk,zk,xv,yv,zv,yp,zp;
int xkx,xkxr,zkx,zkxr,ykx,ykxr,xky,yky,zky,xkyr,ykyr,zkyr;
int apomoc,konec,rezl=1,rez2=40;

float xx,yy,zz,xxx,yyy,zzz,b,c,d,energie=0.,deltaE=0.;
int r=10,xs,ys,zs,vzd;//drop parameters r - drop diameter
//a[xs][ys][zs] - central point of the drop
/* exchange energies C[1][1] liquid-liquid, C[1][0] liquid-air, C[0][0] air-air*/
//float C[2][2]={ {-1.,+7.},{+7.,-91.}}; C1=91; C2=+7; C3=-1;
//float C[2][2]={ {-1.,+10.},{+10.,-92.}}; //113/2=56 (0.9%NaCl); C1=-92; C2=+10; C3=-1;
//float C[2][2]={ {-1.,+4.},{+4.,-57.}}; //66/2=33 (oil); C1=57; C2=+4; C3=-1;
//30-33*cos(46.2)=7; surface tension of oil-surface energy of PP*cos(angle)=46.2
//surface tensin of oil = 2*4-(-47)-(-10)=66/2=33
//surface tensin of PP = 2*(+10)-(-30)-(-10)=60/2=30
//interface tension oil-PP = 2*(-31)-(-47)-(-30)=15/2=7

/* C[1][1] liquid-liquid; C[1][2] liquid-solid; C[1][16] liquid-air;
   C[2][2] solid-solid; C[2][16] air-solid; C[16][16] air-air;
   //lower liquid surface tension, contact angle less than zero
   //30=>13*1+(20,19,18,17,...)
   /*liquid surface tension = 2*1-(-20)-(-2)=24/2=12;
   C[1][1]=-20; C[1][16]=1; C[16][16]=-2;*/
   /*PP surface energy = 2*(+14)-(-30)-(-2)=60/3=30;
   C[2][2]=-30; C[2][16]=+14; C[16][16]=-2;*/
   /*interface tension liquid-PP = 2*(-6)-(-21)-(-30)=38/2= 19.5
   C[1][1]=-21; C[1][2]=-6; C[2][2]=-30;*/
   /*interface tensin liquid-PP = 2*(-10)-(-21)-(-30)=31/2= 15.5
   C[1][1]=-21; C[1][2]=-10; C[2][2]=-30;*/
   /*interface tension liquid-PP = 2*(-4)-(-21)-(-30)=43/2= 21.5
   C[1][1]=-21; C[1][2]=-4; C[2][2]=-30;*/

float C[16][16]={ {0.,0.,0.,0.,0.,0.,0.,0.,0.,0.,0.,0.,0.,0.,0.,0.},
                  {0.,-21.,-4.,0.,0.,0.,0.,0.,0.,0.,0.,0.,0.,+1.,},
                  {0.,-4.,-30.,0.,0.,0.,0.,0.,0.,0.,0.,0.,0.,+14.,},
                  {0.,0.,0.,0.,0.,0.,0.,0.,0.,0.,0.,0.,0.,0.,},
                  {0.,0.,0.,0.,0.,0.,0.,0.,0.,0.,0.,0.,0.,0.,},
                  {0.,0.,0.,0.,0.,0.,0.,0.,0.,0.,0.,0.,0.,0.,},
                  {0.,0.,0.,0.,0.,0.,0.,0.,0.,0.,0.,0.,0.,0.,},
                  {0.,0.,0.,0.,0.,0.,0.,0.,0.,0.,0.,0.,0.,0.,},
                  {0.,0.,0.,0.,0.,0.,0.,0.,0.,0.,0.,0.,0.,0.,},
                  {0.,0.,0.,0.,0.,0.,0.,0.,0.,0.,0.,0.,0.,0.,},
                  {0.,0.,0.,0.,0.,0.,0.,0.,0.,0.,0.,0.,0.,0.,},
                  {0.,0.,0.,0.,0.,0.,0.,0.,0.,0.,0.,0.,0.,0.,},
                  {0.,0.,0.,0.,0.,0.,0.,0.,0.,0.,0.,0.,0.,0.,},
                  {0.,0.,0.,0.,0.,0.,0.,0.,0.,0.,0.,0.,0.,0.,},
                  {0.,0.,0.,0.,0.,0.,0.,0.,0.,0.,0.,0.,0.,0.,},
                  {0.,0.,0.,0.,0.,0.,0.,0.,0.,0.,0.,0.,0.,0.,}
```

[illegible]


```

for(x=0;x<=SMERX-1;x++)
    {for(y=0;y<=SMERY-1;y++)
        {putpixel(x,y,a[x][y][rez1]);}
    }
//grafical outout - cross section (x,z)
for(x=0;x<=SMERX-1;x++)
    {for(z=0;z<=SMERZ-1;z++)
        {putpixel(x+SMERX+100,SMERZ-z,a[x][rez2][z]);}
    }

//open output field 1
//test of opening
if((vystup1=fopen("c:\\energie.cpp","w"))==NULL)
    {printf("output file error\n");getch();return 1;
    }
//open output field 2
//test of opening
if((vystup2=fopen("c:\\konec.cpp","w"))==NULL)
    {printf("output file error\n");getch();return 1;
    }
//open output filed 4
//test of opening
if((vystup4=fopen("c:\\souradnice.cpp","w"))==NULL)
    {printf("output file error\n");getch();return 1;
    }
//open output field 5
//test of opening
if((vystup5=fopen("c:\\enepole.cpp","w"))==NULL)
    {printf("output file error\n");getch();return 1;
    }

//open output field 6
//test of opening
if((vystup6=fopen("c:\\xz.cpp","w"))==NULL)
    {printf("output file error\n");getch();return 1;
    }

//open output field 7
//test of opening
if((vystup7=fopen("c:\\yz.cpp","w"))==NULL)
    {printf("output file error\n");getch();return 1;
    }

//the enegy of the system

for(z=2;z<SMERZ-2;z++)
{for(x=2;x<SMERX-2;x++)
    {for(y=2;y<SMERY-2;y++)
        {xp=x;yp=y;zp=z;
        enpole=0.;cenpole=0.;
        for(i=-1;i<=1;i++)
            {for(j=-1;j<=1;j++)
                {for(l=-1;l<=1;l++)
                    {enpole=enpole+C[a[xp][yp][zp]][a[xp+i][yp+j][zp+l]];}
                } }
        cenpole=enpole-C[a[xp][yp][zp]][a[xp][yp][zp]];
        enepole=enepole+cenpole;
    }
    }
} //1,j,i

fprintf(vystup5,"%8.5f\n",enepole);

//the beginning of simulation cycle
cas=0;
krok=0;
srand((unsigned)time(NULL));
nav1:

```

```

//choose random cell a[x][y][z]

x=random(SMERX-2)+1;
y=random(SMERY-2)+1;
z=random(SMERZ-2)+1;

//look for liquid cell
kont=0;
if(a[x][y][z]==1)
{for(i=x-1;i<x+2;i++)
  {for(j=y-1;j<y+2;j++)
    {for(l=z-1;l<z+2;l++)
      {//liquid - air interface
        if(a[i][j][l]==15)
          {xk=x;yk=y;zk=z;kont=1;goto nav11;}
      }
    }
  }
}

} //if
else {goto nav1;}
if (kont==0){goto nav1;}

nav11:
//choose random cell a[x][y][z]

x=random(SMERX-2)+1;
y=random(SMERY-2)+1;
z=random(SMERZ-2)+1;

//look for air cell
kont=0;
if(a[x][y][z]==15)
{for(i=x-1;i<x+2;i++)
  {for(j=y-1;j<y+2;j++)
    {for(l=z-1;l<z+2;l++)
      {//liquid - air interface
        if(a[i][j][l]==1)
          {xv=x;yv=y;zv=z;kont=1;goto nav111;}
      }
    }
  }
}

} //if
else {goto nav11;}
if(kont==0){goto nav11;}

nav111:
krok++;
//calculation of the energy of liquid cell a[xk][yk][zk] and air cell a[xv][yv][zv]
enkap1=0.;envz1=0.;enpred=0.;
for(i=1;i<=1;i++)
  {for(j=1;j<=1;j++)
    {for(l=1;l<=1;l++)
      {enkap1=enkap1+C[a[xk][yk][zk]][a[xk+i][yk+j][zk+l]];
        envz1=envz1+C[a[xv][yv][zv]][a[xv+i][yv+j][zv+l]];}
    }
  }
} //l,j,i
//without central cell
enkap11=enkap1-C[a[xk][yk][zk]][a[xk][yk][zk]];
envz11=envz1-C[a[xv][yv][zv]][a[xv][yv][zv]];
//gravitational energy
engpr=G*zk;
//total energy
enpred=enkap11+envz11;

//exchange of cell positins.. liquid a[xv][yv][zv]; air a[xk][yk][zk]
apomoc=a[xk][yk][zk];a[xk][yk][zk]=a[xv][yv][zv];a[xv][yv][zv]=apomoc;

```



```

//calculaiton of the liquid cell and air cell after exchange of positions
enkap2=0.;envz2=0.;enpo=0.;
for(i=1;i<=1;i++)
    {for(j=1;j<=1;j++)
        {for(l=1;l<=1;l++)
            {enkap2=enkap2+C[a[xv][yv][zv]][a[xv+i][yv+j][zv+l]];
            envz2=envz2+C[a[xk][yk][zk]][a[xk+i][yk+j][zk+l]];}
        } } //l,j,i
//without centrall cell
enkap22=enkap2-C[a[xv][yv][zv]][a[xv][yv][zv]];
envz22=envz2-C[a[xk][yk][zk]][a[xk][yk][zk]];

//gravitational energy
engpo=G*zv;
//total energy
enpo=engpo+enkap22+envz22;
//energy difference
deltaE=enpo-enpred;

//Boltzmanuv faktor BF, randomlly generated number P
P=0.;BF=0.;
if(deltaE>0.){P=(rand()/(float)RAND_MAX);BF=(float)exp(-deltaE/kT);
    if(P>BF)
        { //exchange of cell positions - bact to initial positins
        apomoc=a[xk][yk][zk];a[xk][yk][zk]=a[xv][yv][zv];a[xv][yv][zv]=apomoc;
        energie=energie;
        goto nav1;
        } //end position exchange
}

} //end if(enpred<enpo)

energie=energie+deltaE;
cas++;

if(fmod(cas,10.)==0.){fprintf(vystup1,"%8d %8.5f\n",krok,energie);}

    if(zk==rez1){putpixel(xk,yk,a[xk][yk][rez1]);}
    if(zv==rez1){putpixel(xv,yv,a[xv][yv][rez1]);}
    if(yk==rez2){putpixel(xk+SMERX+100,SMERZ-zk,a[xk][rez2][zk]);}
    if(yv==rez2){putpixel(xv+SMERX+100,SMERZ-zv,a[xv][rez2][zv]);}

    bar(getmaxx()-70,getmaxy()-30,getmaxx(),getmaxy()-10);
    outtextxy(getmaxx()-100,getmaxy()-20,"k=");
    outtextxy(getmaxx()-70,getmaxy()-20,gcvf(krok,sig,str));
    if(krok>pockr){goto konec;}

//output of energy in simulation time intervals

    outtextxy(getmaxx()-250,getmaxy()-20,"cas=");
    bar(getmaxx()-220,getmaxy()-30,getmaxx()-150,getmaxy()-10);
    outtextxy(getmaxx()-200,getmaxy()-20,gcvf(cas,sig,str));

    goto nav1;

konec:// end of simulation cycle

fprintf(vystup2,"%8d %8d %8.5f\n",cas,krok,energie);
//co-ordinates of liquid cells
for(z=0;z<SMERZ;z++)
    {for(x=0;x<SMERX;x++)
        {for(y=0;y<SMERY;y++)
            {if(a[x][y][z]==1){fprintf(vystup4,"%8d %8d %8d %8d\n",x,y,z,a[x][y][z]);}
        }
    }
}

```

```

    }
    } //l,j,i

//curves of liquid surface
/*
for(x=2;x<SMERX-2;x++)
{for(z=2;z<SMERZ-2;z++)
    {if(a[x][25][z]==1)
        xky=x;zky=z;
        {for(i=-1;i<=1;i++)
            {for(j=-1;j<=1;j++)
                {for(l=-1;l<=1;l++)
                    {if(a[xky+i][25+j][zky+l]==15){fprintf(vystup6,"%8d %8d %8d\n",xky,zky,a[xky][25][zky]);}}
                }
            } //l,i
        }
    } //z,y
}
*/
for(x=2;x<SMERX-2;x++)
    {for(z=1;z<SMERZ-2;z++)
        {if(a[x][40][SMERZ-z-1]==1){goto print1;}}
print1: xky=x;zky=SMERZ-z-1;fprintf(vystup6,"%8d %8d %8d\n",xky,zky,a[xky][40][zky]);
    } //z,y

for(y=2;y<SMERY-2;y++)
    {for(z=1;z<SMERZ-2;z++)
        {if(a[40][y][SMERZ-z-1]==1){goto print2;}}
print2: ykx=y;zkx=SMERZ-z-1;fprintf(vystup7,"%8d %8d %8d\n",ykx,zkx,a[40][ykx][zkx]);
    } //z,y

fclose (vystup1);
fclose (vystup2);
fclose (vystup4);
fclose (vystup5);
fclose (vystup6);
fclose (vystup7);
getch ();
closegraph();
return 0;
}

```


Appendix 4

Microsoft Visual Studio Program for simulation of liquid drop on a heterogeneous substrate

The computer simulation results are mentined in the Chapter 5.5.

```
/*3D lattice model - liquid drop on heterogeneous substrate*/

# include<graphics.h>
# include<stdlib.h>
# include<stdio.h>
# include<conio.h>
# include<math.h>
# include<float.h>
# include<time.h>

# define SMERX 100
# define SMERY 100
# define SMERZ 40

//global variables
int a[SMERX][SMERY][SMERZ];
int q,cas,caskonec=6,krok,pockr=2,kont;
int x,y,z,cidlo,i,j,l,xk,yk,zk,xv,yv,zv,apomoc,konec,rez1=0,rez2=85;
float C1=-60.,C2=-30.,C3=-40.,C4=-75.,C5=-10.,C6=-10.,C7=-1.;
/* exchange energies C1 liquid - liquid, C2 liquid - air, C3 liquid - surface, C4 liquid - cross, C5 air - air,
   C6 air - surface, C7 air - cross*/
float xx,yy,zz,xxx,yyy,zzz,b,c,d,energie=0.;
int r=36,xs,ys,zs,vzd;//drop parameters

float J[5][5]={ {0.,C7,0.,C4,0.},{C7,C5,0.,C2,C6},
                {0.,0.,0.,0.,0.},{C4,C2,0.,C1,C3},
                {0.,C6,0.,C3,0.}};

float G=20.;
int sig=10;
char str[25];

float enkap1,envz1,engpr,enpred,enkap2,envz2,engpo,enpo;
int main(void)
{
FILE *vystup1;
/*request auto detection*/
int gdriver = DETECT, gmode, errorcode;
int xmax, ymax;

/*initialiye graphics and local variables*/
initgraph(&gdriver, &gmode, "D:\\BC\\BGI");

/*read result of initialization*/
errorcode =graphresult();

/*an error occured*/
if (errorcode != grOk)
{
printf("Graphics error: %s/n",grapherrormsg(errorcode));
printf("Press any key to halt:");
getch();
exit(1);
}
```

```

    }
    setfillstyle(1,0);

//a[x][y][z] - initial Ising variables of 3D space
for(x=0;x<SMERX;x++)
    {for(y=0;y<SMERY;y++)
        {for(z=0;z<SMERZ;z++)
            {a[x][y][z]=-1;}}
    }

//Ising variables of initial configuration of homogeneous surface
for(x=0;x<SMERX;x++)
    {for(y=0;y<SMERY;y++)
        {a[x][y][0]=2;}}

//Ising variables of initial configuration of cross
xs=(SMERX-1)/2;ys=(SMERY-1)/2;
for(x=xs-4;x<=xs+4;x++)
    {for(y=0;y<=SMERY-1;y++)
        {a[x][y][0]=-2;}}
for(x=0;x<=SMERX-1;x++)
    {for(y=ys-4;y<=ys+4;y++)
        {a[x][y][0]=-2;}}

//Ising variables of initial configuration of liquid
xs=(SMERX-1)/2;ys=(SMERY-1)/2;
xx=xs+0.1*r;yy=ys-0.2*r;zz=1;
for(x=0;x<SMERX-1;x++)
    {for(y=0;y<SMERY-1;y++)
        {for(z=1;z<SMERZ-1;z++)
            {vzd=sqrt(pow(x-xx,2)+pow(y-yy,2)+pow(z,2));
            if(vzd<=r){a[x][y][z]=1;}}
        }
    }

//grafical output - cross section (x,y)
for(x=0;x<=SMERX-1;x++)
    {for(y=0;y<=SMERY-1;y++)
        {putpixel(x,y,a[x][y][rez1]+2);}
    }

//grafical outout - cross section (x,z)
for(x=0;x<=SMERX-1;x++)
    {for(z=0;z<=SMERZ-1;z++)
        {putpixel(x+SMERX+100,SMERZ-z,a[x][rez2][z]+2);}
    }

//open output field 1
//test of opening
if((vystup1=fopen("e:\\vera\\energie.cpp", "w"))==NULL)
    {printf("output file error\n");getch();return 1;
    }

//the beginning of simulation cycle
cas=0;
krok=0;
randomize();
navl:

//choose random cell a[x][y][z]

x=random(SMERX-2)+1;
y=random(SMERY-2)+1;
z=random(SMERZ-2)+1;

//look for liquid cell
kont=0;
if(a[x][y][z]==1)
    {for(i=x-1;i<x+2;i++)
        {for(j=y-1;j<y+2;j++)
            {for(l=z-1;l<z+2;l++)

```



```

        {if(a[i][j][l]==-1)
        {xk=x;yk=y;zk=z;kont=1;goto nav11;}
        }}//z,j,i
    }//if
    else {goto nav1;}
    if (kont==0){goto nav1;}

nav11:
//choose random cell a[x][y][z]

x=random(SMERX-2)+1;
y=random(SMERY-2)+1;
z=random(SMERZ-2)+1;

//look for air cell
kont=0;
if(a[x][y][z]==-1)
    {for(i=x-1;i<=x+2;i++)
        {for(j=y-1;j<=y+2;j++)
            {for(l=z-1;l<=z+2;l++)
                {if(a[i][j][l]==1)
                    {xv=x;yv=y;zv=z;kont=1;goto nav11;}
                }}//z,j,i
            }
        }
    }//if
    else {goto nav1;}
    if(kont==0){goto nav1;}

nav11:
//calculation of the energy of liquid cell a[xk][yk][zk] and air cell a[xv][yv][zv]
    enkap1=0.;envz1=0.;enpred=0.;
    for(i=1;i<=1;i++)
        {for(j=1;j<=1;j++)
            {for(l=1;l<=1;l++)
                {enkap1=enkap1+J[a[xk][yk][zk]+2][a[xk+i][yk+j][zk+l]+2]
                    *a[xk][yk][zk]*a[xk+i][yk+j][zk+l];
                envz1=envz1+J[a[xv][yv][zv]+2][a[xv+i][yv+j][zv+l]+2]
                    *a[xv][yv][zv]*a[xv+i][yv+j][zv+l];}
            }
        }
    }//l,j,i
    //gravitational energy
    engpr=G*zk;
    //total energy
    enpred=engpr+enkap1+envz1;

//exchange of cell positins.. liquid a[xv][yv][zv]; air a[xk][yk][zk]
apomoc=a[xk][yk][zk];a[xk][yk][zk]=a[xv][yv][zv];a[xv][yv][zv]=apomoc;

//calcaiton of the liquid cell and air cell after exchange of positions
    enkap2=0.;envz2=0.;enpo=0.;
    for(i=1;i<=1;i++)
        {for(j=1;j<=1;j++)
            {for(l=1;l<=1;l++)
                {enkap2=enkap2+J[a[xk][yk][zk]+2][a[xk+i][yk+j][zk+l]+2]
                    *a[xk][yk][zk]*a[xk+i][yk+j][zk+l];
                envz2=envz2+J[a[xv][yv][zv]+2][a[xv+i][yv+j][zv+l]+2]
                    *a[xv][yv][zv]*a[xv+i][yv+j][zv+l];}
            }
        }
    }//l,j,i
    //gravitational energy
    engpo=G*zk;
    //total energy
    enpo=engpo+enkap2+envz2;

//energy difference
if(enpred>enpo)
    {if(zk==rez1){putpixel(xk,yk,a[xk][yk][rez1]+2);}
    if(zv==rez1){putpixel(xv,yv,a[xv][yv][rez1]+2);}
    if(yk==rez2){putpixel(xk+SMERX+100,SMERZ-zk,a[xk][rez2][zk]+2);}
    if(yv==rez2){putpixel(xv+SMERX+100,SMERZ-zv,a[xv][rez2][zv]+2);}
    }

```

```

        krok++;
        bar(getmaxx()-70,getmaxy()-30,getmaxx(),getmaxy()-10);
        outtextxy(getmaxx()-100,getmaxy()-20,"k=");
        outtextxy(getmaxx()-70,getmaxy()-20,gcv(t(krok,sig,str));
        if(krok>pockr){goto konec;}
//output of energy in simulation time intervals
energie=energie+(enpo-enpred);

//konec if(enpred<enpo)

else{//exchange of cell positions - bact to initial positins
apomoc=a[xk][yk][zk];a[xk][yk][zk]=a[xv][yv][zv];a[xv][yv][zv]=apomoc;
}

if(fmod(cas,50.)==0.){fprintf(vystup1,"%8d %8.5f\n",cas,energie);}

cas++;
outtextxy(getmaxx()-250,getmaxy()-20,"cas=");
bar(getmaxx()-220,getmaxy()-30,getmaxx()-150,getmaxy()-10);
outtextxy(getmaxx()-200,getmaxy()-20,gcv(t(cas,sig,str));

goto nav1;

konec: // end of simulation cycle
fclose (vystup1);
getch ();
closegraph();
return 0;
}

```


Appendix 5

Microsoft Visual Studio Program for simulation of liquid drop on a single fibre

The computer simulation results are shown in the Chapter 5.6.

```
/*3D lattice model - liquid drop on a single fibre*/
/*pharmaceutical oil*/

# include"graphics.h"
# include<stdlib.h>
# include<stdio.h>
# include<conio.h>
# include<math.h>
# include<float.h>
# include<time.h>
//dimensions of 3D system
# define SMERX 40
# define SMERY 100
# define SMERZ 40

//global variables
int a[SMERX][SMERY][SMERZ];
int q,cas,caskonec=6,krok,pockr=700,kont;
int x,y,z,cidlo,i,j,l,xk,yk,zk,xv,yv,zv,yp,zp;
int xkx,ykx,zkx,zky,yky,zky,zkxd,zkxh,ykxd,ykxh,xkyd,xkyh,zkyd,zkyh;
int apomoc,konec,rez1=20,rez2=20,rez3=50;

float xx,yy,zz,xxx,yyy,zzz,b,c,d,energie=0,deltaE=0;
int r=15,xs,ys,zs,vzd;//parametry kapky

/* exchange constant
C[1][1] liquid-liquid; C[1][2] liquid-solid; C[1][16] liquid-air;
C[2][2] solid-solid; C[2][16] solid-air; C[16][16] air-air;*/

//30-33*cos(46.2)=7 = interface tension between of oil-surface energy of PP*cos(angle)=46.2
//surface tension of oil = 2*4*(-47)-(-10)=66/2=33
//surface energy of PP = 2*(+10)-(-30)-(-10)=60/2=30
//interface energy of oil-PP = 2*(-31)-(-47)-(-30)=15/2=7
/*C[1][1]=-47; C[1][2]=-31;C[1][16]=4; C[2][2]=-30; C[2][16]=10; C[16][16]=-10;*/

float C[16][16]={ {0,0,0,0,0,0,0,0,0,0,0,0,0,0,0,0},
                  {0,-47,-31,0,0,0,0,0,0,0,0,0,0,0,0,+4},
                  {0,-31,-30,0,0,0,0,0,0,0,0,0,0,0,0,+10},
                  {0,0,0,0,0,0,0,0,0,0,0,0,0,0,0,0},
                  {0,0,0,0,0,0,0,0,0,0,0,0,0,0,0,0},
                  {0,0,0,0,0,0,0,0,0,0,0,0,0,0,0,0},
                  {0,0,0,0,0,0,0,0,0,0,0,0,0,0,0,0},
                  {0,0,0,0,0,0,0,0,0,0,0,0,0,0,0,0},
                  {0,0,0,0,0,0,0,0,0,0,0,0,0,0,0,0},
                  {0,0,0,0,0,0,0,0,0,0,0,0,0,0,0,0},
                  {0,0,0,0,0,0,0,0,0,0,0,0,0,0,0,0},
                  {0,0,0,0,0,0,0,0,0,0,0,0,0,0,0,0},
                  {0,0,0,0,0,0,0,0,0,0,0,0,0,0,0,0},
                  {0,0,0,0,0,0,0,0,0,0,0,0,0,0,0,0},
                  {0,+4,+10,0,0,0,0,0,0,0,0,0,0,0,0,-10}};
```

```

float G=0.,kT=30.,P,BF;//G - gravitational acceleration
//kT - parameter of thermodynamic temperature
int sig=10;
char str[25];

float enkap1, enkap11, envz1, envz11, engpr, enpred;
float enkap2, enkap22, envz2, envz22, engpo, enpo, enpole, cenpole, enepole;

int main(void)
{
FILE *vystup1, *vystup2, *vystup4, *vystup5, *vystup6, *vystup7, *vystup8, *vystup9;
/*request auto detection*/
int gdriver = DETECT, gmode, errorcode;

/*initialiye graphics and local variables*/
initgraph(&gdriver, &gmode, "");

/*read result of initialization*/
errorcode = graphresult();

/*an error occured*/
if (errorcode != grOk)
{
printf("Graphics error: %s/n", grapherrormsg(errorcode));
printf("Press any key to halt:");
getch();
exit(1);
}
setfillstyle(1,0);

//a[x][y][z] - Ising variables of 3D space
for(x=0;x<SMERX;x++)
{for(y=0;y<SMERY;y++)
{for(z=0;z<SMERZ;z++)
{a[x][y][z]=15;}}
}

//Ising variables of initial configuration of liquid
xs=(SMERX-1)/2;ys=(SMERY-1)/2;zs=(SMERZ-1)/2; //central point of liquid drop
for(x=0;x<SMERX-1;x++)
{for(y=0;y<SMERY-1;y++)
{for(z=1;z<SMERZ-1;z++)
{vzd=sqrt(pow(x-xs,2)+pow(y-ys,2)+pow(z-zs,2));
if(vzd<=r){a[x][y][z]=1;}
}} } //z,y,x

//Ising variables of initial configuration of single fibre
for(y=1;y<SMERY;y++)

{a[xs-3][y][zs-1]=2;
a[xs-3][y][zs]=2;
a[xs-3][y][zs+1]=2;
a[xs-2][y][zs-2]=2;
a[xs-2][y][zs-1]=2;
a[xs-2][y][zs]=2;
a[xs-2][y][zs+1]=2;
a[xs-2][y][zs+2]=2;
a[xs-1][y][zs-3]=2;
a[xs-1][y][zs-2]=2;
a[xs-1][y][zs-1]=2;
a[xs-1][y][zs]=2;
a[xs-1][y][zs+1]=2;
a[xs-1][y][zs+2]=2;
a[xs-1][y][zs+3]=2;
a[xs][y][zs-3]=2;
a[xs][y][zs-2]=2;

```



```

a[xs][y][zs-1]=2;
a[xs][y][zs]=2;
a[xs][y][zs+1]=2;
//a[xs][y][zs+2]=2;
//a[xs][y][zs+3]=2;
//a[xs+1][y][zs-3]=2;
//a[xs+1][y][zs-2]=2;
//a[xs+1][y][zs-1]=2;
a[xs+1][y][zs]=2;
//a[xs+1][y][zs+1]=2;
//a[xs+1][y][zs+2]=2;
//a[xs+1][y][zs+3]=2;
//a[xs+2][y][zs-2]=2;
//a[xs+2][y][zs-1]=2;
//a[xs+2][y][zs]=2;
//a[xs+2][y][zs+1]=2;
//a[xs+2][y][zs+2]=2;
//a[xs+3][y][zs-1]=2;
//a[xs+3][y][zs]=2;
//a[xs+3][y][zs+1]=2;
}

//grafical output - cross section (x,y)
for(x=0;x<=SMERX-1;x++)
    {for(y=0;y<=SMERY-1;y++)
        {putpixel(x,y,a[x][y][rez1]);}
    }
//grafical output - cross section (x,z)
for(y=0;y<=SMERY-1;y++)
    {for(z=0;z<=SMERZ-1;z++)
        {putpixel(y+SMERY+100,SMERZ-z,a[rez2][y][z]);}
    }

//grafical output - cross section (y,z)
for(x=0;x<=SMERX-1;x++)
    {for(z=0;z<=SMERZ-1;z++)
        {putpixel(x+SMERX+300,SMERZ-z,a[x][rez3][z]);}
    }

//open output field 1
//test of openinf
if((vystup1=fopen("c:\\energie.cpp","w"))==NULL)
    {printf("output file error\n");getch();return 1;
    }
//open output field 2
//test of opening
if((vystup2=fopen("c:\\konec.cpp","w"))==NULL)
    {printf("output file error\n");getch();return 1;
    }
//open output field 4
//test of opening
if((vystup4=fopen("c:\\souradnice.cpp","w"))==NULL)
    {printf("output file error\n");getch();return 1;
    }
//open output field 5
//test of opening
if((vystup5=fopen("c:\\enepole.cpp","w"))==NULL)
    {printf("output file error\n");getch();return 1;
    }

//open output field 6
//test of opening
if((vystup6=fopen("c:\\xzh.cpp","w"))==NULL)
    {printf("output file error\n");getch();return 1;
    }

```

```

//open output field 8
//test of opening
if((vystup8=fopen("c:\\xzd.cpp","w"))==NULL)
    {printf("output file error\n");getch();return 1;
    }

//open output field 7
//test of opening
if((vystup7=fopen("c:\\yzh.cpp","w"))==NULL)
    {printf("output file error\n");getch();return 1;
    }

//open output field 9
//test of opening
if((vystup9=fopen("c:\\yzd.cpp","w"))==NULL)
    {printf("output file error\n");getch();return 1;
    }

//energy of the sysytem

for(z=2;z<SMERZ-2;z++)
for(x=2;x<SMERX-2;x++)
    {for(y=2;y<SMERY-2;y++)
        {xp=x;yp=y;zp=z;
        enpole=0.;cenpole=0.;
            for(i=-1;i<=1;i++)
                {for(j=-1;j<=1;j++)
                    {for(l=-1;l<=1;l++)
                        {enpole=enpole+C[a[xp][yp][zp]][a[xp+i][yp+j][zp+l]];
                    } }
                cenpole=enpole-C[a[xp][yp][zp]][a[xp][yp][zp]];
                enepole=enepole+cenpole;
            } }
        } } //l,j,i

fprintf(vystup5,"%8.5f\n",enepole);

//beginning of simulation cycle
cas=0;
krok=0;
srand((unsigned)time(NULL));
nav1:

//choose random cell a[x][y][z]

x=random(SMERX-2)+1;
y=random(SMERY-2)+1;
z=random(SMERZ-2)+1;

//look for liquid cell
kont=0;
if(a[x][y][z]==1)
    {for(i=x-1;i<x+2;i++)
        {for(j=y-1;j<y+2;j++)
            {for(l=z-1;l<z+2;l++)
                { //liquid - air interface
                    if(a[i][j][l]==15)
                        {xk=x;yk=y;zk=z;kont=1;goto nav1;}
                } } } //z,j,i
    } } //if
else {goto nav1;}
if (kont==0){goto nav1;}

nav1:
//choose random cell a[x][y][z]

```



```

x=random(SMERX-2)+1;
y=random(SMERY-2)+1;
z=random(SMERZ-2)+1;

//look for air cell
kont=0;
if(a[x][y][z]==15)
{for(i=x-1;i<x+2;i++)
    {for(j=y-1;j<y+2;j++)
        {for(l=z-1;l<z+2;l++)
            {liquid - air interface
            if(a[i][j][l]==1)
                {xv=x;yv=y;zv=z;kont=1;goto nav111;}

            }}}//z,j,i
    }//if
    else {goto nav111;}
    if(kont==0){goto nav111;}

nav111:

krok++;
//calculation of energy of liquid cell and air cell in initial positions

enkap1=0.;envz1=0.;enpred=0.;
for(i=-1;i<=1;i++)
    {for(j=-1;j<=1;j++)
        {for(l=-1;l<=1;l++)
            {enkap1=enkap1+C[a[xk][yk][zk]][a[xk+i][yk+j][zk+l]];
            envz1=envz1+C[a[xv][yv][zv]][a[xv+i][yv+j][zv+l]];}
        } }//l,j,i
//without central cell
enkap11=enkap1-C[a[xk][yk][zk]][a[xk][yk][zk]];
envz11=envz1-C[a[xv][yv][zv]][a[xv][yv][zv]];
//gravitational energy
engpr=G*zk;
//total energy
enpred=engpr+enkap11+envz11;

//position exchange of liquid and air cell
apomoc=a[xk][yk][zk];a[xk][yk][zk]=a[xv][yv][zv];a[xv][yv][zv]=apomoc;

//calculation of energy of liquid cell and air cell after position exchange

enkap2=0.;envz2=0.;enpo=0.;
for(i=-1;i<=1;i++)
    {for(j=-1;j<=1;j++)
        {for(l=-1;l<=1;l++)
            {enkap2=enkap2+C[a[xv][yv][zv]][a[xv+i][yv+j][zv+l]];
            envz2=envz2+C[a[xk][yk][zk]][a[xk+i][yk+j][zk+l]];}
        } }//l,j,i
//without central cell
enkap22=enkap2-C[a[xv][yv][zv]][a[xv][yv][zv]];
envz22=envz2-C[a[xk][yk][zk]][a[xk][yk][zk]];

//gravitational energy
engpo=G*zv;
//total energy
enpo=engpo+enkap22+envz22;
//difference of energie before and after position exchange
deltaE=enpo-enpred;

//Boltzmanuv faktor - BF; randomly generated number P
P=0.;BF=0.;
if(deltaE>0.){P=(rand()/(float)RAND_MAX);BF=(float)exp(-deltaE/kT);

```

```

                                if(P>BF)
                                { //position exchange - bact to initial positions
apomoc=a[xk][yk][zk];a[xk][yk][zk]=a[xv][yv][zv];a[xv][yv][zv]=apomoc;
energie=energie;
                                goto nav1;
                                } //end of positin exchange

//end if(enpred<enpo)

energie=energie+deltaE;
cas++;

if(fmod(cas,10.)==0.){fprintf(vystup1,"%8d %8.5f\n",cas,energie);}

                                if(zk==rez1){putpixel(xk,yk,a[xk][yk][rez1]);}
                                if(zv==rez1){putpixel(xv,yv,a[xv][yv][rez1]);}
                                if(xk==rez2){putpixel(yk+SMERY+100,SMERZ-zk,a[rez2][yk][zk]);}
                                if(xv==rez2){putpixel(yv+SMERY+100,SMERZ-zv,a[rez2][yv][zv]);}
                                if(yk==rez2){putpixel(xk+SMERX+300,SMERZ-zk,a[xk][rez3][zk]);}
                                if(yv==rez2){putpixel(xv+SMERX+300,SMERZ-zv,a[xv][rez3][zv]);}

                                bar(getmaxx()-70,getmaxy()-30,getmaxx(),getmaxy()-10);
                                outtextxy(getmaxx()-100,getmaxy()-20,"k=");
                                outtextxy(getmaxx()-70,getmaxy()-20,gcvt(krok,sig,str));
                                if(krok>pockr){goto konec;}

//output of energy in simultin time intervals

                                outtextxy(getmaxx()-250,getmaxy()-20,"cas=");
                                bar(getmaxx()-220,getmaxy()-30,getmaxx()-150,getmaxy()-10);
                                outtextxy(getmaxx()-200,getmaxy()-20,gcvt(cas,sig,str));

                                goto nav1;

                                konec://end of simulatio cycle
                                fprintf(vystup2,"%8d %8d %8.5f\n",cas,krok,energie);
                                //co-ordination of liquid cells
                                for(z=0;z<SMERZ;z++)
                                        {for(x=0;x<SMERX;x++)
                                                {for(y=0;y<SMERY;y++)
                                                        {if(a[x][y][z]==1){fprintf(vystup4,"%8d %8d %8d %8d\n",x,y,z,a[x][y][z]);}
                                                        }
                                                }
                                        } //l,j,i

                                //crves of liquid surface
                                /*
                                for(x=2;x<SMERX-2;x++)
                                {for(z=2;z<SMERZ-2;z++)
                                        {if(a[x][25][z]==1)
                                                xky=x,zky=z;
                                                {for(i=-1;i<=1;i++)
                                                        {for(j=-1;j<=1;j++)
                                                                {for(l=-1;l<=1;l++)
                                                                        {if(a[xky+i][25+j][zky+l]==15){fprintf(vystup6,"%8d %8d %8d\n",xky,zky,a[xky][25][zky]);}
                                                                        }
                                                                }
                                                        }
                                                }
                                        } //z,y
                                }
                                */
                                for(x=2;x<SMERX-2;x++)
                                {for(z=2;z<SMERZ-2;z++)
                                        {if(a[x][50][SMERZ-z]==1){goto print1;}}
                                }
                                print1: xkyh=x,zkyh=SMERZ-z;fprintf(vystup6,"%8d %8d %8d\n",xkyh,zkyh,a[xkyh][50][zkyh]);
                                } //z,y

```



```

for(x=2;x<SMERX-2;x++)
    {for(z=2;z<SMERZ-2;z++)
        {if(a[x][50][z]==1){goto print3;}}
print3: xkyd=x;zkyd=z;fprintf(vystup8,"%8d %8d %8d\n",xkyd,zkyd,a[xkyd][50][zkyd]);
        }
        //z,y

for(y=2;y<SMERY-2;y++)
    {for(z=2;z<SMERZ-2;z++)
        {if(a[15][y][z]==1){goto print4;}}
print4: ykxd=y;zkxd=z;fprintf(vystup9,"%8d %8d %8d\n",ykxd,zkxd,a[15][ykxd][zkxd]);
        }
        //z,y

for(y=2;y<SMERY-2;y++)
    {for(z=2;z<SMERZ-2;z++)
        {if(a[15][y][SMERZ-z]==1){goto print2;}}
print2: ykxh=y;zkxh=SMERZ-z;fprintf(vystup7,"%8d %8d %8d\n",ykxh,zkxh,a[15][ykxh][zkxh]);
        }
        //z,y

fclose (vystup1);
fclose (vystup2);
fclose (vystup4);
fclose (vystup5);
fclose (vystup6);
fclose (vystup7);
fclose (vystup8);
fclose (vystup9);
getch ();
closegraph();
return 0;
}

```

Appendix 6

Microsoft Visual Studio Program for simulation of liquid drop on parallel fibres ordered into horizontal fibrous assemblies

The computer simulation results are shown in the Chapter 5.7.2.

```
/*3D lattice model – assemblies of parallel fibres*/
/*pharmaceutical oil*/

# include"graphics.h"
# include<stdlib.h>
# include<stdio.h>
# include<conio.h>
# include<math.h>
# include<float.h>
# include<time.h>

# define SMERX 40
# define SMERY 300
# define SMERZ 40

//global variables
int a[SMERX][SMERY][SMERZ];
int q,cas,caskonec=6,krok,pockr=2000,kont;
int x,y,z,cidlo,i,j,l,xk,yk,zk,xv,yv,zv,xp,yp,zp;
int xkx,ykx,zkx,zky,yky,zky,zkxd,zkxh,ykxd,ykxh,xkyd,xkyh,zkyd,zkyh;
int apomoc,konec,rez1=20,rez2=20,rez3=150;

float xx,yy,zz,xxx,yyy,zzz,b,c,d,energie=0.,deltaE=0.;
int r=15,xs,ys,zs,x1,z1,x2,z2,x3,z3,x4,z4,x5,z5,x6,z6,vzd;//parametry kapky
int x11,z11,x11,z11;

// exchange constant
//float C[2][2]={ {-1.,+7.},{+7.,-91.}};
//float C[2][2]={ {-1.,+10.},{+10.,-92.}}; //113/2=56 (0.9%NaCl)
//float C[2][2]={ {-1.,+4.},{+4.,-57.}}; //66/2=33 (olej)
//30-33*cos(46.2)=7 = nap oil-PP, angle = 46.2
//surface tension of oil = 2*4*(-47)-(-10)=66/2=33
//surface energy of PP = 2*(+10)-(-30)-(-10)=60/2=30
//interface tension oil-PP = 2*(-31)-(-47)-(-30)=15/2=7

float C[16][16]={ {0.,0.,0.,0.,0.,0.,0.,0.,0.,0.,0.,0.,0.,0.,0.,0.},
{0.,-47.,-31.,0.,0.,0.,0.,0.,0.,0.,0.,0.,0.,0.,+4.},
{0.,-31.,-30.,0.,0.,0.,0.,0.,0.,0.,0.,0.,0.,0.,+10.},
{0.,0.,0.,0.,0.,0.,0.,0.,0.,0.,0.,0.,0.,0.,0.},
{0.,0.,0.,0.,0.,0.,0.,0.,0.,0.,0.,0.,0.,0.,0.},
{0.,0.,0.,0.,0.,0.,0.,0.,0.,0.,0.,0.,0.,0.,0.},
{0.,0.,0.,0.,0.,0.,0.,0.,0.,0.,0.,0.,0.,0.,0.},
{0.,0.,0.,0.,0.,0.,0.,0.,0.,0.,0.,0.,0.,0.,0.},
{0.,0.,0.,0.,0.,0.,0.,0.,0.,0.,0.,0.,0.,0.,0.},
{0.,0.,0.,0.,0.,0.,0.,0.,0.,0.,0.,0.,0.,0.,0.},
{0.,0.,0.,0.,0.,0.,0.,0.,0.,0.,0.,0.,0.,0.,0.},
{0.,0.,0.,0.,0.,0.,0.,0.,0.,0.,0.,0.,0.,0.,0.},
{0.,0.,0.,0.,0.,0.,0.,0.,0.,0.,0.,0.,0.,0.,0.},
{0.,+4.,+10.,0.,0.,0.,0.,0.,0.,0.,0.,0.,0.,0.,-10.}};
```



```

float G=0.,kT=30.,P,BF; //G – gravitational constant, kT – temperature parameter, BF – Boltzman factor
int sig=10;
char str[25];

float enkap1, enkap11, envz1, envz11, engpr, enpred;
float enkap2, enkap22, envz2, envz22, engpo, enpo, enpole, cenpole, enepole;
int main(void)
{
FILE *vystup1,*vystup2,*vystup3,*vystup4,*vystup5,*vystup6,*vystup7,*vystup8,*vystup9,*vystup77;
/*request auto detection*/
int gdriver = DETECT, gmode, errorcode;

/*initialiye graphics and local variables*/
initgraph(&gdriver, &gmode, "");

/*read result of initialization*/
errorcode = graphresult();

/*an error occured*/
if (errorcode != grOk)
{
printf("Graphics error: %s/n", grapherrormsg(errorcode));
printf("Press any key to halt:");
getch();
exit(1);
}
setfillstyle(1,0);

//a[x][y][z] - initial Ising variables of 3D space
for(x=0;x<SMERX;x++)
{
for(y=0;y<SMERY;y++)
{
for(z=0;z<SMERZ;z++)
{
a[x][y][z]=15;
}
}
}

//Ising variables of initial configuration of liquid
xs=(SMERX-1)/2;ys=(SMERY-1)/2;zs=(SMERZ-1)/2;
for(x=0;x<SMERX-1;x++)
{
for(y=0;y<SMERY-1;y++)
{
for(z=1;z<SMERZ-1;z++)
{
vzd=sqrt(pow(x-xs,2)+pow(y-ys,2)+pow(z-zs,2));
if(vzd<=r){a[x][y][z]=1;}
}
}
}

x1=xs+2; z1=zs-2; x2=xs-1; z2=zs-2; x3=xs+3; z3=zs; x4=xs-3; z4=zs; x5=xs-2; z5=zs+2; x6=xs+1; z6=zs+2;

//Ising variables of initial configuration of fibre A - assemble
/*for(y=1;y<SMERY;y++)

{
a[xs-1][y][zs]=2; a[xs][y][zs-1]=2; a[xs][y][zs]=2; a[xs][y][zs+1]=2; a[xs+1][y][zs]=2;
//a[x1-1][y][z1]=2; a[x1][y][z1-1]=2; a[x1][y][z1]=2; a[x1][y][z1+1]=2; a[x1+1][y][z1]=2;
// a[x2-1][y][z2]=2; a[x2][y][z2-1]=2; a[x2][y][z2]=2; a[x2][y][z2+1]=2; a[x2+1][y][z2]=2;
a[x3-1][y][z3]=2; a[x3][y][z3-1]=2; a[x3][y][z3]=2; a[x3][y][z3+1]=2; a[x3+1][y][z3]=2;
//a[x4-1][y][z4]=2; a[x4][y][z4-1]=2; a[x4][y][z4]=2; a[x4][y][z4+1]=2; a[x4+1][y][z4]=2;
//a[x5-1][y][z5]=2; a[x5][y][z5-1]=2; a[x5][y][z5]=2; a[x5][y][z5+1]=2; a[x5+1][y][z5]=2;
//a[x6-1][y][z6]=2; a[x6][y][z6-1]=2; a[x6][y][z6]=2; a[x6][y][z6+1]=2; a[x6+1][y][z6]=2;
}
*/

/*
//Ising variables of initial configuration of fibre C
for(y=1;y<SMERY;y++)

{
a[xs-2][y][zs-1]=2; a[xs-2][y][zs]=2; a[xs-2][y][zs+1]=2;
a[xs-1][y][zs-2]=2; a[xs-1][y][zs-1]=2; a[xs-1][y][zs]=2; a[xs-1][y][zs+1]=2; a[xs-1][y][zs+2]=2;
}
*/

```

```

a[xs][y][zs-2]=2;a[xs][y][zs-1]=2;a[xs][y][zs]=2;a[xs][y][zs+1]=2;a[xs][y][zs+2]=2;
a[xs+1][y][zs-2]=2;a[xs+1][y][zs-1]=2;a[xs+1][y][zs]=2;a[xs+1][y][zs+1]=2;a[xs+1][y][zs+2]=2;
a[xs+2][y][zs-1]=2;a[xs+2][y][zs]=2;a[xs+2][y][zs+1]=2;}

// fibrous assemble
//1
x11=xs+5;z11=zs;
for(y=1;y<SMERY;y++)

{a[x11-2][y][z11-1]=2;a[x11-2][y][z11]=2;a[x11-2][y][z11+1]=2;
a[x11-1][y][z11-2]=2;a[x11-1][y][z11-1]=2;a[x11-1][y][z11]=2;a[x11-1][y][z11+1]=2;a[x11-1][y][z11+2]=2;
a[x11][y][z11-2]=2;a[x11][y][z11-1]=2;a[x11][y][z11]=2;a[x11][y][z11+1]=2;a[x11][y][z11+2]=2;
a[x11+1][y][z11-2]=2;a[x11+1][y][z11-1]=2;a[x11+1][y][z11]=2;a[x11+1][y][z11+1]=2;a[x11+1][y][z11+2]=2;
a[x11+2][y][z11-1]=2;a[x11+2][y][z11]=2;a[x11+2][y][z11+1]=2;}

//2
x11=xs+3;z11=zs-5;
for(y=1;y<SMERY;y++)

{a[x11-2][y][z11-1]=2;a[x11-2][y][z11]=2;a[x11-2][y][z11+1]=2;
a[x11-1][y][z11-2]=2;a[x11-1][y][z11-1]=2;a[x11-1][y][z11]=2;a[x11-1][y][z11+1]=2;a[x11-1][y][z11+2]=2;
a[x11][y][z11-2]=2;a[x11][y][z11-1]=2;a[x11][y][z11]=2;a[x11][y][z11+1]=2;a[x11][y][z11+2]=2;
a[x11+1][y][z11-2]=2;a[x11+1][y][z11-1]=2;a[x11+1][y][z11]=2;a[x11+1][y][z11+1]=2;a[x11+1][y][z11+2]=2;
a[x11+2][y][z11-1]=2;a[x11+2][y][z11]=2;a[x11+2][y][z11+1]=2;}

//3
x11=xs-2;z11=zs-5;
for(y=1;y<SMERY;y++)

{a[x11-2][y][z11-1]=2;a[x11-2][y][z11]=2;a[x11-2][y][z11+1]=2;
a[x11-1][y][z11-2]=2;a[x11-1][y][z11-1]=2;a[x11-1][y][z11]=2;a[x11-1][y][z11+1]=2;a[x11-1][y][z11+2]=2;
a[x11][y][z11-2]=2;a[x11][y][z11-1]=2;a[x11][y][z11]=2;a[x11][y][z11+1]=2;a[x11][y][z11+2]=2;
a[x11+1][y][z11-2]=2;a[x11+1][y][z11-1]=2;a[x11+1][y][z11]=2;a[x11+1][y][z11+1]=2;a[x11+1][y][z11+2]=2;
a[x11+2][y][z11-1]=2;a[x11+2][y][z11]=2;a[x11+2][y][z11+1]=2;}

//4
x11=xs-5;z11=zs;
for(y=1;y<SMERY;y++)

{a[x11-2][y][z11-1]=2;a[x11-2][y][z11]=2;a[x11-2][y][z11+1]=2;
a[x11-1][y][z11-2]=2;a[x11-1][y][z11-1]=2;a[x11-1][y][z11]=2;a[x11-1][y][z11+1]=2;a[x11-1][y][z11+2]=2;
a[x11][y][z11-2]=2;a[x11][y][z11-1]=2;a[x11][y][z11]=2;a[x11][y][z11+1]=2;a[x11][y][z11+2]=2;
a[x11+1][y][z11-2]=2;a[x11+1][y][z11-1]=2;a[x11+1][y][z11]=2;a[x11+1][y][z11+1]=2;a[x11+1][y][z11+2]=2;
a[x11+2][y][z11-1]=2;a[x11+2][y][z11]=2;a[x11+2][y][z11+1]=2;}

//5
x11=xs-2;z11=zs+5;
for(y=1;y<SMERY;y++)

{a[x11-2][y][z11-1]=2;a[x11-2][y][z11]=2;a[x11-2][y][z11+1]=2;
a[x11-1][y][z11-2]=2;a[x11-1][y][z11-1]=2;a[x11-1][y][z11]=2;a[x11-1][y][z11+1]=2;a[x11-1][y][z11+2]=2;
a[x11][y][z11-2]=2;a[x11][y][z11-1]=2;a[x11][y][z11]=2;a[x11][y][z11+1]=2;a[x11][y][z11+2]=2;
a[x11+1][y][z11-2]=2;a[x11+1][y][z11-1]=2;a[x11+1][y][z11]=2;a[x11+1][y][z11+1]=2;a[x11+1][y][z11+2]=2;
a[x11+2][y][z11-1]=2;a[x11+2][y][z11]=2;a[x11+2][y][z11+1]=2;}

//6
x11=xs+3;z11=zs+5;
for(y=1;y<SMERY;y++)

{a[x11-2][y][z11-1]=2;a[x11-2][y][z11]=2;a[x11-2][y][z11+1]=2;
a[x11-1][y][z11-2]=2;a[x11-1][y][z11-1]=2;a[x11-1][y][z11]=2;a[x11-1][y][z11+1]=2;a[x11-1][y][z11+2]=2;
a[x11][y][z11-2]=2;a[x11][y][z11-1]=2;a[x11][y][z11]=2;a[x11][y][z11+1]=2;a[x11][y][z11+2]=2;
a[x11+1][y][z11-2]=2;a[x11+1][y][z11-1]=2;a[x11+1][y][z11]=2;a[x11+1][y][z11+1]=2;a[x11+1][y][z11+2]=2;
a[x11+2][y][z11-1]=2;a[x11+2][y][z11]=2;a[x11+2][y][z11+1]=2;}
*/

```

//Using variables of initial configuration of fibre D


```
for(y=1;y<SMERY;y++)
```

```
{
    a[xs-3][y][zs-1]=2;a[xs-3][y][zs]=2;a[xs-3][y][zs+1]=2;
    a[xs-2][y][zs-2]=2;a[xs-2][y][zs-1]=2;a[xs-2][y][zs]=2;a[xs-2][y][zs+1]=2;a[xs-2][y][zs+2]=2;
    a[xs-1][y][zs-3]=2;a[xs-1][y][zs-2]=2;a[xs-1][y][zs-1]=2;a[xs-1][y][zs]=2;a[xs-1][y][zs+1]=2;
    a[xs-1][y][zs+2]=2;a[xs-1][y][zs+3]=2;
    a[xs][y][zs-3]=2;a[xs][y][zs-2]=2;a[xs][y][zs-1]=2;a[xs][y][zs]=2;a[xs][y][zs+1]=2;
    a[xs][y][zs+2]=2;a[xs][y][zs+3]=2;
    a[xs+1][y][zs-3]=2;a[xs+1][y][zs-2]=2;a[xs+1][y][zs-1]=2;a[xs+1][y][zs]=2;a[xs+1][y][zs+1]=2;
    a[xs+1][y][zs+2]=2;a[xs+1][y][zs+3]=2;
    a[xs+2][y][zs-2]=2;a[xs+2][y][zs-1]=2;a[xs+2][y][zs]=2;a[xs+2][y][zs+1]=2;a[xs+2][y][zs+2]=2;
    a[xs+3][y][zs-1]=2;a[xs+3][y][zs]=2;a[xs+3][y][zs+1]=2;}
}
```

```
// fibrous assemble
```

```
//1
```

```
x111=xs+7;z111=zs;
```

```
for(y=1;y<SMERY;y++)
```

```
{ a[x111-3][y][z111-1]=2;a[x111-3][y][z111]=2;a[x111-3][y][z111+1]=2;
    a[x111-2][y][z111-2]=2;a[x111-2][y][z111-1]=2;a[x111-2][y][z111]=2;a[x111-2][y][z111+1]=2;
    a[x111-2][y][z111+2]=2;
    a[x111-1][y][z111-3]=2;a[x111-1][y][z111-2]=2;a[x111-1][y][z111-1]=2;a[x111-1][y][z111]=2;
    a[x111-1][y][z111+1]=2;a[x111-1][y][z111+2]=2;a[x111-1][y][z111+3]=2;
    a[x111][y][z111-3]=2;a[x111][y][z111-2]=2;a[x111][y][z111-1]=2;a[x111][y][z111]=2;
    a[x111][y][z111+1]=2;a[x111][y][z111+2]=2;a[x111][y][z111+3]=2;
    a[x111+1][y][z111-3]=2;a[x111+1][y][z111-2]=2;a[x111+1][y][z111-1]=2;a[x111+1][y][z111]=2;
    a[x111+1][y][z111+1]=2;a[x111+1][y][z111+2]=2;a[x111+1][y][z111+3]=2;
    a[x111+2][y][z111-2]=2;a[x111+2][y][z111-1]=2;a[x111+2][y][z111]=2;
    a[x111+2][y][z111+1]=2;a[x111+2][y][z111+2]=2;
    a[x111+3][y][z111-1]=2;a[x111+3][y][z111]=2;a[x111+3][y][z111+1]=2;}
}
```

```
//2
```

```
x111=xs+4;z111=zs-6;
```

```
for(y=1;y<SMERY;y++)
```

```
{ a[x111-3][y][z111-1]=2;a[x111-3][y][z111]=2;a[x111-3][y][z111+1]=2;
    a[x111-2][y][z111-2]=2;a[x111-2][y][z111-1]=2;a[x111-2][y][z111]=2;a[x111-2][y][z111+1]=2;
    a[x111-2][y][z111+2]=2;
    a[x111-1][y][z111-3]=2;a[x111-1][y][z111-2]=2;a[x111-1][y][z111-1]=2;a[x111-1][y][z111]=2;
    a[x111-1][y][z111+1]=2;a[x111-1][y][z111+2]=2;a[x111-1][y][z111+3]=2;
    a[x111][y][z111-3]=2;a[x111][y][z111-2]=2;a[x111][y][z111-1]=2;a[x111][y][z111]=2;
    a[x111][y][z111+1]=2;a[x111][y][z111+2]=2;a[x111][y][z111+3]=2;
    a[x111+1][y][z111-3]=2;a[x111+1][y][z111-2]=2;a[x111+1][y][z111-1]=2;a[x111+1][y][z111]=2;
    a[x111+1][y][z111+1]=2;a[x111+1][y][z111+2]=2;a[x111+1][y][z111+3]=2;
    a[x111+2][y][z111-2]=2;a[x111+2][y][z111-1]=2;a[x111+2][y][z111]=2;
    a[x111+2][y][z111+1]=2;a[x111+2][y][z111+2]=2;
    a[x111+3][y][z111-1]=2;a[x111+3][y][z111]=2;a[x111+3][y][z111+1]=2;}
}
```

```
//3
```

```
x111=xs-3;z111=zs-7;
```

```
for(y=1;y<SMERY;y++)
```

```
{ a[x111-3][y][z111-1]=2;a[x111-3][y][z111]=2;a[x111-3][y][z111+1]=2;
    a[x111-2][y][z111-2]=2;a[x111-2][y][z111-1]=2;a[x111-2][y][z111]=2;a[x111-2][y][z111+1]=2;
    a[x111-2][y][z111+2]=2;
    a[x111-1][y][z111-3]=2;a[x111-1][y][z111-2]=2;a[x111-1][y][z111-1]=2;a[x111-1][y][z111]=2;
    a[x111-1][y][z111+1]=2;a[x111-1][y][z111+2]=2;a[x111-1][y][z111+3]=2;
    a[x111][y][z111-3]=2;a[x111][y][z111-2]=2;a[x111][y][z111-1]=2;a[x111][y][z111]=2;
    a[x111][y][z111+1]=2;a[x111][y][z111+2]=2;a[x111][y][z111+3]=2;
    a[x111+1][y][z111-3]=2;a[x111+1][y][z111-2]=2;a[x111+1][y][z111-1]=2;a[x111+1][y][z111]=2;
    a[x111+1][y][z111+1]=2;a[x111+1][y][z111+2]=2;a[x111+1][y][z111+3]=2;
    a[x111+2][y][z111-2]=2;a[x111+2][y][z111-1]=2;a[x111+2][y][z111]=2;
    a[x111+2][y][z111+1]=2;a[x111+2][y][z111+2]=2;
    a[x111+3][y][z111-1]=2;a[x111+3][y][z111]=2;a[x111+3][y][z111+1]=2;}
}
```

```
//4
```

```

x111=xs-7;z111=zs-1;
for(y=1;y<SMERY;y++)

{ a[x111-3][y][z111-1]=2;a[x111-3][y][z111]=2;a[x111-3][y][z111+1]=2;
  a[x111-2][y][z111-2]=2;a[x111-2][y][z111-1]=2;a[x111-2][y][z111]=2;a[x111-2][y][z111+1]=2;
  a[x111-2][y][z111+2]=2;
  a[x111-1][y][z111-3]=2;a[x111-1][y][z111-2]=2;a[x111-1][y][z111-1]=2;a[x111-1][y][z111]=2;
  a[x111-1][y][z111+1]=2;a[x111-1][y][z111+2]=2;a[x111-1][y][z111+3]=2;
  a[x111][y][z111-3]=2;a[x111][y][z111-2]=2;a[x111][y][z111-1]=2;a[x111][y][z111]=2;
  a[x111][y][z111+1]=2;a[x111][y][z111+2]=2;a[x111][y][z111+3]=2;
  a[x111+1][y][z111-3]=2;a[x111+1][y][z111-2]=2;a[x111+1][y][z111-1]=2;a[x111+1][y][z111]=2;
  a[x111+1][y][z111+1]=2;a[x111+1][y][z111+2]=2;a[x111+1][y][z111+3]=2;
  a[x111+2][y][z111-2]=2;a[x111+2][y][z111-1]=2;a[x111+2][y][z111]=2;
  a[x111+2][y][z111+1]=2;a[x111+2][y][z111+2]=2;
  a[x111+3][y][z111-1]=2;a[x111+3][y][z111]=2;a[x111+3][y][z111+1]=2;}

//5
x111=xs-4;z111=zs+6;
for(y=1;y<SMERY;y++)

{ a[x111-3][y][z111-1]=2;a[x111-3][y][z111]=2;a[x111-3][y][z111+1]=2;
  a[x111-2][y][z111-2]=2;a[x111-2][y][z111-1]=2;a[x111-2][y][z111]=2;a[x111-2][y][z111+1]=2;
  a[x111-2][y][z111+2]=2;
  a[x111-1][y][z111-3]=2;a[x111-1][y][z111-2]=2;a[x111-1][y][z111-1]=2;a[x111-1][y][z111]=2;
  a[x111-1][y][z111+1]=2;a[x111-1][y][z111+2]=2;a[x111-1][y][z111+3]=2;
  a[x111][y][z111-3]=2;a[x111][y][z111-2]=2;a[x111][y][z111-1]=2;a[x111][y][z111]=2;
  a[x111][y][z111+1]=2;a[x111][y][z111+2]=2;a[x111][y][z111+3]=2;
  a[x111+1][y][z111-3]=2;a[x111+1][y][z111-2]=2;a[x111+1][y][z111-1]=2;a[x111+1][y][z111]=2;
  a[x111+1][y][z111+1]=2;a[x111+1][y][z111+2]=2;a[x111+1][y][z111+3]=2;
  a[x111+2][y][z111-2]=2;a[x111+2][y][z111-1]=2;a[x111+2][y][z111]=2;
  a[x111+2][y][z111+1]=2;a[x111+2][y][z111+2]=2;
  a[x111+3][y][z111-1]=2;a[x111+3][y][z111]=2;a[x111+3][y][z111+1]=2;}

//6
x111=xs+3;z111=zs+6;
for(y=1;y<SMERY;y++)

{ a[x111-3][y][z111-1]=2;a[x111-3][y][z111]=2;a[x111-3][y][z111+1]=2;
  a[x111-2][y][z111-2]=2;a[x111-2][y][z111-1]=2;a[x111-2][y][z111]=2;a[x111-2][y][z111+1]=2;
  a[x111-2][y][z111+2]=2;
  a[x111-1][y][z111-3]=2;a[x111-1][y][z111-2]=2;a[x111-1][y][z111-1]=2;a[x111-1][y][z111]=2;
  a[x111-1][y][z111+1]=2;a[x111-1][y][z111+2]=2;a[x111-1][y][z111+3]=2;
  a[x111][y][z111-3]=2;a[x111][y][z111-2]=2;a[x111][y][z111-1]=2;a[x111][y][z111]=2;
  a[x111][y][z111+1]=2;a[x111][y][z111+2]=2;a[x111][y][z111+3]=2;
  a[x111+1][y][z111-3]=2;a[x111+1][y][z111-2]=2;a[x111+1][y][z111-1]=2;a[x111+1][y][z111]=2;
  a[x111+1][y][z111+1]=2;a[x111+1][y][z111+2]=2;a[x111+1][y][z111+3]=2;
  a[x111+2][y][z111-2]=2;a[x111+2][y][z111-1]=2;a[x111+2][y][z111]=2;
  a[x111+2][y][z111+1]=2;a[x111+2][y][z111+2]=2;
  a[x111+3][y][z111-1]=2;a[x111+3][y][z111]=2;a[x111+3][y][z111+1]=2;}

//grafical output - cross section (x,y)
for(x=0;x<=SMERX-1;x++)
  {for(y=0;y<=SMERY-1;y++)
    {putpixel(x,y,a[x][y][rez1]);}
  }

//grafical outout - cross section (x,z)
for(y=0;y<=SMERY-1;y++)
  {for(z=0;z<=SMERZ-1;z++)
    {putpixel(y+SMERY,SMERZ-z,a[rez2][y][z]);}
  }

//grafical outout - cross section (y,z)
for(x=0;x<=SMERX-1;x++)
  {for(z=0;z<=SMERZ-1;z++)

```



```

        {putpixel(x+SMERX+100,SMERZ-z,a[x][rez3][z]);}
    }

//open output field 1
//test of opening
if((vystup1=fopen("c:\\energie.cpp","w"))==NULL)
    {printf("output file error\n");getch();return 1;}
//open output field 2
//test of opening
if((vystup2=fopen("c:\\rychlost1.cpp","w"))==NULL)
    {printf("output file error\n");getch();return 1;}
//open output field 3
//test of opening
if((vystup3=fopen("c:\\rychlost11.cpp","w"))==NULL)
    {printf("output file error\n");getch();return 1;}
//open output field 4
//test of opening
if((vystup4=fopen("c:\\rychlost2.cpp","w"))==NULL)
    {printf("output file error\n");getch();return 1;}
//open output field 5
//test of opening
if((vystup5=fopen("c:\\rychlost3.cpp","w"))==NULL)
    {printf("output file error\n");getch();return 1;}

//open output field 6
//test of opening
if((vystup6=fopen("c:\\rychlost4.cpp","w"))==NULL)
    {printf("output file error\n");getch();return 1;}
//open output field 8
//test of opening
if((vystup8=fopen("c:\\rychlost6.cpp","w"))==NULL)
    {printf("output file error\n");getch();return 1;}

//open output field 8
//test of opening
if((vystup7=fopen("c:\\yzh.cpp","w"))==NULL)
    {printf("output file error\n");getch();return 1;}
//open output field 9
//test of opening
if((vystup9=fopen("c:\\yzd.cpp","w"))==NULL)
    {printf("output file error\n");getch();return 1;}
//open output field 77
//test of opening
if((vystup77=fopen("c:\\rychlost5.cpp","w"))==NULL)
    {printf("output file error\n");getch();return 1;}

//the beginning of simulation cycle
cas=0;
krok=0;
srand((unsigned)time(NULL));
navl:

//choose random cell a[x][y][z]

x=random(SMERX-2)+1;

```

```

y=random(SMERY-2)+1;
z=random(SMERZ-2)+1;

//look for liquid cell
kont=0;
if(a[x][y][z]==1)
{for(i=x-1;i<x+2;i++)
  {for(j=y-1;j<y+2;j++)
    {for(l=z-1;l<z+2;l++)
      {if(a[i][j][l]==15)
        {xk=x;yk=y;zk=z;kont=1;goto nav11;}}
    }
  }
}

} //if
else {goto nav1; }
if (kont==0){goto nav1;}

nav11:
//choose random cell a[x][y][z]

x=random(SMERX-2)+1;
y=random(SMERY-2)+1;
z=random(SMERZ-2)+1;

//look for air cell
kont=0;
if(a[x][y][z]==15)
{for(i=x-1;i<x+2;i++)
  {for(j=y-1;j<y+2;j++)
    {for(l=z-1;l<z+2;l++)
      {if(a[i][j][l]==1)
        {xv=x;yv=y;zv=z;kont=1;goto nav111;}}
    }
  }
}

} //if
else {goto nav11; }
if(kont==0){goto nav11;}

nav111:

krok++;

rychlost1: //cell 1
if(fmod(krok,5000)==0.)
{for(y=0;y<=SMERY-1;y++)
  {if(a[xs+3][y][zs-2]==1){fprintf(vystup2,"%8d %8d\n",krok,y);goto rychlost11; }
  }
}
else{goto rychlost11;}

rychlost11://cell 11
if(fmod(krok,5000)==0.)
{for(y=0;y<=SMERY-1;y++)
  {if(a[xs+2][y][zs-3]==1){fprintf(vystup3,"%8d %8d\n",krok,y);goto rychlost2; }
  }
}
else{goto rychlost2;}

rychlost2: // cell 2
if(fmod(krok,5000)==0.)
{for(y=0;y<=SMERY-1;y++)
  {if(a[xs+2][y][zs-3]==1){fprintf(vystup4,"%8d %8d\n",krok,y);goto rychlost3; }
  }
}
else{goto rychlost3;}

rychlost3: //cell 3
if(fmod(krok,5000)==0.)

```



```

        {for(y=0;y<=SMERY-1;y++)
        {if(a[xs+3][y][zs+2]==1){fprintf(vystup5,"%8d %8d\n",krok,y);goto rychlost4; }
        } }
    else{goto rychlost4;}

rychlost4: //cell 4
if(fmod(krok,5000.)==0.)
    {for(y=0;y<=SMERY-1;y++)
    {if(a[xs][y][zs-4]==1){fprintf(vystup6,"%8d %8d\n",krok,y);goto rychlost5; }
    } }
    else{goto rychlost5;}

rychlost5: //cell 5
if(fmod(krok,5000.)==0.)
    {for(y=0;y<=SMERY-1;y++)
    {if(a[xs-6][y][zs+3]==1){fprintf(vystup7,"%8d %8d\n",krok,y);goto rychlost6; }
    } }
    else{goto rychlost6;}

rychlost6:
//calculation of the energy of liquid cell a[xk][yk][zk] and air cell a[xv][yv][zv]
    enkap1=0.;envz1=0.;enpred=0.;
    for(i=1;i<=1;i++)
        {for(j=1;j<=1;j++)
        {for(l=1;l<=1;l++)
        {enkap1=enkap1+C[a[xk][yk][zk]][a[xk+i][yk+j][zk+l]];
        envz1=envz1+C[a[xv][yv][zv]][a[xv+i][yv+j][zv+l]];}
        } } //l,j,i
    //without central cell
    enkap11=enkap1-C[a[xk][yk][zk]][a[xk][yk][zk]];
    envz11=envz1-C[a[xv][yv][zv]][a[xv][yv][zv]];
    //gravitational energy
    engpr=G*zk;
    //total energy
    enpred=engpr+enkap11+envz11;

//exchange of cell positins.. liquid a[xv][yv][zv]; air a[xk][yk][zk]
apomoc=a[xk][yk][zk];a[xk][yk][zk]=a[xv][yv][zv];a[xv][yv][zv]=apomoc;

//calculaiton of the liquid cell and air cell after exchange of positions
    enkap2=0.;envz2=0.;enpo=0.;
    for(i=1;i<=1;i++)
        {for(j=1;j<=1;j++)
        {for(l=1;l<=1;l++)
        {enkap2=enkap2+C[a[xv][yv][zv]][a[xv+i][yv+j][zv+l]];
        envz2=envz2+C[a[xk][yk][zk]][a[xk+i][yk+j][zk+l]];}
        } } //l,j,i
    //without central cell
    enkap22=enkap2-C[a[xv][yv][zv]][a[xv][yv][zv]];
    envz22=envz2-C[a[xk][yk][zk]][a[xk][yk][zk]];

    //gravitational energy
    engpo=G*zv;
    //total energy
    enpo=engpo+enkap22+envz22;

//energy difference
deltaE=enpo-enpred;

//porovnani velikosti energie - Boltzmanuv faktor
P=0.;BF=0.;
if(deltaE>0.){P=(rand()/(float)RAND_MAX);BF=(float)exp(-deltaE/kT);
    if(P>BF)
        { //exchange of cell positins into initial state
        apomoc=a[xk][yk][zk];a[xk][yk][zk]=a[xv][yv][zv];a[xv][yv][zv]=apomoc;
        energie=energie;
        goto nav1;
        }
    }

```

```

        } //end of position exchange

//konec if(enpred<enpo)

energie=energie+deltaE;
cas++;

if(fmod(cas,10.)==0.){fprintf(vystup1,"%8d %8.5f\n",cas,energie);}

    if(zk==rez1){putpixel(xk,yk,a[xk][yk][rez1]);}
    if(zv==rez1){putpixel(xv,yv,a[xv][yv][rez1]);}
    if(xk==rez2){putpixel(yk+SMERY,SMERZ-zk,a[rez2][yk][zk]);}
    if(xv==rez2){putpixel(yv+SMERY,SMERZ-zv,a[rez2][yv][zv]);}
    if(yk==rez3){putpixel(xk+SMERX+100,SMERZ-zk,a[xk][rez3][zk]);}
    if(yv==rez3){putpixel(xv+SMERX+100,SMERZ-zv,a[xv][rez3][zv]);}

    bar(getmaxx()-70,getmaxy()-30,getmaxx(),getmaxy()-10);
    outtextxy(getmaxx()-100,getmaxy()-20,"k=");
    outtextxy(getmaxx()-70,getmaxy()-20,gcvt(krok,sig,str));
    if(krok>pockr){goto konec;}

//output of energy in simulation time intervals

    outtextxy(getmaxx()-250,getmaxy()-20,"cas=");
    bar(getmaxx()-220,getmaxy()-30,getmaxx()-150,getmaxy()-10);
    outtextxy(getmaxx()-200,getmaxy()-20,gcvt(cas,sig,str));

goto nav1;

konec: // end of simulation cycle

for(y=2;y<SMERY-2;y++)
    {for(z=2;z<zs;z++)
        {if(a[xs+4][y][z]==1){goto print4;}}
    print4:   ykxd=y,zkxd=z,fprintf(vystup9,"%8d %8d %8d\n",ykxd,zkxd,a[xs+2][ykxd][zkxd]);

        } //z,y

for(y=2;y<SMERY-2;y++)
    {for(z=2;z<SMERZ-2;z++)
        {if(a[xs][y][SMERZ-z]==1){goto print2;}}
    print2:   ykxh=y,zkxh=SMERZ-z,fprintf(vystup7,"%8d %8d %8d\n",ykxh,zkxh,a[xs][ykxh][zkxh]);

        } //z,y

fclose (vystup1);
fclose (vystup2);
fclose (vystup3);
fclose (vystup4);
fclose (vystup5);
fclose (vystup6);
fclose (vystup7);
fclose (vystup8);
fclose (vystup9);
fclose (vystup77);
getch ();
closegraph();
return 0;
}

```


Appendix 7

Microsoft Visual Studio Program for simulation of liquid penetration into fibrous structure

The computer simulation results are shown in the Chapter 5.8.2.

```
/*3D lattice model of liquid penetration into fibrous structure*/

#include "graphics.h"
#include <stdlib.h>
#include <stdio.h>
#include <conio.h>
#include <math.h>
#include <float.h>
#include <time.h>

#define SMERX 201
#define SMERY 201
#define SMERZ 201

//global variables
int a[SMERX][SMERY][SMERZ];
int q,cas,krok,pockr=1000,kont,pocet,pocvl=0,n,xr,yr,zr,delka,objemk,plochak,ubytok;
double xp,yp,zp,kx,ky,kz;
int x,y,z,cidlo,i,j,l,xk,yk,zk,xv,yv,zv,apomoc,konec,rez1=25,rez3=45,rez2=100,okraj=5;
int vlakna=0;
float zaplneni=0.;
double fi,fir,thetar,theta,betar,beta,signumx,signumy,signumz,pi=3.1416,vzdal,vzd;

float xx,yy,zz,xxx,yyy,zzz,b,c,d,energie=0.,deltaE=0.,BF,P;
int r=19,xs,ys,zs;
int xmin,xmax,ymin,ymax,vyska,prumer1,prumer2;//parametry kapky

/* vvalues of exchange energies
J[1][1] liquid-liquid, J[1][0] liquid-solid, J[1][16] liquid-air,
J[0][0] solid-solid; J[0][16] solid-air; J[16][16] air-air */

/*liquid surface tension = 2*10*(-92)-(-1)=113/2=56.5;
C[1][1]=-92;C[1][16]=10;C[16][16]=1;*/
/*fibre surface energy = 2*10*(-59)-(-1)=80/2=40;
C[0][0]=-59; C[0][16]=+10; C[16][16]=1;*/
/*interface tension liquid-fibres = 2*(-102)-(-92)-(-59)=53/2= 26.5
C[1][0]=-102; C[1][1]=-92; C[0][0]=-59;*/

float J[16][16]={ {-59,-102,0,0,0,0,0,0,0,0,0,0,0,0,0,0,+10},
                  {-102,-92,0,0,0,0,0,0,0,0,-82,0,0,0,0,0,+10},
                  {0,0,0,0,0,0,0,0,0,0,0,0,0,0,0,0,0},
                  {0,0,0,0,0,0,0,0,0,0,0,0,0,0,0,0,0},
                  {0,0,0,0,0,0,0,0,0,0,0,0,0,0,0,0,0},
                  {0,0,0,0,0,0,0,0,0,0,0,0,0,0,0,0,0},
                  {0,0,0,0,0,0,0,0,0,0,0,0,0,0,0,0,0},
                  {0,0,0,0,0,0,0,0,0,0,0,0,0,0,0,0,0},
                  {0,-82,0,0,0,0,0,0,0,0,0,0,0,0,0,0,-1},
                  {0,0,0,0,0,0,0,0,0,0,0,0,0,0,0,0,0},
                  {0,0,0,0,0,0,0,0,0,0,0,0,0,0,0,0,0},
                  {0,0,0,0,0,0,0,0,0,0,0,0,0,0,0,0,0},
                  {0,0,0,0,0,0,0,0,0,0,0,0,0,0,0,0,0},
                  {0,0,0,0,0,0,0,0,0,0,0,0,0,0,0,0,0},
                  {0,0,0,0,0,0,0,0,0,0,0,0,0,0,0,0,0},
                  {0,0,0,0,0,0,0,0,0,0,0,0,0,0,0,0,0},
}
```

```

float G=7.,kT=50.; //G gravitational acceleration
// kT parameter fo thermodynamic temperature
int sig=10;
char str[25];

float enkap1,enkap11,envz1,envz11,engpr,enpred;
float enkap2,enkap22,envz2,envz22,engpo,enpo;

int main(voi)
{
FILE *vystup1,*vystup2,*vystup3,*vystup4,*vystup5,*vystup6,*vystup45,*vystup35,*vystup25;
FILE *vystup15,*vystup05,*vystup7,*vystup8;
/*request auto detection*/
int gdriver = DETECT, gmode, errorcode;
int xmax, ymax;

/*initialiye graphics and local variables*/
initgraph(&gdriver, &gmode, "");

/*read result of initialization*/
errorcode =graphresult();

/*an error occured*/
if (errorcode != grOk)
{
printf("Graphics error: %s/n",grapherrormsg(errorcode));
printf("Press any key to halt:");
getch();
exit(1);
}
setfillstyle(1,0);

//Ising variables of 3D space
for(x=0;x<SMERX;x++)
{for(y=0;y<SMERY;y++)
{for(z=0;z<SMERZ;z++)
{a[x][y][z]=15;}}
}

//Ising variables of intial configuration of the fibrous system

//proc jsou uhly theta a fi prehozeny nevim, ale funguje to

pocvl=0;

zs=51;
zacatek:
n=0;
zaplneni=0.;

/*
for(x=0;x<SMERX;x++)
{for(y=0;y<SMERY;y++)
{for(z=0;z<zs;z++)
{if(a[x][y][z]==0){pocvl=pocvl+1;}}
} }*/

/*
zaplneni=100*pocvl/2020000;

if(zaplneni>4.){goto konecvl;}

xr=random(SMERX-1); yr=random(SMERY-1); zr=random((zs-1));a[(int)xr][(int)yr][(int)zr]=2;

if(random(1000)<500){signumx=1.;} else{signumx=-1.;}

```



```

fir=random(20);    fi=pi*fir/180.;
if(random(1000)<500){signumy=1.;} else{signumy=-1.;}

//unit vector parallel with fibre
signumx;ky=signumy*sin(fi);

if(random(1000)<500){signumz=1.;} else{signumz=-1.;}
nav90:thetar=random(5);    theta=pi*thetar/180.;
kz=signumz*sin(theta);
//fprintf(vystup6,"%8.5d %8.5d %8.5d\n",kx,ky,kz);

//delkavl:
delka=1875;
//delka=random(225);
//if(delka<1000){goto delkavl;}
//else{goto postup;}

postup:
xp=(n*kx)+xr;    yp=(n*ky)+yr;    zp=(n*kz)+zr;

if(xp<=0) {n=0;goto zacatek;} if(xp>=SMERX-okraj)    {n=0;goto zacatek;}
if(yp<=0) {n=0;goto zacatek;} if(yp>=SMERY-okraj)    {n=0;goto zacatek;}
if(zp<=0) {n=0;goto zacatek;} if(zp>=zs)    {n=0;goto zacatek;}
vzdal=sqrt( pow(xp-xr,2)+pow(yp-yr,2)+pow(zp-zr,2) );

if(vzdal>delka){n=0;goto zacatek;}

a[(int)xp][(int)yp][(int)zp]=0;
a[(int)xp+1][(int)yp][(int)zp]=0; n=n+1; pocvl=pocvl+2;    goto postup;

/*

*/
zaplneni=100*pocvl/2020000;

if(zaplneni>4.){goto konecvl;}

xr=random(SMERX-1); yr=random(SMERY-1); zr=random((zs-1));a[(int)xr][(int)yr][(int)zr]=2;

if(random(1000)<500){signumx=1.;} else{signumx=-1.;}
nav90: fir=random(45);    fi=2.*pi*fir/360.;

if(random(1000)<500){signumz=1.;} else{signumz=-1.;}

//unit vector parallel with fibre
kx=(float)signumx*sin(fi);kz=(float)signumz;

if(random(1000)<500){signumy=1.;} else{signumy=-1.;}
thetar=random(45); theta=2.*pi*thetar/360.;

ky=(float)signumy*sin(theta);

//delkavl:
delka=1875;
//delka=random(225);
//if(delka<1000){goto delkavl;}
//else{goto postup;}

postup:
xp=(int)(n*kx)+xr; yp=(int)(n*ky)+yr;    zp=(int)(n*kz)+zr;

if(xp<=0) {n=0;goto zacatek;} if(xp>=SMERX-okraj)    {n=0;goto zacatek;}
if(yp<=0) {n=0;goto zacatek;} if(yp>=SMERY-okraj)    {n=0;goto zacatek;}
if(zp<=0) {n=0;goto zacatek;} if(zp>=zs)    {n=0;goto zacatek;}
vzdal=sqrt( pow(xp-xr,2)+pow(yp-yr,2)+pow(zp-zr,2) );

if(vzdal>delka){n=0;goto zacatek;}

```

```

a[(int)xp][(int)yp][(int)zp]=0;
a[(int)xp+1][(int)yp][(int)zp]=0;n=n+1; pocvl=pocvl+2;    goto postup;

```

```

konecvl:

```

```

//Ising variables of glass vessel
xs=(SMERX-1)/2;ys=(SMERY-1)/2;
xx=(int)xs;yy=(int)ys;
for(x=0;x<SMERX-1;x++)
    {for(y=0;y<SMERY-1;y++)
        {for(z=zs-1;z<SMERZ-10;z++)
            {vzd=sqrt(pow(x-xx,2)+pow(y-yy,2));
                if(vzd<=r){a[x][y][z]=8;}
            }
        }
    } //z,y,x*/

```

```

//Ising variable of liquid in initial configuration
xs=(SMERX-1)/2;ys=(SMERY-1)/2;
xx=(int)xs;yy=(int)ys;
for(x=0;x<SMERX-1;x++)
    {for(y=0;y<SMERY-1;y++)
        {for(z=zs-1;z<SMERZ-10;z++)
            {vzd=sqrt(pow(x-xx,2)+pow(y-yy,2));
                if(vzd<=r-3){a[x][y][z]=1;}
            }
        }
    } //z,y,x

```

```

//grafical output - cross section (x,y)
for(x=0;x<=SMERX-1;x++)
    {for(y=0;y<=SMERY-1;y++)
        {putpixel(x,y,a[x][y][rez1]);}
    }

```

```

//grafical output - cross section (x,y)
for(x=0;x<=SMERX-1;x++)
    {for(y=0;y<=SMERY-1;y++)
        {putpixel(x,SMERY-y+250,a[x][y][rez3]);}
    }

```

```

//grafical output - cross section (x,z)
for(x=0;x<=SMERX-1;x++)
    {for(z=0;z<=SMERZ-1;z++)
        {putpixel(x+SMERX+20,SMERZ-z,a[x][rez2][z]);}
    }

```

```

//grafical output - cross section (y,z)
for(y=0;y<=SMERY-1;y++)
    {for(z=0;z<=SMERZ-1;z++)
        {putpixel(y+SMERY+240,SMERZ-z,a[rez2][y][z]);}
    }

```

```

//open output field 1
//test of opening
if((vystup1=fopen("c:\\energie.cpp","w"))==NULL)
    {printf("output file error\n");getch();return 1;
    }

```

```

//open output field 2
//test of opening
if((vystup2=fopen("c:\\krokcasy.cpp","w"))==NULL)
    {printf("output file error\n");getch();return 1;
    }

```

```

//open output field 3
//test of opening
if((vystup3=fopen("c:\\objemk.cpp","w"))==NULL)

```



```

        {printf("output file error\n");getch();return 1;
        }

        //open output field 4
//test of opening
if((vystup4=fopen("c:\\zaplneni.cpp", "w"))==NULL)
    {printf("output file error\n");getch();return 1;
    }

        //open output field 5
//test of opening
if((vystup5=fopen("c:\\vrstvy.cpp", "w"))==NULL)
    {printf("output file error\n");getch();return 1;
    }

        //open output field 6
//test of opening
if((vystup6=fopen("c:\\plochak.cpp", "w"))==NULL)
    {printf("output file error\n");getch();return 1;
    }

        //open output field 45
//test of opening
if((vystup45=fopen("c:\\plocha05.cpp", "w"))==NULL)
    {printf("output file error\n");getch();return 1;
    }

        //open output field 35
//test of opening
if((vystup35=fopen("c:\\plocha15.cpp", "w"))==NULL)
    {printf("output file error\n");getch();return 1;
    }

        //open output field 25
//test of opening
if((vystup25=fopen("c:\\plocha25.cpp", "w"))==NULL)
    {printf("output file error\n");getch();return 1;
    }

        //open output field 15
//test of opening
if((vystup15=fopen("c:\\plocha35.cpp", "w"))==NULL)
    {printf("output file error\n");getch();return 1;
    }

        //open output field 05
//test of opening
if((vystup05=fopen("c:\\plocha45.cpp", "w"))==NULL)
    {printf("output file error\n");getch();return 1;
    }

        //open output field 7
//test of opening
if((vystup7=fopen("c:\\rychlost.cpp", "w"))==NULL)
    {printf("output file error\n");getch();return 1;
    }

        //open output field 8
//test of opening
if((vystup8=fopen("c:\\ubYTEK.cpp", "w"))==NULL)
    {printf("output file error\n");getch();return 1;
    }

    fprintf(vystup4, "%8d %8.5f\n", pocvl, zaplneni);

//beginnign of simulation cycle

```

```

cas=0;
krok=0;
srand((unsigned)time(NULL));
nav1:

/*
//how deep is liquid in fibrous structure?
if(fmod(krok,500.)==0.)
{for(x=0;x<SMERX;x++)
    {for(y=0;y<SMERY;y++)
        {if(a[x][y][1]==1){goto konec;}
    } } */

//choose random cell a[x][y][z]

x=random(SMERX-2)+1;
y=random(SMERY-2)+1;
z=random(SMERZ-2)+1;

//look for liquid cell
kont=0;
if(a[x][y][z]==1)
{for(i=x-1;i<x+2;i++)
    {for(j=y-1;j<y+2;j++)
        {for(l=z-1;l<z+2;l++)
            {//liquid - air interface
                if(a[i][j][l]==15)
                {xk=x;yk=y;zk=z;kont=1;goto nav11;}
            } } } //z,j,i
    } } //if
else {goto nav1;}
if (kont==0){goto nav1;}

nav11:
//choose random cell a[x][y][z]

x=random(SMERX-2)+1;
y=random(SMERY-2)+1;
z=random(SMERZ-2)+1;

//look for air cell
kont=0;
if(a[x][y][z]==15)
{for(i=x-1;i<x+2;i++)
    {for(j=y-1;j<y+2;j++)
        {for(l=z-1;l<z+2;l++)
            {//liquid - air interface
                if(a[i][j][l]==1)
                {xv=x;yv=y;zv=z;kont=1;goto nav111;}
            } } } //z,j,i
    } } //if
else {goto nav11;}
if(kont==0){goto nav11;}

nav111:

krok++;

if(fmod(krok,500.)==0.)
{for(z=0;z<zs;z++)
    {for(y=0;y<=SMERY-1;y++)
        {for(x=0;x<=SMERX-1;x++)
            {if(a[x][y][z]==1){fprintf(vystup7,"%8d %8d\n",krok,z);

```



```

        goto nave; }
    }
}
else { goto nave; }

nave:
if(fmod(krok,10000.)==0.)
{
    for(z=zs;z<SMERZ-10;z++)
    {
        for(y=0;y<=SMERY-1;y++)
        {
            for(x=0;x<=SMERX-1;x++)
            {
                if(a[x][y][z]==1){ubytex=ubytex+1;}
            }
        }
    }
    fprintf(vystup8,"%8d %8d\n",krok,ubytex);goto naven;
}
else { goto naven; }

naven:
//calculatin of energies of liquid and air cells in initial positions

    enkap1=0.;envz1=0.;enpred=0.;
    for(i=-1;i<=1;i++)
    {
        for(j=-1;j<=1;j++)
        {
            for(l=-1;l<=1;l++)
            {
                enkap1=enkap1+J[a[xk][yk][zk]][a[xk+i][yk+j][zk+l]];
                envz1=envz1+J[a[xv][yv][zv]][a[xv+i][yv+j][zv+l]];
            }
        }
    }
    //without central cell
    enkap11=enkap1-J[a[xk][yk][zk]][a[xk][yk][zk]];
    envz11=envz1-J[a[xv][yv][zv]][a[xv][yv][zv]];
    //gravitational energy
    engpr=G*zk;
    //total energy
    enpred=enpred+enkap11+envz11;

//exchange of positins of liquid cell and air cell
    apomoc=a[xk][yk][zk];a[xk][yk][zk]=a[xv][yv][zv];a[xv][yv][zv]=apomoc;

//calculation of energies f liquid cell and air cell after positins exchange

    enkap2=0.;envz2=0.;enpo=0.;
    for(i=-1;i<=1;i++)
    {
        for(j=-1;j<=1;j++)
        {
            for(l=-1;l<=1;l++)
            {
                enkap2=enkap2+J[a[xv][yv][zv]][a[xv+i][yv+j][zv+l]];
                envz2=envz2+J[a[xk][yk][zk]][a[xk+i][yk+j][zk+l]];
            }
        }
    }
    //without central cell
    enkap22=enkap2-J[a[xv][yv][zv]][a[xv][yv][zv]];
    envz22=envz2-J[a[xk][yk][zk]][a[xk][yk][zk]];

    //gravitational energy
    engpo=G*zv;
    //total energy
    enpo=enpo+enkap22+envz22;

//difference of energies before and after positin exchange
    deltaE=enpo-enpred;

//if(fmod(krok,1.)==0.){fprintf(vystup5,"%8d %8.5f\n",krok,P);}

// Boltzman factor BF, randomly generated number P
    P=0.;BF=0.;
    if(deltaE>0.){P=(rand()/(float)RAND_MAX);BF=(float)exp(-deltaE/kT);

        if(P>BF)
        {
            //exchange of positions of liquid cell and air cell
            apomoc=a[xk][yk][zk];a[xk][yk][zk]=a[xv][yv][zv];a[xv][yv][zv]=apomoc;

```

```

energie=energie;
    goto nav1;

} //end if(enpred<enpo)                                } //end of position exchange

energie=energie+deltaE;

if(fmod(cas,50.)==0.){fprintf(vystup1,"%8d %8.5f\n",cas,energie);}

    if(zk==rez1){putpixel(xk,yk,a[xk][yk][rez1]);}
    if(zv==rez1){putpixel(xv,yv,a[xv][yv][rez1]);}
    if(zk==rez3){putpixel(xk,SMERY-yk+250,a[xk][yk][rez3]);}
    if(zv==rez3){putpixel(xv,SMERY-yv+250,a[xv][yv][rez3]);}
    if(yk==rez2){putpixel(xk+SMERX+20,SMERZ-zk,a[xk][rez2][zk]);}
    if(yv==rez2){putpixel(xv+SMERX+20,SMERZ-zv,a[xv][rez2][zv]);}
    if(xk==rez2){putpixel(yk+SMERY+240,SMERZ-zk,a[rez2][yk][zk]);}
    if(xv==rez2){putpixel(yv+SMERY+240,SMERZ-zv,a[rez2][yv][zv]);}

    outtextxy(getmaxx()-100,getmaxy()-20,"k=");
    setfillstyle(1,0);
    bar(getmaxx()-70,getmaxy()-30,getmaxx(),getmaxy()-10);
    setcolor(15);
    outtextxy(getmaxx()-70,getmaxy()-20,gcvrt(krok,sig,str));

    if(krok>pockr){goto konec;}

//output of energy in simulation time intervals
cas++;

outtextxy(getmaxx()-270,getmaxy()-20,"cas=");
setfillstyle(1,0);
bar(getmaxx()-220,getmaxy()-30,getmaxx()-150,getmaxy()-10);
setcolor(15);
outtextxy(getmaxx()-200,getmaxy()-20,gcvrt(cas,sig,str));

goto nav1;

konec:// end of simulation cycle

//liquid volume in fibrous structure
objemk=0;
for(x=0;x<SMERX;x++)
    {for(y=0;y<SMERY;y++)
        {for(z=0;z<zs;z++)
            {if(a[x][y][z]==1){objemk=objemk+1;}
        }
    }
    fprintf(vystup2,"%8d %8d\n",cas,krok);
    fprintf(vystup3,"%8d\n",objemk);

//liquid volume in horizontal layers of fibrous structure
for(z=0;z<zs;z++)
    //plochak=0;
    {for(y=0;y<=SMERY-1;y++)
        {for(x=0;x<=SMERX-1;x++)
            {if(a[x][y][z]==1){plochak=plochak+1;}
        }
    }
    fprintf(vystup6,"%8d %8d\n",z,plochak); }

//layer z=45
for(z=45;z<46;z++)
    {for(y=0;y<=SMERY-1;y++)
        {for(x=0;x<=SMERX-1;x++)

```



```

        {if(a[x][y][45]==1){fprintf(vystup05,"%8d %8d %8d\n",a[x][y][45],x,y);}
    }
}

//layer z=35
for(z=35;z<36;z++)
{for(y=0;y<=SMERY-1;y++)
    {for(x=0;x<=SMERX-1;x++)
        {if(a[x][y][35]==1){fprintf(vystup15,"%8d %8d %8d\n",a[x][y][35],x,y);}
    }
}

//layer z=25
for(z=25;z<26;z++)
{for(y=0;y<=SMERY-1;y++)
    {for(x=0;x<=SMERX-1;x++)
        {if(a[x][y][25]==1){fprintf(vystup25,"%8d %8d %8d\n",a[x][y][25],x,y);}
    }
}

//layer z=15
for(z=15;z<16;z++)
{for(y=0;y<=SMERY-1;y++)
    {for(x=0;x<=SMERX-1;x++)
        {if(a[x][y][15]==1){fprintf(vystup35,"%8d %8d %8d\n",a[x][y][15],x,y);}
    }
}

//layer 5
for(z=5;z<6;z++)
{for(y=0;y<=SMERY-1;y++)
    {for(x=0;x<=SMERX-1;x++)
        {if(a[x][y][5]==1){fprintf(vystup45,"%8d %8d %8d\n",a[x][y][5],x,y);}
    }
}

outtextxy(getmaxx()-470,getmaxy()-20,"ob=");
setfillstyle(1,0);
bar(getmaxx()-420,getmaxy()-30,getmaxx()-350,getmaxy()-10);
setcolor(15);
outtextxy(getmaxx()-400,getmaxy()-20,gcvrt(objemk,sig,str));

fclose (vystup1);fclose (vystup2);fclose (vystup3);fclose (vystup4);fclose (vystup5);
fclose (vystup6);fclose (vystup45);fclose (vystup35);fclose (vystup25);fclose (vystup15);
fclose (vystup05);fclose (vystup7);fclose (vystup8);
getch ();
closegraph();
return 0;
}

```

Appendix 8

Microsoft Visual Studio Program for simulation of liquid penetration into fibrous composite structure

The computer simulation results are shown in the Chapter 5.8.2.

[illegible]


```

float G=7.,kT=50.;
int sig=10;
char str[25];

float enkap1, enkap11, envz1, envz11, engpr, enpred;
float enkap2, enkap22, envz2, envz22, engpo, enpo;

int main(voi)
{
FILE *vystup1, *vystup2, *vystup3, *vystup4, *vystup5, *vystup6, *vystup45, *vystup35, *vystup25;
FILE *vystup15, *vystup05, *vystup7, *vystup8;
/*request auto detection*/
int gdriver = DETECT, gmode, errorcode;
int xmax, ymax;

/*initialiye graphics and local variables*/
initgraph(&gdriver, &gmode, "");

/*read result of initialization*/
errorcode = graphresult();

/*an error occured*/
if (errorcode != grOk)
{
printf("Graphics error: %s/n", grapherrormsg(errorcode));
printf("Press any key to halt:");
getch();
exit(1);
}
setfillstyle(1,0);

//Ising variables of 3D space
for(x=0;x<SMERX;x++)
{for(y=0;y<SMERY;y++)
{for(z=0;z<SMERZ;z++)
{a[x][y][z]=15;}}
}

//Ising variables of fibrous structure in initial configuration
//proc jsou uhly theta a fi prehozeny nevim, ale funguje to
pocvl=0;

zs=51;

//top layer
zacatek1:
n=0;
zaplneni=0.;

/*
for(x=0;x<SMERX;x++)
{for(y=0;y<SMERY;y++)
{for(z=0;z<zs;z++)
{if(a[x][y][z]==0){pocvl=pocvl+1;}}
} }*/

zaplneni=100*pocvl/1000000;

if(zaplneni>4.){goto konec1;}

xr=random(SMERX-1); yr=random(SMERY-1); zr=random((zs-1)); a[(int)xr][(int)yr][(int)zr]=0;

if(random(1000)<500){signumx=1.;} else{signumx=-1.;}
fir=random(5); fi=pi*fir/180.;
if(random(1000)<500){signumz=1.;} else{signumz=-1.;}

```

```

//unit vector parallel with fibre
x=signumx*sin(fi); kz=signumz;

if(random(1000)<500){signumy=1.;} else{signumy=-1.;}
nav90.thetar=random(20); theta=pi*thetar/180.;
ky=signumy*sin(theta);
//fprintf(vystup6,"%8.5d %8.5d %8.5d\n",kx,ky,kz);

//delkavl:
delka=1875;
//delka=random(225);
//if(delka<1000){goto delkavl;}
//else{goto postup1;}

postup1:
xp=(n*kx)+xr; yp=(n*ky)+yr; zp=(n*kz)+zr;

if(xp<=0) {n=0;goto zacatek1;} if(xp>=SMERX-okraj) {n=0;goto zacatek1;}
if(yp<=0) {n=0;goto zacatek1;} if(yp>=SMERY-okraj) {n=0;goto zacatek1;}
if(zp<=0) {n=0;goto zacatek1;} if(zp>=zs) {n=0;goto zacatek1;}
vzda1=sqrt( pow(xp-xr,2)+pow(yp-yr,2)+pow(zp-zr,2) );

if(vzda1>delka){n=0;goto zacatek1;}

a[(int)xp][(int)yp][(int)zp]=0;n=n+1; pocvl=pocvl+1; goto postup1;
//a[(int)xp+1][(int)yp][(int)zp]=0;
konecvl1:

//vstupni hodnoty pole a
for(x=0;x<SMERX;x++)
{for(y=0;y<SMERY;y++)
{for(z=0;z<21;z++)
{a[x][y][z]=15;}}
}

//bottom layer
zaplneni=0;
pocvl=0;
n=0;
vzda1=0.;
zacatek2:

zaplneni=100*pocvl/1000000;

if(zaplneni>4.){goto konecvl2;}

xr=random(SMERX-1); yr=random(SMERY-1); zr=random(25);a[(int)xr][(int)yr][(int)zr]=0;

if(random(1000)<500){signumx=1.;} else{signumx=-1.;}
fir=random(5); fi=2.*pi*fir/360.;
if(random(1000)<500){signumz=1.;} else{signumz=-1.;}

//unit vector parallel with fibre
kx=(float)signumx;kz=(float)signumz*sin(fi);

if(random(1000)<500){signumy=1.;} else{signumy=-1.;}
thetar=random(20); theta=pi*thetar/180.;

ky=signumy*sin(theta);

//delkavl:
delka=1875;
//delka=random(225);
//if(delka<1000){goto delkavl;}
//else{goto postup1;}

```



```

postup2:
xp=(int)(n*kx)+xr; yp=(int)(n*ky)+yr;          zp=(int)(n*kz)+zr;

if(xp<=1) {n=0;goto zacatek2;} if(xp>=SMERX-okraj) {n=0;goto zacatek2;}
if(yp<=1) {n=0;goto zacatek2;} if(yp>=SMERY-okraj) {n=0;goto zacatek2;}
if(zp<=1) {n=0;goto zacatek2;} if(zp>=26) {n=0;goto zacatek2;}
vzdal=sqrt( pow(xp-xr,2)+pow(yp-yr,2)+pow(zp-zr,2) );

if(vzdal>delka){n=0;goto zacatek2;}

a[(int)xp][(int)yp][(int)zp]=0; n=n+1; pocvl=pocvl+1;    goto postup2;

//a[(int)xp+1][(int)yp][(int)zp]=0;

konecvl2:

```

```

//Ising variables of glass vesel
xs=(SMERX-1)/2;ys=(SMERY-1)/2;
xx=(int)xs;yy=(int)ys;
for(x=0;x<SMERX-1;x++)
    {for(y=0;y<SMERY-1;y++)
        {for(z=zs-1;z<SMERZ-10;z++)
            {vzd=sqrt(pow(x-xx,2)+pow(y-yy,2));
                if(vzd<=r){a[x][y][z]=8;}
            }
        }
    } //z,y,x*/

```

```

//Ising variables of liquid in initial configuration
xs=(SMERX-1)/2;ys=(SMERY-1)/2;
xx=(int)xs;yy=(int)ys;
for(x=0;x<SMERX-1;x++)
    {for(y=0;y<SMERY-1;y++)
        {for(z=zs-1;z<SMERZ-10;z++)
            {vzd=sqrt(pow(x-xx,2)+pow(y-yy,2));
                if(vzd<=r-3){a[x][y][z]=1;}
            }
        }
    } //z,y,x

```

```

//grafical output - cross section (x,y)
for(x=0;x<=SMERX-1;x++)
    {for(y=0;y<=SMERY-1;y++)
        {putpixel(x,y,a[x][y][rez1]);}
    }

//grafical output - cross section (x,y)
for(x=0;x<=SMERX-1;x++)
    {for(y=0;y<=SMERY-1;y++)
        {putpixel(x,SMERY-y+250,a[x][y][rez3]);}
    }

//grafical output - cross section (x,z)
for(x=0;x<=SMERX-1;x++)
    {for(z=0;z<=SMERZ-1;z++)
        {putpixel(x+SMERX+20,SMERZ-z,a[x][rez2][z]);}
    }

//grafical output - cross section (y,z)
for(y=0;y<=SMERY-1;y++)
    {for(z=0;z<=SMERZ-1;z++)
        {putpixel(y+SMERY+240,SMERZ-z,a[rez2][y][z]);}
    }

```

```

//open output field 1
//test of opening
if((vystup1=fopen("c:\\energie.cpp","w"))==NULL)
    {printf("output file error\n");getch();return 1;
    }

```

```

//open output field 2
//test of opening
if((vystup2=fopen("c:\\krokcas.cpp","w"))==NULL)
    {printf("output file error\n");getch();return 1;
    }

//open output field 3
//test of opening
if((vystup3=fopen("c:\\objemk.cpp","w"))==NULL)
    {printf("output file error\n");getch();return 1;
    }

//open output field 4
//test of opening
if((vystup4=fopen("c:\\zaplneni.cpp","w"))==NULL)
    {printf("output file error\n");getch();return 1;
    }

//open output field 5
//test of opening
if((vystup5=fopen("c:\\vrstvy.cpp","w"))==NULL)
    {printf("output file error\n");getch();return 1;
    }

//open output field 6
//test of opening
if((vystup6=fopen("c:\\plochak.cpp","w"))==NULL)
    {printf("output file error\n");getch();return 1;
    }

//open output field 45
//test of opening
if((vystup45=fopen("c:\\plocha05.cpp","w"))==NULL)
    {printf("output file error\n");getch();return 1;
    }

//open output field 35
//test of opening
if((vystup35=fopen("c:\\plocha15.cpp","w"))==NULL)
    {printf("output file error\n");getch();return 1;
    }

//open output field 25
//test of opening
if((vystup25=fopen("c:\\plocha25.cpp","w"))==NULL)
    {printf("output file error\n");getch();return 1;
    }

//open output field 15
//test of opening
if((vystup15=fopen("c:\\plocha35.cpp","w"))==NULL)
    {printf("output file error\n");getch();return 1;
    }

//open output field 05
//test of opening
if((vystup05=fopen("c:\\plocha45.cpp","w"))==NULL)
    {printf("output file error\n");getch();return 1;
    }

//open output field 7
//test of opening
if((vystup7=fopen("c:\\rychlost.cpp","w"))==NULL)
    {printf("output file error\n");getch();return 1;
    }

```



```

//open output field 8
//test of opening
if((vystup8=fopen("c:\\ubYTEk.cpp","w"))==NULL)
    {printf("output file error\n");getch();return 1;
    }

fprintf(vystup4,"%8d %8.5f\n",pocvl,zaplneni);

//beginning of simulation cycle
cas=0;
krok=0;
srand((unsigned)time(NULL));
nav1:
/*
//how deep is liquid in fibrous structure?
if(fmod(krok,500.)==0.)
{for(x=0;x<SMERX;x++)
    {for(y=0;y<SMERY;y++)
        {if(a[x][y][1]==1){goto konec;}}
    } }*/

//choose random cell a[x][y][z]

x=random(SMERX-2)+1;
y=random(SMERY-2)+1;
z=random(SMERZ-2)+1;

//look for liquid cell
kont=0;
if(a[x][y][z]==1)
    {for(i=x-1;i<x+2;i++)
        {for(j=y-1;j<y+2;j++)
            {for(l=z-1;l<z+2;l++)
                {//liquid - air interface
                    if(a[i][j][l]==15)
                        {xk=x,yk=y,zk=z,kont=1;goto nav11;}
                }
            }
        }
    } } //z,j,i

} //if
else {goto nav1;}
if (kont==0){goto nav1;}

nav11:
//choose random cell a[x][y][z]

x=random(SMERX-2)+1;
y=random(SMERY-2)+1;
z=random(SMERZ-2)+1;

//look for air cell
kont=0;
if(a[x][y][z]==15)
    {for(i=x-1;i<x+2;i++)
        {for(j=y-1;j<y+2;j++)
            {for(l=z-1;l<z+2;l++)
                {//liquid - air interface
                    if(a[i][j][l]==1)
                        {xv=x,yv=y,zv=z,kont=1;goto nav111;}
                }
            }
        }
    } } //z,j,i

} //if
else {goto nav11;}
if(kont==0){goto nav11;}

```

```

navl11:

krok++;

if(fmod(krok,5000.)==0.)
{
for(z=0;z<zs;z++)
{
for(y=0;y<=SMERY-1;y++)
{
for(x=0;x<=SMERX-1;x++)
{
if(a[x][y][z]==1){fprintf(vystup7,"%8d %8d\n",krok,z);
goto nave; }
}
}
}
}
else{goto nave;}

nave:
if(fmod(krok,10000.)==0.)
{
for(z=zs;z<SMERZ-10;z++)
{
for(y=0;y<=SMERY-1;y++)
{
for(x=0;x<=SMERX-1;x++)
{
if(a[x][y][z]==1){ubYTEK=ubYTEK+1;}
}
}
}
}
fprintf(vystup8,"%8d %8d\n",krok,ubYTEK);goto naven;}
else{goto naven;}

naven:
//calculation of energies of liquid and air cells in initial positions

enkap1=0.;envz1=0.;enpred=0.;
for(i=1;i<=1;i++)
{
for(j=1;j<=1;j++)
{
for(l=1;l<=1;l++)
{
enkap1=enkap1+J[a[xk][yk][zk]][a[xk+i][yk+j][zk+l]];
envz1=envz1+J[a[xv][yv][zv]][a[xv+i][yv+j][zv+l]];}
}
}
} //l,j,i
//without central cell
enkap11=enkap1-J[a[xk][yk][zk]][a[xk][yk][zk]];
envz11=envz1-J[a[xv][yv][zv]][a[xv][yv][zv]];
//gravitational energy
engpr=G*zk;
//total energy
enpred=enpred+enkap11+envz11;

//exchange of positions of liquid cell and air cell
apomoc=a[xk][yk][zk];a[xk][yk][zk]=a[xv][yv][zv];a[xv][yv][zv]=apomoc;

//calculation of energies of liquid and air cells after position exchange

enkap2=0.;envz2=0.;enpo=0.;
for(i=1;i<=1;i++)
{
for(j=1;j<=1;j++)
{
for(l=1;l<=1;l++)
{
enkap2=enkap2+J[a[xv][yv][zv]][a[xv+i][yv+j][zv+l]];
envz2=envz2+J[a[xk][yk][zk]][a[xk+i][yk+j][zk+l]];}
}
}
} //l,j,i
//without central cell
enkap22=enkap2-J[a[xv][yv][zv]][a[xv][yv][zv]];
envz22=envz2-J[a[xk][yk][zk]][a[xk][yk][zk]];

//gravitational energy
engpo=G*zv;
//total energy
enpo=enpo+enkap22+envz22;

//difference of energies before and after position exchange
deltaE=enpo-enpred;

```



```

//if(fmod(krok,1.)==0.){fprintf(vystup5,"%8d %8.5f\n",krok,P);}
// Boltzman factor BF, randomly generated number P
P=0.;BF=0.;
if(deltaE>0.){P=(rand()/(float)RAND_MAX);BF=(float)exp(-deltaE/kT);

                                if(P>BF)
                                { //position exchange, cells back to initial positions
apomoc=a[xk][yk][zk];a[xk][yk][zk]=a[xv][yv][zv];a[xv][yv][zv]=apomoc;
energie=energie;
                                goto nav1;
                                } //end position exchange
} //end if(enpred<enpo)

energie=energie+deltaE;

if(fmod(cas,50.)==0.){fprintf(vystup1,"%8d %8.5f\n",cas,energie);}

    if(zk==rez1){putpixel(xk,yk,a[xk][yk][rez1]);}
    if(zv==rez1){putpixel(xv,yv,a[xv][yv][rez1]);}
    if(zk==rez3){putpixel(xk,SMERY-yk+250,a[xk][yk][rez3]);}
    if(zv==rez3){putpixel(xv,SMERY-yv+250,a[xv][yv][rez3]);}
    if(yk==rez2){putpixel(xk+SMERX+20,SMERZ-zk,a[xk][rez2][zk]);}
    if(yv==rez2){putpixel(xv+SMERX+20,SMERZ-zv,a[xv][rez2][zv]);}
    if(xk==rez2){putpixel(yk+SMERY+240,SMERZ-zk,a[rez2][yk][zk]);}
    if(xv==rez2){putpixel(yv+SMERY+240,SMERZ-zv,a[rez2][yv][zv]);}

    outtextxy(getmaxx()-100,getmaxy()-20,"k=");
    setfillstyle(1,0);
    bar(getmaxx()-70,getmaxy()-30,getmaxx(),getmaxy()-10);
    setcolor(15);
    outtextxy(getmaxx()-70,getmaxy()-20,gcvt(krok,sig,str));

    if(krok>pockr){goto konec;}

//output of energy in simulation time intervals
cas++;

    outtextxy(getmaxx()-270,getmaxy()-20,"cas=");
    setfillstyle(1,0);
    bar(getmaxx()-220,getmaxy()-30,getmaxx()-150,getmaxy()-10);
    setcolor(15);
    outtextxy(getmaxx()-200,getmaxy()-20,gcvt(cas,sig,str));

goto nav1;

konec://end of simulation cycle

//liquid volume in fibrous structure
objemk=0;
for(x=0;x<SMERX;x++)
    {for(y=0;y<SMERY;y++)
        {for(z=0;z<zs;z++)
            {if(a[x][y][z]==1){objemk=objemk+1;}
        }
    }
}
fprintf(vystup2,"%8d %8d\n",cas,krok);
fprintf(vystup3,"%8d\n",objemk);

//liquid volume in horizontal layers of fibrous structure
for(z=0;z<zs;z++)
    //plochak=0;
    {for(y=0;y<=SMERY-1;y++)
        {for(x=0;x<=SMERX-1;x++)
            {if(a[x][y][z]==1){plochak=plochak+1;}
        }
    }
}

```

```

    }
    fprintf(vystup6, "%8d %8d\n", z, plochak); }

//layer z=45
for(z=45; z<46; z++)
{for(y=0; y<=SMERY-1; y++)
    {for(x=0; x<=SMERX-1; x++)
        {if(a[x][y][45]==1){fprintf(vystup05, "%8d %8d %8d\n", a[x][y][45], x, y);}}
    }
}

//layer z=35
for(z=35; z<36; z++)
{for(y=0; y<=SMERY-1; y++)
    {for(x=0; x<=SMERX-1; x++)
        {if(a[x][y][35]==1){fprintf(vystup15, "%8d %8d %8d\n", a[x][y][35], x, y);}}
    }
}

//layer z=25
for(z=25; z<26; z++)
{for(y=0; y<=SMERY-1; y++)
    {for(x=0; x<=SMERX-1; x++)
        {if(a[x][y][25]==1){fprintf(vystup25, "%8d %8d %8d\n", a[x][y][25], x, y);}}
    }
}

//layer z=15
for(z=15; z<16; z++)
{for(y=0; y<=SMERY-1; y++)
    {for(x=0; x<=SMERX-1; x++)
        {if(a[x][y][15]==1){fprintf(vystup35, "%8d %8d %8d\n", a[x][y][15], x, y);}}
    }
}

//layer z=5
for(z=5; z<6; z++)
{for(y=0; y<=SMERY-1; y++)
    {for(x=0; x<=SMERX-1; x++)
        {if(a[x][y][5]==1){fprintf(vystup45, "%8d %8d %8d\n", a[x][y][5], x, y);}}
    }
}

outtextxy(getmaxx()-470, getmaxy()-20, "ob=");
setfillstyle(1, 0);
bar(getmaxx()-420, getmaxy()-30, getmaxx()-350, getmaxy()-10);
setcolor(15);
outtextxy(getmaxx()-400, getmaxy()-20, gcvt(objemk, sig, str));

fclose (vystup1); fclose (vystup2); fclose (vystup3); fclose (vystup4); fclose (vystup5);
fclose (vystup6); fclose (vystup45); fclose (vystup35); fclose (vystup25); fclose (vystup15);
fclose (vystup05); fclose (vystup7); fclose (vystup8);
getch ();
closegraph();
return 0;
}

```


U 594 T

1000000